SILICON CARBIDE NANOTUBES: PROMISES BEYOND CARBON NANOTUBES

by

KAZI MOHAMMAD MONIRUL ALAM

Presented to the Faculty of the Graduate School of

The University of Texas at Arlington in Partial Fulfillment

of the Requirements

for the Degree of

MASTER OF SCIENCE IN PHYSICS

THE UNIVERSITY OF TEXAS AT ARLINGTON

August 2008

ACKNOWLEDGEMENTS

I would like to express my deep gratefulness to my thesis advisor, Prof. Dr. A. K. Ray who made the whole work possible. His stimulating suggestions and encouragement helped me throughout my research and writing of this thesis. My experience of working as a student of Prof. A. K. Ray is an invaluable treasure, which will benefit my entire life. I also would like to extend my thanks to my committee members, Dr. Zhang and Dr. Sharma, for their advice and opinions. I am thankful to Welch Foundation, Houston, Texas for support and the entire physics department for providing an excellent work environment.

It was my pleasure to work with my research group members; Raymond, Somil, Souptik, Pratik, and Fakrul who have given help and valuable hints. I particularly enjoyed our group meetings. My stay in UTA Physics department was peaceful and interesting. I found the departmental activities very conducive to gain knowledge and build up social networks.

Finally, I would like to be thankful to my family members whose continuous support and encouragement helped complete this work.

June 26, 2008

ABSTRACT

SILICON CARBIDE NANOTUBES: PROMISES BEYOND CARBON NANOTUBES

Kazi Mohammad Monirul Alam, M. S.

The University of Texas at Arlington, 2008

Supervising Professor: Dr. A. K. Ray

First-principles calculations for the electronic and geometric structures of *three* different types of armchair and zigzag silicon carbide nanotubes from (3, 3) to (11, 11) and (3, 0) to (11, 0) have been performed using hybrid density functional theory and the finite cluster approximation. Full geometry and spin optimizations have been performed without any symmetry constraints. A detailed comparison of the structures and stabilities of the three types of nanotubes is presented. The dependence of the electronic band gaps on the respective tube diameters, energy density of states and dipole moments as well as Mulliken charge distributions have been investigated. For type 1 armchair nanotubes Si atoms moved toward the tube axis and C atoms moved in the opposite direction after relaxation, consistent with other SiC nanotubes found in literature. For type 2 and the *newly* proposed type 3 armchair, this displacement direction is reversed. For all types of zigzag SiC nanotubes Si atoms moved outward the tube axis making two concentric cylinders of Si and C atoms after relaxation contrary to some published results in the literature for type 1 nanotubes. The band gaps for type 1 armchair nanotubes are larger than bulk 3C-SiC gap, while type 2 and type 3 armchair nanotubes have significantly lower band gaps. The band gaps for type 2 armchair

nanotubes, also type 1 and type 2 zigzag nanotubes show an oscillatory pattern as the diameter increases. Unlike the other two types, band gap for type 3 nanotubes in both chirality decreases monotonically with increasing tube diameter. None of the armchair tubes appear to be magnetic. On the other hand all the zigzag tubes studied here appear to have triplet ground states except for type 1 (3, 0). As a continuation we have also investigated the interaction of Fe atom with these SiC nanotubes. A systematic study of Fe atom encapsulation and adsorption in both armchair and zigzag SiC nanotubes has been performed using the same computational formalism. A detailed comparison of the binding energies, equilibrium positions, Mulliken charges, spin magnetic moments of Fe atoms, the electronic states, HOMO-LUMO gaps, and changes in gaps with respect to the bare nanotube gaps have been investigated. Our results show that the properties of SiC nanotubes can be modified by Fe atom encapsulation and adsorption. All the structures are found to have magnetic ground states with high magnetic moments. It is expected that both pristine and Fe doped SiC nanotubes will have interesting and important applications in the field of band gap engineering, molecular electronics and spintronics.

TABLE OF CONTENTS

LIST OF ILLUSTRATIONS

LIST OF TABLES

CHAPTER 1

INTRODUCTION

1.1 Important applications of carbon nanotubes

Nanotubes have attracted significant academic and industrial interest due to their outstanding and unique mechanical, electronic and optical properties. They are one of the most studied nanostructures in the current literature. Since the discovery of multi-walled carbon nanotubes (CNT) in 1991[1], there has been an explosive growth of interest in these kinds of quasi-one-dimensional structures due to their fascinating physical properties and huge potential applications in the electronics industry. Exploring the underlying physics of these structures constitutes the basic building blocks of modern fields of nanoscience and nanotechnology. One distinguishing feature of carbon among other group IV elements in the periodic table is that it can participate in either sp^2 or sp^3 bond configurations and can form a variety of phases, such as diamond, graphite, and fullerenes.[2] Single-walled carbon nanotubes have unique characteristics in that they can behave either as metals or semiconductors depending on the tube diameter and chirality. Armchair carbon nanotubes are metallic, while zigzag structures are semiconductors. Length and curvature also play a significant role on structures and energetics.[3-7] Also, carbon nanotube based field effect transistors (CNT-FET) have advantages over conventional silicon metal-oxide-semiconductor-field-effect transistors (MOSFETs) such as, strong one dimensional electron confinement and full depletion in the nanoscale diameter of single-walled carbon nanotubes lead to a suppression of short-channel effects in transistor devices.[8-11] Nanotube-based nonlinear devices can be compact, fast, and sensitive because nanotubes are strong, stable, and uniquely conductive. Researchers have demonstrated that nanotube transistors can have a large current density, high gain, and high carrier mobility.[12-15] Prototype nanotube sensors have demonstrated high sensitivity

detection of electromagnetic and acoustic signals as well as different chemicals.[16-18] Carbon nanotube based field effect transistor, depending on the biasing conditions, can serve as an electrical switch, a novel light source and a light detector. Carbon nanotubes provide an ideal model system to study the electrical transport properties of one dimensional nanostructures and molecules.[19-20]

1.2 Nanostructures of other elements

The extraordinary success in synthesizing and in applications of CNTs has prompted significant experimental and theoretical research on nanostructures of other elements. Group-III nitrides, such as BN, AlN and GaN have been synthesized through different techniques.[21-23] Synthesis of several other nanotubes have been reported, for example, NiCl, $H_2Ti_3O_3$, TiO_2, and Si.[24-27] Silicon carbide (SiC) in bulk form is one of the hardest materials and is very suitable for electronic devices designed for operations in extreme environments. In fact, SiC, with its wide band gap, high thermal conductivity, and radiation resistance, is particularly important for use in high temperature and radiation environments. It is reasonable to assume that the unique properties of bulk SiC, along with properties due to quantum size-effects, would also reflect in SiC nanostructures. Indeed, possibilities and promises abound for SiC nanostructures for applications such as nanosensors and nanodevices which can be operated at high temperature, high frequency, and high power. Our group has studied, in detail, the stability of Si_{60} fullerene-like cage by substitutional and endohedral placements of carbon atoms. We found that substitutional carbon doping made the Si_{60} clusters more stable than endohedral doping. Also stability is higher when the Si and the C atoms are in separate sub-units on the cage.[28-30] First principles calculations based on density functional theory has been performed on the electronic and structural properties of silicon substitutional doping in carbon nanotubes.[31]

1.3 Silicon carbide nanotubes

Except carbon, group IV elements have considerable energy differences between sp^2 and sp^3 bonds which suppress the realization of graphitic phase.[32] SiC, in fact, also has a significant energy difference between the sp^2 and sp^3 bonds. Despite these facts, SiC nanotubes have been successfully synthesized by different groups.[33-41] Sun *et al*.[33] have reported the synthesis of SiC nanotubes trough a substitutional reaction with Si atoms replacing half of the C atoms from a multi-walled carbon nanotube. The observed SiC nanotubes were also multi-walled but with higher interplanar spacings than those of multi-walled carbon nanotubes. This indicated weak coupling between inner and outer tubes and possibility of separating them with ease. This motivated us to explore the properties of single wall SiC nanotubes. Indeed from technological points of view single wall nanotubes play more important rolls in molecular electronics. Borowiak-Palen *et al*.[35] produced SiC nanotubes based on high-temperature reactions between silicon powders and multi-walled carbon nanotubes. Hu *et al*.[37] formed SiC nanotubes by reacting CH_4 with SiO. SiC nanotubes are expected to have some advantages over carbon nanotubes. They may possess high reactivity of exterior surface facilitating sidewall decoration and stability at high temperature, harsh environment nanofiber and nanotube reinforced ceramics.[42] Some *ab initio* methods[43] have shown that the most stable SiC nanotube has the ratio of Si to C one to one. These studies claim that other ratios will eventually collapse the tube into nanowire or clusters with solid interiors. M. Menon et al.[44] have shown that there are two different arrangements (type 1 and type 2) for the most stable SiC nanotubes. They have studied certain nanotubes in armchair and zigzag configuration. Type 1 consists of alternating Si and C atoms with each Si atoms having three C neighbors and vice versa. In type 2 configuration each Si atom has two C neighbors and one Si neighbor and vice versa. Generalized tight-binding molecular-dynamics and *ab initio* methods were used to study only armchair (6, 6) and zigzag (12, 0). Their calculations

revealed that SiC nanotubes with alternating Si and C atoms (type 1) are energetically preferred over the forms that contain C-C and Si-Si bonds (type 2) in addition to Si-C bonds.

We propose in this work a new type 3 SiC tube which has the same number of Si and C atoms, but differs in the relative spatial positions of Si and C atoms. In this type, each Si has two C and one Si neighbors, has the same constraint as type 2, but Si and C atoms are arranged alternatively in each layer (the layer perpendicular to the tube axis) unlike in type 2 where each layer contains either Si or C atoms. As the results below show, type 3 is indeed found to be less stable than types 1 and 2 in armchair configuration but is more stable in zigzag configuration; however, depending on particular applications, type3 SiC nanotubes can provide an alternate choice. This study is the first ab initio study of the evolution of physical and electronic properties with size (the tube diameter) of three different types of SiC nanotubes. In particular, in this work we have studied detailed electronic and geometric structure properties of three different types of single wall armchair SiC nanotubes from (3, 3) to (11, 11) and zigzag SiC nanotubes from (3, 0) to (11, 0).

1.4 Interactions of transition metal atoms with nanotubes

Theoretical [45-49] and experimental[50] research on interactions of transition metal atoms with single wall carbon nanotubes (SWCNTs) have reported dramatic changes in the structural, electronic, and magnetic properties of the nanotubes and provide valuable information about possible uses of them as nanowires, nanomagnets, interconnects in molecular electronic network, spintronics, recording media, and magnetic links, among others. Doping metal atoms inside silicon clusters and nanotubes has also acquired significant attention since this stabilizes the structures [51, 52]. In addition, it was found that electrical, magnetic and optical properties of the silicon nanostructures can be tailored by changing the metal atoms.

1.5 Interactions of transition metal atoms with SiC nanotubes

Unlike carbon and silicon nanotubes, interaction of transition metal atoms with SiC nanotubes has *not* been explored extensively. Recently first principles method has been used to investigate the adsorption of Ti atom on type 1 single wall SiCNT with the corresponding adsorption of hydrogen molecules.[53] Using periodic boundary conditions and the Dmol3 suite of software, Zhao and Ding have very recently studied the silicon carbide nanotubes functionalized by transition metal atoms. They primarily studied interactions with a (8, 0) zigzag SiC nanotube and four of them, not including Fe, with a (6, 6) armchair type 1 nanotube.[54] They concluded that transition metal-SiC nanotube materials could be used in various interesting applications, such as nanomagnets and hydrogen storage.[55] To the best of our knowledge, *no* other study has been reported regarding the interaction of transition metal atoms with SiCNT. As is known, the most common experimental methods for fabricating carbon nanotubes are arc discharge, laser ablation, and chemical vapor deposition. Transition metals such as Mn, Fe, Co and Ni or metal alloys are required as catalyst in those methods. As mentioned before SiCNTs were synthesized using carbon nanotubes as template, so it is particularly important to analyze the interaction of these metal atoms with both CNT and SiCNT. In this present work we have systematically studied the encapsulation and adsorption of a Fe atom in all three types of single wall armchair and zigzag SiC nanotubes.

CHAPTER 2

THEORY

2.1 Density functional theory

Two standard methods in computational condensed matter physics are based on Hartree-Fock (HF) theory and density functional theory (DFT). Both of these theories are simplifications of the full problem of many electrons moving in the potential field. Density functional theory, which results from work of Hohenberg, Kohn and Sham. [56-63] is the most popular method. In many cases the problems related to electronic structures can be studied by the time-independent Schrödinger equation. For an isolated system with N electrons in the Born-Oppenheimer nonrelativistic approximation, this is given by

$$H\Psi = E\Psi \tag{2.1}$$

Where H is the Hamiltonian in atomic units,

$$H = \sum_{i=1}^{N} (-\frac{1}{2}\nabla_i^2) + \sum_{i=1}^{N} v(r_i) + \sum_{i<j}^{N} \frac{1}{r_{ij}} \tag{2.2}$$

in which

$$v(r) = -\sum_{\alpha} \frac{Z_\alpha}{| r_i - R_\alpha |} \tag{2.3}$$

is the "external" potential due to nuclei of charges Z_α acting on the i^{th} electron. E is the electronic energy and $\Psi = \Psi(x_i, x_2, ..., x_n)$ is the many-electron wave function, where x_i denote the particle coordinates and spins. It has been an important goal of physics to solve this many particle problem for a few decades. Generally speaking, there are two approaches. One is to consider the many-electron wave function $\Psi(x_i, x_2, ..., x_n)$. In the Hartree

approximation [64], in which the many-electron wave function is constructed from the product of single particle functions,

$$\Psi(x_i, x_2, ..., x_n) = \Psi_1(x_1)\Psi_2(x_2)...\Psi_n(x_n) \tag{2.4}$$

Each of the functions $\Psi_1(x_1)$ satisfies a one-electron Schrödinger equation with a potential term arising from the average field of the other electrons,

$$\left[-\frac{h^2}{2m}\nabla^2 + V_{ext} + \Phi_i\right]\Psi_i(x) = \varepsilon_i\Psi_i(x) \tag{2.5}$$

where the Coulomb potential Φ_i is given by Poisson's equation

$$\nabla^2\Phi_i = 4\pi e^2 \sum_{j=1, i\neq j}^{N} |\Psi_j|^2 \tag{2.6}$$

and V_{ext} is the potential due to the nuclei. Considering Pauli Exclusion Principle, the simple product wave function can be replaced by a single determinantal function, which leads to the so-called Hartree-Fock approximation [65-66]. The inclusion of Fermi statistics which introduces an additional, nonlocal exchange term in the Schrödinger equation improves the total energy calculation, but the single particle picture, with the wave function described in terms of orbital with particular spins and occupation numbers is unchanged. It has noted that a single configuration (Slater determinant) wave function must inevitably lead to a poor energy since the lowest-lying configuration is generally only one of very many with comparable energies, and a better approximation would result from taking a linear combination [67]. This approach known as "configuration interaction" (CI) includes the correlation effects beyond Hartree-Fock approximation by improving the many-particle wave functions. In principle, CI provides an exact solution of the many-electron problems. In practice, however, the explosive increase in the number of configurations with increasing electron number limits its application to only small

systems with relatively few electrons. Furthermore, the complexity of the resulting solutions means that a simple interpretation of the results is often difficult.

An alternative approach which is originated from the Thomas-Fermi model [68-69] is based on the density of electrons in the system, n(r),

$$n(r) = N\int dr_2 ... \int dr_n \Psi^*(r_1, r_2, ..., r_n)\Psi(r_1, r_2, ..., r_n). \quad (2.7)$$

The Thomas-Fermi model assumes that the motions of the electrons are uncorrelated and that the corresponding kinetic energy can be described by a local approximation based on the results for uniform electron gas, $[n(r)]^{5/3}$. Shortly after, Dirac [70] proposed that exchange effects can be included by incorporating a term derived from the exchange energy density in a homogenous system. The exchange potential in a system of variable density could be approximated by a term with a local dependence ~ $[n(r)]^{1/3}$ on electron density. In fact, this dependence on the density is a consequence of the concept of the "exchange" or "Fermi" hole, i.e., the region near an electron is avoided by electrons of the same spin, and not on the exchange potential in a homogenous system. The Thomas-Fermi model provided a prototype for modern density functional theory based upon two Hohenberg-Kohn theorems [57].

Note that the Hamiltonian in (2.2), contains the number of electrons N and the external potential $v(r)$. Hence, N and $v(r)$ will determine all properties for the ground state. In place of N and $v(r)$, the first two Hohenberg-Kohn theorem legitimizes the use of electron density $n(r)$ as the basic variable. It states: *The external potential* $v(r)$ *is determined, within a trivial additive constant, by the electron density* $n(r)$.

The proof is rather straightforward. Consider the electron density $n(r)$ for the nondegenerate ground state of some N-electron system. It determines the number of electrons by

$$\int n(r)dr = N \tag{2.8}$$

If $n(r)$ also determines $v(r)$, it follows that $n(r)$ determines the ground-state wave function Ψ and hence all other electronic properties of the system. Suppose that there were two external potentials v and v_1 differing by more than a constant, each giving the same $n(r)$ for its ground state, we would then have two Hamiltonians H and H_1 whose ground-state densities were the same although the normalized wave functions Ψ and Ψ_1 would be different,

$$H\Psi = E\Psi \tag{2.9}$$

$$H_1\Psi_1 = E_1\Psi_1 \tag{2.10}$$

E and E_1 are the ground-state energies for H and H_1 respectively. Therefore, the expectation value of H in Ψ_1 would be greater than E, namely,

$$E < \langle \Psi_1 \mid H \mid \Psi_1 \rangle = \langle \Psi_1 \mid H + H_1 - H_1 \mid \Psi_1 \rangle$$

$$= \langle \Psi_1 \mid H_1 \mid \Psi_1 \rangle + \langle \Psi_1 \mid H - H_1 \mid \Psi_1 \rangle \tag{2.11}$$

$$= E_1 + \int n(r)[v(r) - v_1(r)]dr$$

Similarly, the expectation value of H_1 in Ψ would be greater than E_1,

$$E_1 < \langle \Psi \mid H_1 \mid \Psi \rangle = \langle \Psi \mid H_1 + H - H \mid \Psi \rangle$$

$$= \langle \Psi \mid H \mid \Psi \rangle + \langle \Psi \mid H - H_1 \mid \Psi \rangle \tag{2.12}$$

$$= E + \int n(r)[v(r) - v_1(r)]dr$$

Adding (2.11) and (2.12), we obtain

$$E + E_1 < E_1 + E \tag{2.13}$$

This is a contradiction, and so there cannot be two different external potentials that give the same ground-state densities.

Thus, $n(r)$ determines both N and v and hence all properties of the ground state. Therefore, the ground state total energy can be written as a functional of the electron density,

$$E[n] = T[n] + V_{ne}[n] + V_{ee}[n] = \int n(r)v(r)dr + F_{HK}[n] \tag{2.14}$$

where $T[n]$ is the kinetic energy, $V_{ne}[n]$ is the nuclei-electron interaction energy and $V_{ee}[n]$ is the electron-electron Coulomb interaction energy and $F_{HK}[n]$ is a universal functional of $n(r)$ in a sense that $F_{HK}[n]$ is defined independently of the external potential $v(r)$,

$$F_{HK}[n] = T[n] + V_{ee}[n] \tag{2.15}$$

The second Hohenberg-Kohn theorem states: *For a trial density* $n_1(r)$, *such that* $n_1(r) \geq 0$ *and* $\int n_1(r)dr = N$,

$$E_0 \leq E[n_1] \tag{2.16}$$

where $E[n_1]$ *is the energy functional of (2.14).*

This theorem gives the energy variational principle. It means that the ground-state electron density is the density that minimizes $E[n]$. The proof is as follows. Since the first theorem assures that $n_1(r)$ which determines its own v_1, Hamiltonian H_1, and wave function Ψ_1, can be taken as a trial function for the Hamiltonian H of interest with external potential v. Thus,

$$\langle \Psi_1 \mid H \mid \Psi_1 \rangle = \int n_1(r)v(r)dr + F_{HK}[n_1] = E[n_1] \geq E[n] \tag{2.17}$$

The variational principle (2.16) requires that the ground-state density satisfy the following stationary principle,

$$\delta\{E[n] - \mu[\int n(r)dr - N]\} = 0 \tag{2.18}$$

which gives the Euler-Lagrange equation

$$\mu = \frac{\delta \mathrm{E}[n]}{\delta n(r)} = v(r) + \frac{\delta F_{HK}[n]}{\delta n(r)} \tag{2.19}$$

The quantity μ is the chemical potential.

If we knew the exact $F_{HK}[n]$ (2.18) would be an exact equation for the ground-state density. Once we have an explicit form either approximate or accurate for $F_{HK}[n]$, we can apply this method to any system. Equation (2.19) is the basic working equation of density-functional theory. However, accurate computational implementations of the density-functional theory are far from easy to achieve, because of the unfortunate fact that is hard to obtain the explicit form of the functional $F_{HK}[n]$. Although the Hohenberg-Kohn theorems do not give insights of actual methods of calculation, and it is usually $v(r)$ rather than $n(r)$ that is known, that is known, they provide confidence that it is sensible to seek solutions of many-body problems based on the density rather than the wave functions.

Early attempts to approximate the universal functional $F_{HK}[n]$ used the Thomas-Fermi approximation for the kinetic component $T[n]$. It was soon realized that only very crude answers can be obtained with this local functional for the kinetic energy, no matter how sophisticated the approximation for the $V_{ee}[n]$ component is. Kohn and Sham therefore proposed a highly nonlocal functional giving the major part of the kinetic energy and the scheme makes the density functional theory practical. They invoked a noninteracting reference system, with the Hamiltonian,

$$H_s = \sum_i^N (-\frac{1}{2}\nabla_i^{\,2}) + \sum_i^N v_{eff}(r_i) \tag{2.20}$$

For which the ground-state electron density is exactly $n(r)$. There will be an exact determinantal ground-state wave function for this system.

$$\Psi_s = \frac{1}{\sqrt{N!}} \det\left[\Psi_1 \Psi_2 ... \Psi_n\right] \tag{2.21}$$

where the Ψ_i are the N lowest eigenstates of the one-electron Hamiltonian h_s:

$$h_s \Psi_i = \left[-\tfrac{1}{2}\nabla^2 + v_{eff}(r)\right]\Psi_i = \varepsilon_i \Psi_i \tag{2.22}$$

and

$$n(r) = \sum_i^N \sum_s \left|\Psi_i(r,s)\right|^2 \tag{2.23}$$

The kinetic energy is then given by $T_s[n]$,

$$T_s[n] = \sum_{i=1}^{N} \left\langle \Psi_i \left| -\frac{1}{2}\nabla^2 \right| \Psi_i \right\rangle \tag{2.24}$$

This is the kinetic energy of the independent electrons (i.e. electrons without mutual Coulomb repulsion) in their ground state, under the action of an external potential such that their ground state density is $n(r)$. Then the universal functional can now be rewritten as

$$\begin{aligned} F_{HK}[n] &= T[n] + V_{ee}[n] \\ &= T_s[n] + J[n] + \left(T[n] - T_s[n] + V_{ee}[n] - J[n]\right) \\ &= T_s[n] + J[n] + E_{xc}[n] \end{aligned} \tag{2.25}$$

where $J[n]$ is the classical Coulomb interaction energy,

$$J[n] = \frac{1}{2}\int \frac{n(r)n(r')}{\left|r - r'\right|} dr dr' \tag{2.26}$$

while the defined quantity

$$E_{xc}[n] \equiv T[n] - T_s[n] + V_{ee}[n] - J[n] \tag{2.27}$$

is called the exchange-correlation energy. Here, we note that $T_s[n]$ is not the true kinetic energy of the interacting system whose ground state density is $n(r)$, but in the final optimized

description it is much closer to the kinetic energy $T[n]$ than the Thomas-Fermi kinetic energy. The exchange correlation energy $E_{xc}[n]$ includes two parts of contributions: one is from the non-classical effects of the electron-electron interactions and the other is from the kinetic energy. The Euler equation now becomes

$$\mu = v_{eff}(r) + \frac{\delta T_s[n]}{\delta n(r)} \tag{2.28}$$

where the Kohn-Sham effective potential is defined by

$$v_{eff}(r) = v(r) + \frac{\delta J[n]}{\delta n(r)} + \frac{\delta E_{xc}[n]}{\delta n(r)} \tag{2.29}$$

$$= v(r) + \int \frac{n(r')}{|r - r'|} dr' + v_{xc}(r)$$

which the exchange-correlation potential

$$v_{xc}(r) = \frac{\delta E_{xc}[n]}{\delta n(r)} \tag{2.30}$$

The Kohn-Sham computational scheme for DFT is shown in the flowchart in figure 2.1. As we can see from equation (2.29) that the effective potential v_{eff} is also a functional of the electron density, such that equations (2.22) to (2.30) have to be solved self-consistently. We can start with a guessed density $n_0(r)$ which is usually constructed from the atomic wave functions. Then calculate the effective potential v_{eff} through equation (2.29) and use it in equation (2.22) to solve the single-electron Schrödinger equation. A new electron density $n(r)$ will be formed from equation (2.23). Once the convergent requirement is achieved, we can compute the total energy from equations. (2.14, 2.24 to 2.27).

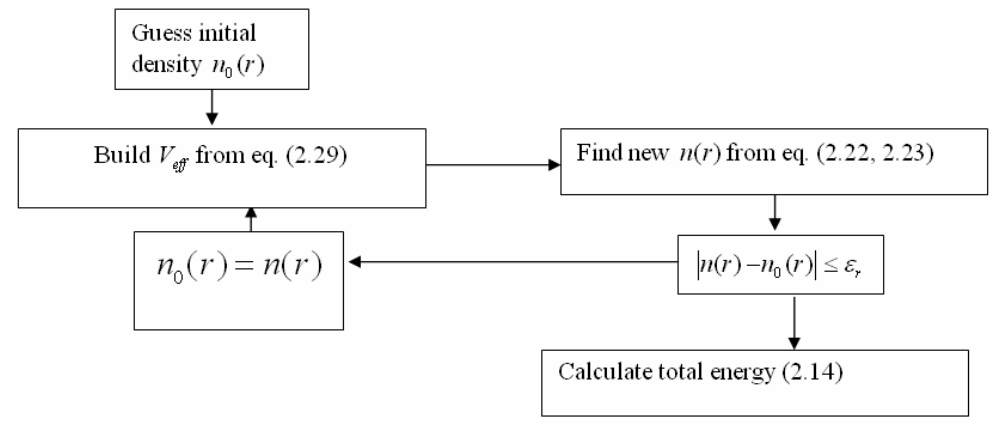

Figure 2.1 Flow-chart for DFT self-consistency loop

The single Euler equation (2.22) has the same form as the Hartree equation but includes a more general local effective potential that incorporates the exchange and correlation interactions between electrons. Therefore, the computational efforts to solve the Kohn-Sham equations will be the same as to solve the Hartree equations and significantly less than to solve the Hartree-Fock equations, which, by definition lack of correlation effects. In principle, the Kohn-Sham equations will yield exact ground state properties if exact exchange correlation potential is given. However, the Kohn-Sham scheme does not provide methods to obtain the explicit exchange and correlation functionals and therefore, approximations have to be considered.

2.2 Exchange and correlation functionals

There are basically three distinct approximations in DFT to the exchange correlation functionals, namely, the local density approximation (LDA), the generalized gradient approximation (GGA) and the hybrid approximation.

2.2.1. Local density approximation

This local density approximation was proposed by Kohn and Sham. They showed that it could be applied to the limiting case of a slowly varying density [58].

$$E_{xc}^{LDA}[n] = \int n(r)\varepsilon_{xc}(n)dr \tag{2.31}$$

where $\varepsilon_{xc}(n)$ is the exchange and correlation energy per particle of a uniform electron gas of density $n(r)$. The functional derivative of $E_{xc}^{LDA}[n]$ gives the local approximation to the Kohn-Sham exchange-correlation potential

$$v_{xc}^{LDA}(r) = \frac{\delta E_{xc}^{LDA}}{\delta n(r)} = \varepsilon_{xc}(n(r)) = n(r)\frac{\delta \varepsilon_{xc}(n)}{\delta n} \tag{2.32}$$

The Kohn-Sham equation becomes

$$\left[-\frac{1}{2}\nabla^2 + v(r) + \int \frac{n(r')}{|r-r'|}dr' + v_{xc}^{LDA}(r)\right]\Psi_1 = \varepsilon_i \Psi_i \tag{2.33}$$

$$\varepsilon_{xc}(n) = \varepsilon_x(n) + \varepsilon_c(n) \tag{2.34}$$

where $\varepsilon_x(n)$ is the exchange energy per particle of a homogenous electron gas,

$$\varepsilon_{xc}(n) = -\frac{3}{4}\left(\frac{3}{\pi}\right)^{1/3} n(r)^{1/3} = -\frac{0.4582}{r_s} \tag{2.35}$$

and $\varepsilon_c(n)$ is the correlation energy per particle of a homogenous electron gas,

$$\varepsilon_c(n) = \frac{1}{2}\left(\frac{g_0}{r_s} + \frac{g_1}{r_s^{3/2}} + \frac{g_2}{r_s^{2}} + \ldots\right) \qquad \text{for } r_s >> 1 \tag{2.36}$$

Here r_s is the Wigner-Seitz radius,

$$\frac{4}{3}\pi r_s^3 = \frac{1}{n} \tag{2.37}$$

The Kohn-Sham-LDA is further extended to the spin dependent case by replacing the scalar external potential $v(r)$ by a spin dependent potential $v_{\alpha\beta}(r)$ and replacing the charge density $n(r)$ by the density matrix $n_{\alpha\beta}(r)$ [71-73]. The electron densities with spin projection up $n_\alpha(r)$ and down $n_\beta(r)$ are treated separately. Similarly, one can deal with $n(r) = n_\alpha(r) + n_\beta(r)$,along with the polarization $\zeta(r) = \left\lfloor n_\alpha(r) - n_\beta(r) \right\rfloor / n(r)$. ζ takes values between -1 (fully polarized downwards) and +1 (fully polarized upwards). The spin-up and spin-down densities are generated from the spin-up and spin-down Kohn-Sham wave functions. This so-called local spin density (LSD) approximation improved LDA for atomic and molecular systems with unpaired spins.

LDA and its spin generalization LSD allow one to use the knowledge of the uniform electron gas to predict properties of the in homogenous electron gases occurring in atoms, molecules and solids. The success and importance of LDA and LSD computational schemes in the solid state computations can hardly be exaggerated. Specifically, LSD usually has moderate accuracy for most systems of interest, making errors of order 5-10%. It's most remarkable feature is it's reliability, making the same kinds of errors on every system it's applied to. The success of LDA and LSD is attributed to the fact that the exchange-correlation hole $n_{xc}^{LDA}(r_1, r_2)$ is spherically symmetric and it obeys the sum rule which corresponds to the fact that, if an electron has been found at r_1 , then there is one less electron left to find elsewhere (i.e , by integral over all r_2),

$$\int n_{xc}^{LDA}(r_1, r_2) dr_2 = -1 \tag{2.38}$$

where the exchange-correlation hole $n_{xc}^{LDA}(r_1, r_2)$ is defined by

$$V_{ee} = \iint \frac{1}{r_{12}} n_2(r_1, r_2) dr_1 dr_2 = J[n] + \frac{1}{2} \iint \frac{1}{r_{12}} n(r_1) n_{xc}^{LDA}(r_1, r_2) dr_1 dr_2 \tag{2.39}$$

with $J[n]$ being the classical Coulomb interaction. This is true because for every r_1, $n_{xc}^{LDA}(r_1, r_2)$ is the exact exchange-correlation hole of a homogenous electron gas with density $n(r_1)$. Hence, the LDA and LSD describe the total charge of $n_{xc}^{LDA}(r_1, r_2)$ correctly.

2.2.2. Generalized gradient approximation

Since the LDA formula for E_{xc} is formally justified for systems with slow varying densities, it seemed natural to seek gradient corrections to E_{xc}^{LDA} by the gradient expansion approximation (GGA), which expands the functional in a Taylor series in gradients of the density[74],

$$E_{xc}^{GEA}[n_\alpha, n_\beta] = E_{xc}^{LSD}[n_\alpha, n_\beta] + \sum_{\alpha\beta} \int C_{\alpha\beta}(n_\alpha(r), n_\beta(r)) \frac{\nabla n_\alpha(r)}{n_\alpha^{2/3}} . \frac{\nabla n_\beta(r)}{n_\beta^{2/3}} d^3 r \qquad (2.40)$$

However, GGA does not give better energy than LDA for systems such as atom and molecule. The reasons can be summarized as (1) GGA exchange-correlation hole improves the LDA hole only at short separations, but is poorly damped and oscillatory at large separations, and (2) GGA violates the sum rule of the exchange-correlation hole. Accordingly, Perdew and others introduced the so-called generalized gradient approximation [75-80] such that the exchange correlation energy can be written as a functional of both the density and its gradient:

$$E_{xc}^{GGA}[n_\alpha, n_\beta] = \int d^3 r f(n_\alpha(r), n_\beta(r), \nabla n_\alpha(r), \nabla n_\beta(r)) \qquad (2.41)$$

The first modern GGA was that of Langreth and Mehl [87], who proposed the idea of truncating the gradient expansion for the exchange-correlation hole. Considering the problems encountered by GGA, Perdew *et al*. [79,80] proposed several versions of GGA functional by introducing the real-space cutoff procedure on the hole, which restores the sum rule or the normalization and negativity conditions on the GGA hole and generates a short-ranged hole whose angular and system average was much closer to the true hole. The Perdew-Wang 1991 (PW91) GGA functional [80] incorporates no free parameters and is entirely determined from

uniform electron gas properties and extract constraints. The Perdew-Burke-Ernzerhof [79] functional is a simplified and refined version of the PW91 functional. Becke [76] derived an exchange functional known as B88 incorporating the known behavior of the exchange hole at large distances outside a finite system. Lee, Yang and Parr [77] obtained the correlation energy as an explicit functional of the density and it's gradient and Laplacian, now generally known as the "LYP" functional.

The well-known GGA functionals systematically improve the LDA and, in some calculations, approach the accuracy of traditional quantum chemical (e.g. Configuration Interaction) methods, at much less computational cost. However, according to the quasilocal nature of GGA, the dispersion or long-ranged van der Waals interaction arising from long-ranged correlated electronic density fluctuations in the weak bonding systems such as noble gas dimmers could not be accurately described by either LDA or GGA. On the other hand, similar to LDA, GGA has the difficulty to describe the hole centered for from the electron causing the hole.

2.2.3. Hybrid density functional method

Considering the local or semi local nature of LDA and GGA, Becke proposed the so-called Hybrid Density Functional method which incorporates the exact treatment of exchange by Hartree-Fock theory with DFT approximations for dynamical correlation. This idea was motivated by re-examination of the adiabatic connection,

$$H_\lambda = T + \lambda V_{ee} + \sum_i v_\lambda(r_i) \qquad (2.42)$$

where λ is an inter-electronic coupling-strength parameter that "switches on" the $1/r_{12}$ Coulomb repulsion between electrons. $\lambda = 0$ corresponds to the non-interacting Kohn-Sham reference system, while $\lambda = 1$ corresponds to the fully interacting real system, with $n(r)$ being fixed as the exact ground state density of H_λ. The $E_{xc}[n]$ can be written as

$$E_{xc}[n] = \int_0^1 d\lambda U_{xc}^{\lambda}[n] \tag{2.43}$$

where,

$$U_{xc}^{\lambda}[n] = \left\langle \Psi_n^{\lambda} \mid V_{ee} \mid \Psi_n^{\lambda} \right\rangle - J[n] \tag{2.44}$$

The obvious first approximation for the λ dependence of the integrated in equation (2.43) is a linear interpolation, resulting in the Becke's half-and-half functional:

$$E_{xc}^{h\&h}[n] = \frac{1}{2}\left(U_{xc}^{0} + U_{xc}^{1}\right) \tag{2.45}$$

where U_{xc}^{o} is the exact exchange energy of the KS determinant and U_{xc}^{1} is the potential energy contribution to the exchange-correlation energy of the fully interacting system. This half and half functional has the merit of having a finite slope as $\lambda \to 0$, and becomes exact if $E_{xc,\lambda=1}^{DFT}$ is exact and the system has high density. However, its does not provide a good quality of the total energy and the uniform gas limit is not obtained. Due to this Becke proposed the semi-empirical generalization of 3-parameter hybrid exchange-correlation functional

$$E_{xc}^{B3} = E_{xc}^{LSDA} + a_o(E_x^{exact} - E_x^{LSDA}) + a_x \Delta E_x^{GGA} + a_c \Delta E_c^{GGA} \tag{2.46}$$

Where a_o, a_x and a_c are semiempirical coefficients to be determined by an appropriate fit to experimental data. E_x^{exact} is the exchange energy of the Slater determinant of the Kohn-Sham orbitals. ΔE_x^{GGA} is the gradient correction for the exchange and ΔE_c^{GGA} is the gradient correction for the correlation.

Both methods based on Hartree-Fock (HF) theory and density functional theory (DFT) have their advantages and disadvantages.[56-59,81] For example, DFT within the local spin density approximation (LSDA) calculations underestimate the band gaps of semiconductors. The discontinuity of exchange-correlation Kohn-Sham potential results in this discrepancy

between theoretical and experimental band gaps.[82, 83] On the other hand, hybrid density functional theory incorporating HF exchange with DFT exchange-correlation has proved to be an efficient method for many systems. It has been recently verified that hybrid functionals can reproduce the band gaps of semiconductors and insulators quite well.[84, 85] In particular, screened hybrid functionals can accurately reproduce band gaps in carbon based materials.[86-89] Thus, in these works, we have opted to use hybrid density functional theory for a detailed step by step investigation of SiC nanotubes and their interactions with Fe atom. In particular, we have used the B3LYP[76, 77] hybrid functional and the Los Alamos National Laboratory double-ζ basis set[90] as implemented in the Gaussian 03 suite of programs[91]. For silicon and iron atom, the Hay-Wadt pseudo potential[92] and the associated basis set are used for the core and the valence electrons, respectively. For carbon and hydrogen atoms, the Dunning-Huzinaga double-ζ basis set has been employed. Here we have used finite cluster approach with dangling bonds terminated by hydrogen atoms to simulate the effect of infinite nanotubes. All computations reported here have been performed at the supercomputing facilities of the University of Texas at Arlington.

CHAPTER 3

ARMCHAIR SILICON CARBIDE NANOTUBES

3.1 Construction of different types of nanotubes

We have used the finite cluster-CNT based approach for single wall CNT to construct SiC nanotubes. This approach comprises of rolling a graphene-like sheet of Si and C to form a nanotube. This rolling up can be described in terms of the chiral vector C_h, which connects two sites of the two-dimensional graphene-like sheet that are crystallographically equivalent. This chiral vector maps an atom from the left hand border onto an atom on the right border line and is an integer multiple of the two basis vectors a_1 and a_2, i. e., $C_h = na_1 + ma_2$. So the geometry of any nanotube can be described by the integer pair (n, m) which determines the chiral vector. An armchair nanotube corresponds to the case of n = m with the chiral angle 30°, and a zigzag nanotube corresponds to the case of m = 0 with the chiral angle 0°. All other (n, m) chiral vectors correspond to chiral nanotubes with chiral angles intermediate between 0° and 30°.Here we are concerned about the armchair nanotube only. As mentioned before, in the type 1 arrangement, silicon and carbon atoms are placed alternatively without any adjacent Si or C atoms. In type 2 and type 3 arrangements, the nearest neighbors of each Si atom consist of two C atoms and another Si atom and vice versa. The difference between type 2 and type 3 lies in the relative spatial position of Si and C atoms. If we consider one layer perpendicular to the tube axis, in type 3, Si and C atoms are alternating while in type 2 each layer contains either Si or C atoms. Fig. 3.1 shows the relative positions of Si and C atoms, while figs. 3.2-3.4 show the top and side views of (4,4) and (10,10) of all three types of armchair nanotubes.

3.2 Results and discussions

Table 3.1 and fig. 3.5 show the variations of the cohesive energies per atom with respect to the total number of Si and C atoms for all three types of nanotubes. The cohesive energy or the binding energy per atom for each system was calculated according to the following formula:

$$E_b = \{[a\ E\ (Si) + b\ E\ (C) + c\ E\ (H)] - [E\ (Si_a\ C_b\ H_c)]\} / (a + b + c) \quad (1)$$

where *a, b,* and *c* are the number of Si, C, and H atoms, respectively. *E (Si), E (C)* and *E (H)* are the ground state total energies of Si, C, and H atoms, respectively and $E\ (Si_a\ C_b\ H_c)$ is the total energy of the optimized clusters representing the nanotubes. The default energy convergence criterion was set to 0.0001 a.u.. It is evident that type 1 tubes are most stable while types 2 and 3 have almost the same binding energy. The energy differences are, however, quite small between all three types of armchair SiC nanotubes and *we believe that suitable experimental conditions can design and produce all three types of nanotubes*. As the number of atoms increases, the cohesive energy per atom also increases and approaches saturation. This phenomenon is a common feature for all types of nanotubes. For comparison the largest type 1 silicon carbide nanotube (SiCNT) studied (11, 11) has a cohesive energy of 4.638eV/atom, about 67.67% of the bulk (3C-SiC) cohesive energy of 6.854eV/atom. As Si-C bonds are stronger than Si-Si bonds, type 1 nanotubes are more stable than the other two types. The overall symmetry is another reason for their higher binding energies since clusters tend to prefer symmetric structures with higher binding energies.

Table 3.2 summarizes the bond length distribution for all nanotubes studied. This bond length distribution rather than fixed bond length is reminiscent of our *ab initio* calculations performed on hydrogen passivated finite SiC clusters. Generalized tight binding molecular dynamics calculations performed on infinite nanotubes usually gives fixed bond lengths unlike *ab initio* calculations. As the diameter or total number of Si and C atoms increase, this bond alteration or the variation range tends to decrease. Tubes of higher curvature with smaller

diameter have weaker bonds, resulting in a possible reduction of Young modulus, similar to the cases of C and composite $B_xC_yN_z$ nanotubes.[93] Si-C bond lengths are more widely spread in type 3 than the other two types. This range is narrowest for type 2. On the other hand Si-Si and C-C bond lengths have more wide range in type 2 than type 3 suggesting possible less electron delocalization in type 2 structures.

After optimization the nanotube surfaces were found to be slightly rippled. For type 1, more electronegative C atoms moved outward and more electropositive Si moved inward resulting in two concentric cylinders. This is in good agreement with other *ab initio* results.[42, 44, 94, 95] This surface reconstruction has similar feature observed for group-III nitride nanotubes, where N atoms move away from the tube axis and group III elements like Ga, Al, B move toward the axis.[96-98]. For type 2 and type 3 tubes, the average radial distance of Si atoms were higher than that for C atoms, because in those structures in addition to Si-C bonds there are Si-Si and C-C covalent type bonds. For the latter two cases, this reverse buckling makes the nanotubes Si coated. As mentioned before, figs. 3.2-3.4 show the views of three different types of nanotubes along the axis of symmetry and side views for the armchair configurations. Tight binding studies [99,100] and Monte Carlo simulations using semi-empirical potentials[101] gave an inward displacement of Si and C atoms by relaxation. In contrast to that, one *ab initio* study[102] on 3C SiC surface reported displacements of Si and C atoms into different directions. These radial bucklings caused by bond bending will create surface dipoles and modify the surface band structure, indicating some relevant potential applications of SiC nanotube. Table 3.3 shows the average tube diameter and the amount of radial buckling. Type 2 tubes have maximum diameter, followed by type 3 and type 1 nanotubes. The radial buckling has been calculated by subtracting the mean Si radius from the mean C radius (for type 1) and for type 2 and 3, subtracting the mean C radius from the mean Si radius. The common feature for all types is that, the amount of buckling decreases as the tube diameter increases. This has been shown in fig. 3.6. Similar trends were observed for BN nanotubes[93] which has the same

arrangement as type 1. However, the amounts of buckling for type 1 nanotubes are smaller than the values found in another *ab initio* calculation[42]. The reason for this difference is attributed to the fact that we have first rolled up the unoptimized graphene like SiC sheet and then performed full optimization rather than rolling up the optimized sheet. We believe this is more reasonable since graphene like SiC sheets do not exist in nature and because typically in experimental works as mentioned here and reported in the literature, SiC nanotubes were synthesized using carbon nanotubes as templates.[33-41] This difference can also be attributed to different theoretical approaches. Nonetheless, the variation of these bucklings with diameter, namely the reduction of buckling with diameter increases, well matched with type 1 SiC[42] and BN nanotube cases[93]. The buckling effect is most pronounced in type 2, then type 3 followed by type 1. We need to stress here that the surface reconstruction appears to be a minor effect and might possibly be related to the finite length of the tubes.

We also performed Mulliken charge analysis for the nanotubes studied here. All the structures show significant electron transfer from Si to C atoms. Figure 3.7 implies type 1 armchair structures are more ionic than type 2 and type 3 nanotubes, as they have only Si-C bonds. In fact, the Si-C bonds in type1 are fully ionic whereas in type 2 and 3, the bonds, Si-C, Si-Si, and C-C, are a mixture of ionic and covalent bonds. The asymmetry in charge distribution in SiC nanotubes has been and can further be exploited to achieve different electronic properties by exterior-wall decoration at different adsorption sites.[103,104] This charge transfer is consistent with the radial buckling for type 1 SiCNT as the charge transfer is presumed to occur in one of the C valence orbitals, to which electrons flow from Si atom. The probable existence of more point charges on the wall of type 1 nanotubes might make them better hydrogen storage device than carbon nanotubes.[105] However, the same possibilities might also exist for type 2 and 3 nanotubes. Table 3.4 shows the calculated dipole moment for all three types of SiC nanotubes from (3, 3) to (11, 11). Despite the fact that type 1 has ionic bonding between Si and C atoms, the overall dipole moment is low compared to type 2 and

type 3 nanotubes. The almost zero dipole moments of type 1 structures indicate an overall highly symmetric charge distribution though all the Si-C bonds are ionic. It is clearly shown that type 3 has slightly higher dipole moment than type1; thus it can probably be attributed the same charge symmetry as type 1. In contrast, type 2 structures have significantly higher values which indicate overall charge asymmetry. This fact reveals that symmetric configurations of type 2 nanotubes are characterized by a higher potential energy than the asymmetric configurations implying that type 2 symmetric nanotubes are less stable than asymmetric type 2 nanotubes. This will have the effect of adherence of the type 2 nanotubes into bundles if experimentally synthesized. It is worth noting that type 2 nanotubes have two ends populated by either Si or C atoms. Here the separations of the positive and negative charges are comparatively large, causing increases in dipole moments. Also, accumulations of charges increase with increases in tube diameters. In type 1 and type 3, the layers perpendicular to the tube axis have alternating C and Si atoms, resulting in low dipole moments. Type 1 nanotubes have almost zero dipole moment due the existence of all perfect hexagons in those structures. In the case of type 3 nanotubes though we do not see any charge polarization, there are two different types of imperfect hexagons, with each having two different orientations. This is the origin of their slightly higher dipole moment than type 1 nanotubes. .

The highest occupied molecular orbital (HOMO) and the lowest unoccupied molecular orbital (LUMO) gap gives a measure of the “band gap” for the infinite periodic SiC nanotubes. This measure is qualitative in the sense that the tubes studied are finite in length and any extrapolation to infinite tubes should be viewed with caution. After optimization, the lengths of type 1 nanotubes varied from 16.211Å to 16.257Å, with the average length being 16.228Å. The corresponding numbers for type 2 are 16.014Å and 16.346Å, with the average being 16.297Å. For type 3, the lengths varied from 16.278Å and 16.345Å, the average being 16.335Å. The effects of finite size for carbon nanotubes have been studied in detail in the literature[106--109] and we intend to pursue such studies in the future for SiC nanotubes. Table 3.5 and fig. 3.8 provide

the evolution of these gaps as a function of tube diameters for all the structures. The electronic states are also listed in table 3.5. All the ground state structures we have studied here are in singlet state, i. e., no magnetic structures have been found. The gap is increasing with increasing diameter for the type 1 nanotubes and approaching saturation. A slight decreasing trend is observed after (7, 7) but not significant. Type 1 nanotubes have larger band gaps than bulk 3C-SiC (2.4eV). Type 2 and 3 nanotubes have significantly lower gaps. In case of type 2, gap and tube diameter have an alternating relationship, while for type 3, band gap decreases monotonically with increasing tube diameter and is expected to approach small gap semiconducting to semi-metallic regime. These wide ranges of SiC armchair nanotube gaps are in sharp contrast to carbon nanotubes, which are essentially metallic in armchair configuration. Carbon nanotubes are semiconductors in other helicity. The origin of wide band gap for type 1 SiC nanotubes lies in the fact that, they have only ionic like Si-C bonds as compared to the covalent C-C bonds in carbon nanotubes and some Si-Si and C-C bonds in other two types SiC nanotubes in addition to Si-C bonds. More ionic type bonding localizes the electronic states in type 1 nanotubes and consequently increases the band gap[42]. The band gap variation with tube diameter indicates that type 1 tubes are always wide band gap structures while type 2 and specifically type 3 tubes are small gap semiconductors and might exhibit metallic behavior. The evolution of band gap with the tube diameter can be analyzed by the curvature induced σ-π hybridization[35]. In the case of type 1 SiC nanotube, as the diameter decreases, curvature increases and the induced σ-π hybridization has the effect of down-shifting the conduction bands, resulting in lower gaps with decreasing diameters. For type 3, this trend is reversed in that the curvature induced σ-π hybridization has the effect of uplifting the conduction bands for type 3 structures, resulting in higher band gaps with decreasing diameters. This reverse trend is related to the existence of different bonds in two types of nanotubes. Figure 3.9 demonstrates energy density of states (DOS) for largest nanotubes (11, 11) in three different configurations. The DOS is built by fitting a Gaussian function in each

eigenvalue and then summing them up. The Gaussian width used to broaden the eigenvalues is 0.05 eV and E=0 refers to the HOMO. The comparatively large gap of type 1 (11, 11) to the gaps in the other two types is clearly visible.

Tuning the band gap of semiconductors is an important task and challenging endeavor in molecular electronics as it facilitates the integration of devices and systems for performing a specific work. Among all three types of SiC nanotubes we studied, type 1 which is the most stable one, has valence charge density strongly accumulated around C atoms. Significant electron transfer from Si to C atoms results in charge accumulation which makes the nanotube wall highly reactive to the external atom or group of atoms. This asymmetry has been exploited to band structure modification by side wall decoration with H, CH_3, SiH_3, N, NH, NH_2[103,104,110] and Si or C substitution by N atom.[110] In this work it has been shown that by changing the relative positions of C and Si atoms it is possible to have nanotubes with various band gaps. In nanotube based technology Schottky barriers form at the metal/nanotube junctions, through which carriers must tunnel.[111] These barriers have a profound effect on the function and performance of CNT-based transistors. In general, the charge transfer takes place at the metal nanotube interface leading to band-bending and the creation of Schottky barrier.[112] The newly proposed type 3 single wall SiC armchair nanotube gap is inversely proportional to tube diameter, as is the effective mass, for electrons and holes. Thus, at a given temperature, a larger diameter nanotube will have a larger free carrier concentration than a smaller diameter nanotube, and they will have a lower effective mass. Consequently, because of the smaller band gap of large diameter nanotubes, the band line-up at the metal/nanotube interface will result in lower Schottky barriers at the transistor source and drain. Tunneling through these barriers will be facilitated because of the smaller effective mass. Though type 2 nanotubes do not show any continuous gap decrease with the increasing diameter, the relationship between HOMO-LUMO gap with the diameter shows they might possess smaller gap at the larger diameters. These indicate that in SiCNT based junctions, type 3 and type 2 might play

important role at the nanoscale molecular electronic networks, where SiC nanotubes are desirable over carbon nanotubes for some specific reasons. For example, one of the limitations of CNTs is their inability to survive in high-temperature, harsh-environment applications. Silicon carbide nanotubes are preferred for their superior material properties under such conditions.

Table 3.1. Cohesive Energies/atom (in eV) for Armchair SiC Nanotubes.

Nanotube	Stoichiometry	Total number of atoms	Cohesive energy per atom (eV)		
			Type1	Type2	Type3
SiC (3, 3)	$Si_{30}C_{30}H_{12}$	72	4.398	4.328	4.228
SiC (4, 4)	$Si_{40}C_{40}H_{16}$	96	4.507	4.344	4.325
SiC (5, 5)	$Si_{50}C_{50}H_{20}$	120	4.560	4.388	4.373
SiC (6, 6)	$Si_{60}C_{60}H_{24}$	144	4.589	4.411	4.399
SiC (7, 7)	$Si_{70}C_{70}H_{28}$	168	4.607	4.425	4.416
SiC (8, 8)	$Si_{80}C_{80}H_{32}$	192	4.619	4.437	4.427
SiC (9, 9)	$Si_{90}C_{90}H_{36}$	216	4.628	4.443	4.435
SiC (10, 10)	$Si_{100}C_{100}H_{40}$	240	4.634	4.448	4.440
SiC (11, 11)	$Si_{110}C_{110}H_{44}$	264	4.638	4.451	4.444

Table 3.2. Bond Length Distributions (in Å) for Armchair SiC Nanotubes.

Nanotube	Type 1	Type 2			Type 3		
	Si-C (Å)	Si-C (Å)	Si-Si (Å)	C-C (Å)	Si-C (Å)	Si-Si (Å)	C-C (Å)
SiC (3, 3)	1.75-1.83	1.82-1.88	2.25-2.31	1.38-1.43	1.75-1.89	2.25-2.27	1.43-1.45
SiC (4, 4)	1.75-1.82	1.82-1.87	2.24-2.30	1.39-1.45	1.76-1.87	2.23-2.25	1.44-1.45
SiC (5, 5)	1.76-1.82	1.82-1.86	2.23-2.27	1.39-1.45	1.76-1.85	2.23-2.24	1.44-1.45
SiC (6, 6)	1.76-1.81	1.82-1.85	2.25-2.26	1.39-1.44	1.76-1.85	2.22-2.23	1.44-1.46
SiC (7, 7)	1.76-1.81	1.82-1.85	2.24-2.27	1.39-1.45	1.76-1.85	2.22-2.23	1.44-1.46
SiC (8, 8)	1.76-1.82	1.82-1.85	2.23-2.25	1.39-1.45	1.77-1.85	2.22-2.23	1.44-1.46
SiC (9, 9)	1.76-1.81	1.82-1.85	2.23-2.25	1.39-1.45	1.77-1.85	2.22-2.23	1.44-1.46
SiC(10,10)	1.76-1.82	1.82-1.84	2.23-2.25	1.39-1.45	1.77-1.84	2.22-2.23	1.44-1.46
SiC(11,11)	1.76-1.81	1.82-1.84	2.25-2.25	1.39-1.45	1.77-1.85	2.22-2.23	1.44-1.46

Table 3.3. Tube Diameters (in Å) and Radial Buckling (in Å) for Armchair SiC Nanotubes.

Nanotube	Type 1		Type 2		Type 3	
	Tube diameter (Å)	Radial buckling (Å)	Tube diameter (Å)	Radial buckling (Å)	Tube diameter (Å)	Radial buckling (Å)
SiC (3, 3)	5.313	0.037	5.412	0.214	5.375	0.182
SiC (4, 4)	7.022	0.033	7.162	0.202	7.116	0.093
SiC (5, 5)	8.760	0.028	8.936	0.164	8.841	0.071
SiC (6, 6)	10.451	0.023	10.694	0.133	10.582	0.052
SiC (7, 7)	11.786	0.021	12.161	0.115	12.050	0.043
SiC (8, 8)	13.905	0.016	14.240	0.108	14.070	0.035
SiC (9, 9)	15.723	0.013	16.012	0.107	15.816	0.031
SiC (10, 10)	17.351	0.011	17.793	0.092	17.562	0.027
SiC (11, 11)	19.087	0.009	19.576	0.082	19.304	0.022

Table 3.4. Dipole Moments of Armchair SiC Nanotubes (in Debye).

Nanotube	Type 1 (Debye)	Type 2 (Debye)	Type 3 (Debye)
SiC (3, 3)	0.018	1.242	0.307
SiC (4, 4)	0.001	6.067	0.446
SiC (5, 5)	0.001	7.713	0.226
SiC (6, 6)	0.001	9.767	0.033
SiC (7, 7)	0.050	11.499	0.007
SiC (8, 8)	0.018	13.398	1.311
SiC (9, 9)	0.001	13.337	0.024
SiC (10, 10)	0.000	14.669	0.011
SiC (11, 11)	0.010	16.378	0.371

Table 3.5. HOMO-LUMO Gaps (in eV) and Electronic States for Armchair SiC Nanotubes.

SiC Nanotube	Type 1 Armchair		Type 2 Armchair		Type 3 Armchair	
	HOMO-LUMO Gap	Electronic State	HOMO-LUMO Gap	Electronic State	HOMO-LUMO Gap	Electronic State
SiC (3, 3)	2.776	^{1}A	1.487	^{1}A	1.216	^{1}A
SiC (4, 4)	2.823	^{1}A	0.806	^{1}A	1.084	^{1}A
SiC (5, 5)	2.889	^{1}A	0.839	^{1}A	0.905	^{1}A
SiC (6, 6)	2.932	^{1}A	0.876	^{1}A	0.835	^{1}A
SiC (7, 7)	2.937	^{1}A	0.727	^{1}A	0.808	^{1}A
SiC (8, 8)	2.923	^{1}A	0.882	^{1}A	0.799	^{1}A
SiC (9, 9)	2.919	^{1}A	0.897	^{1}A	0.795	^{1}A
SiC(10, 10)	2.913	^{1}A	0.905	^{1}A	0.792	^{1}A
SiC(11, 11)	2.906	^{1}A	0.907	^{1}A	0.791	^{1}A

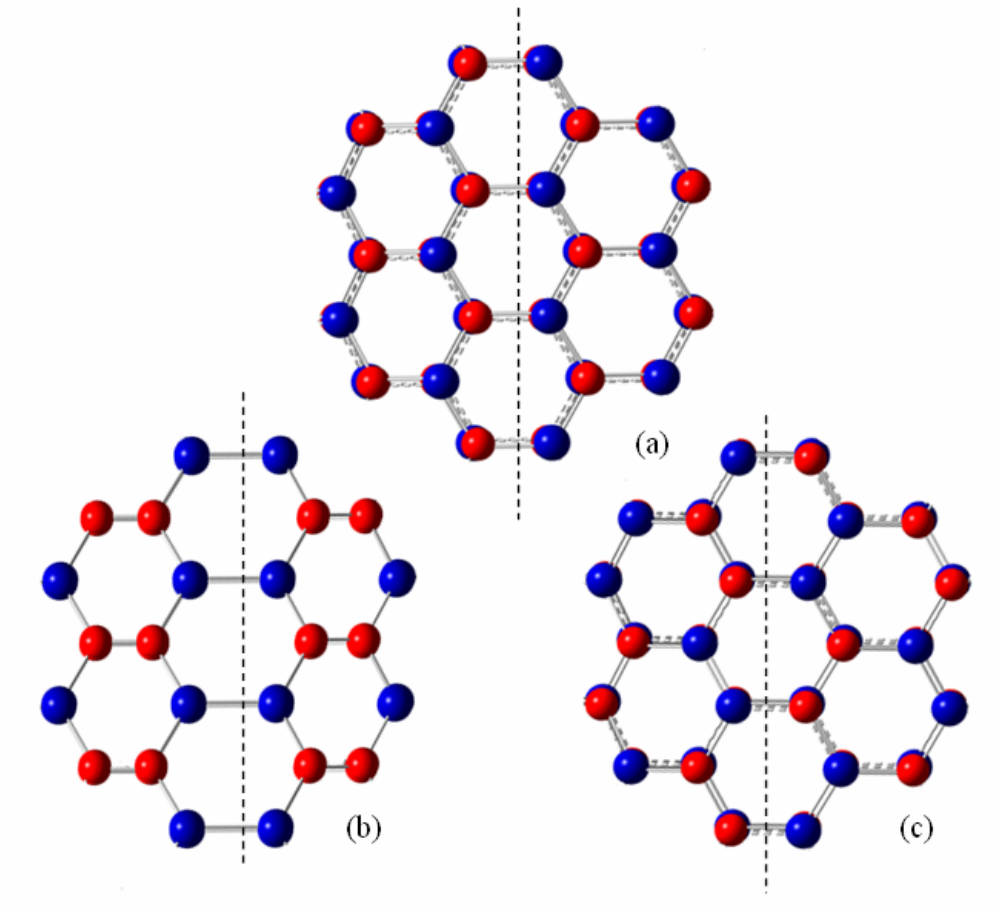

Fig. 3.1. Atomic arrangements for (a) type 1, (b) type 2 and (c) type 3 armchair nanotubes. The carbon atoms are red and silicon atoms are blue. The dashed lines represent the orientation of tube axis.

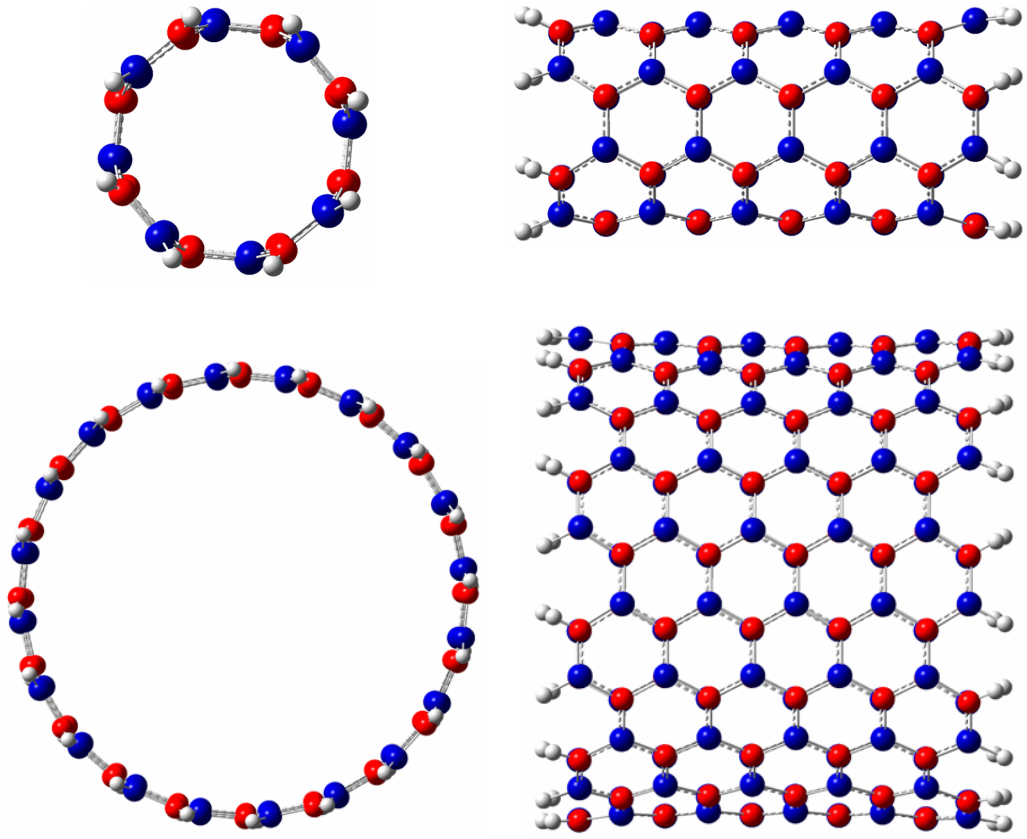

Fig. 3.2. Top and side views of single wall type 1 (4, 4) and (10, 10) SiC nanotubes. Red atoms are carbon and blue atoms are Si.

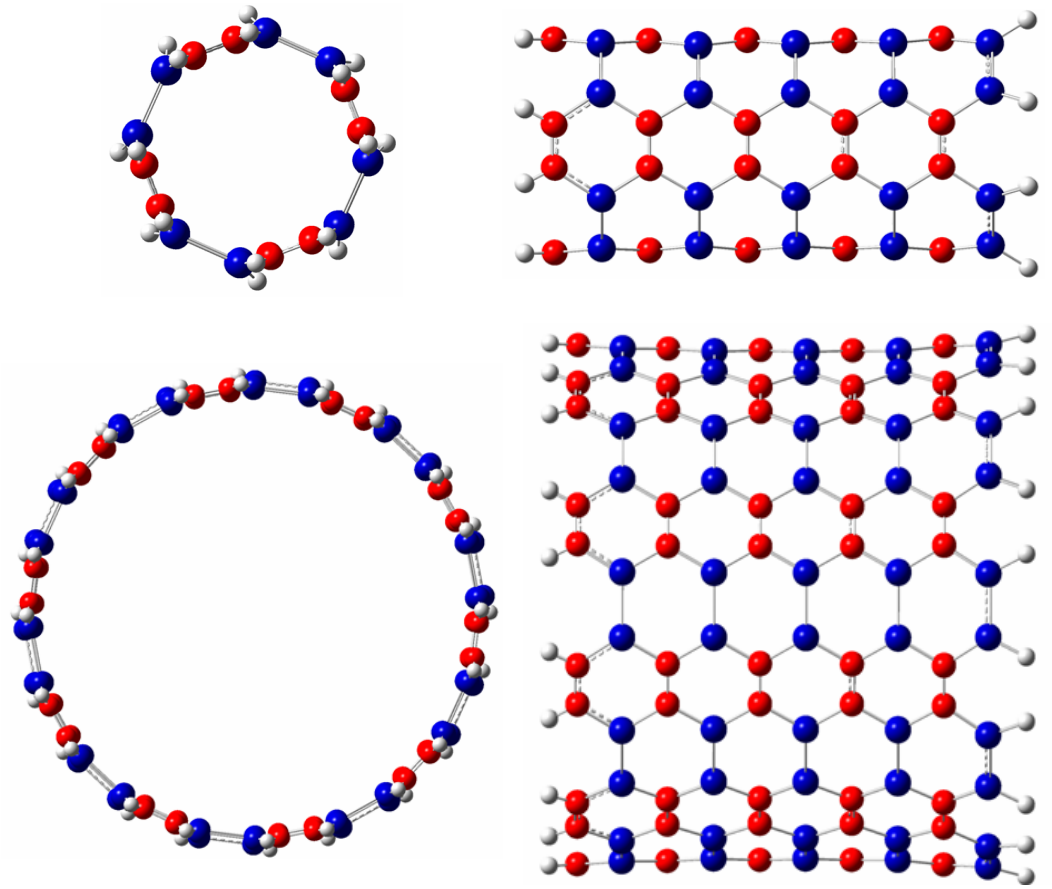

Fig. 3.3. Top and side views of single wall type 2 (4, 4) and (10, 10) SiC nanotubes. Red atoms are carbon and blue atoms are Si.

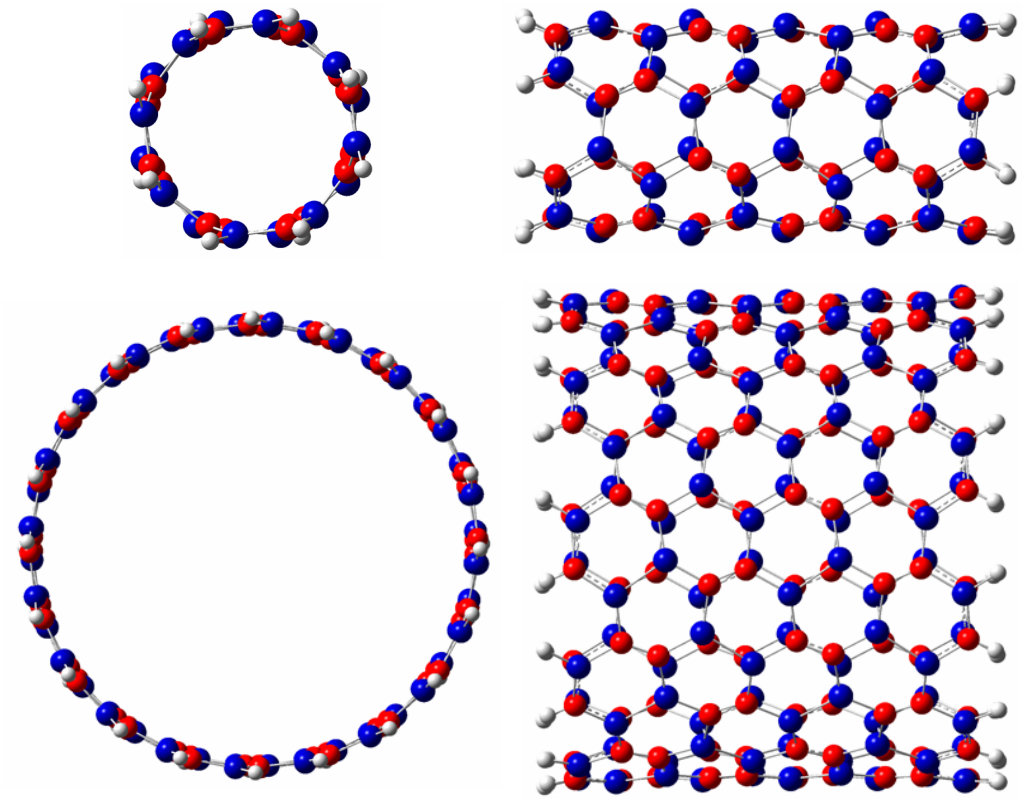

Fig. 3.4. Top and side views of single wall type 3 (4, 4) and (10, 10) SiC nanotubes. Red atoms are carbon and blue atoms are Si.

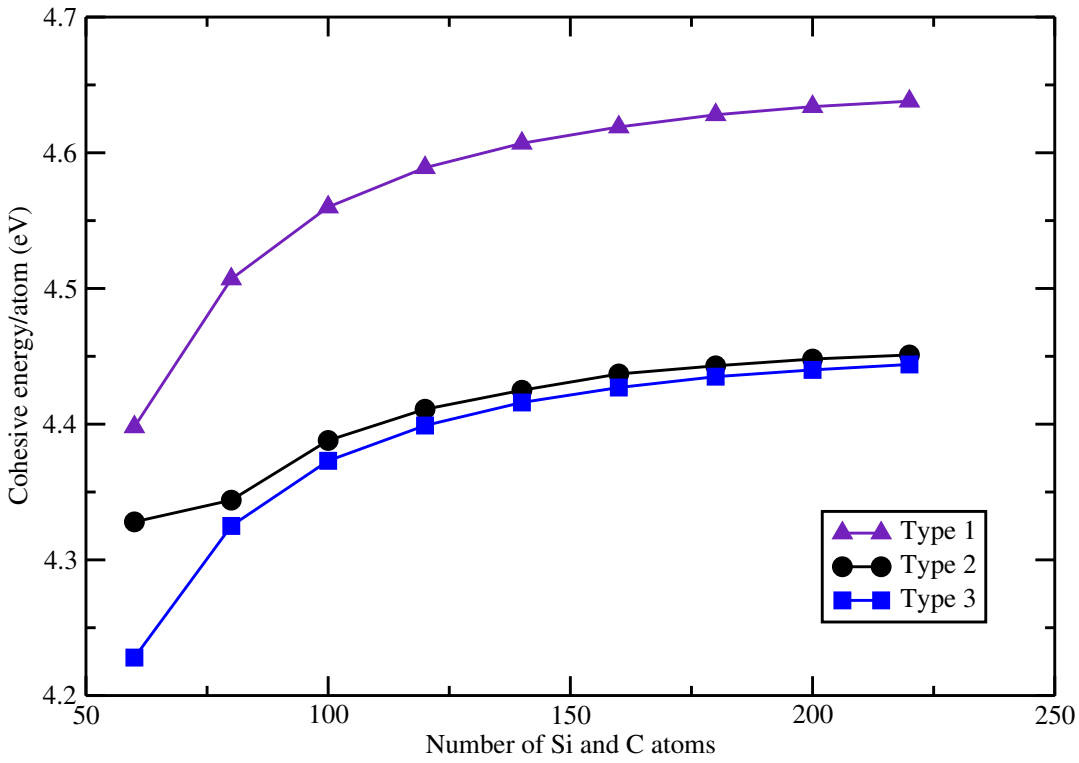

Fig. 3.5. Cohesive energy/atom (eV) vs. total number of Si and C atoms.

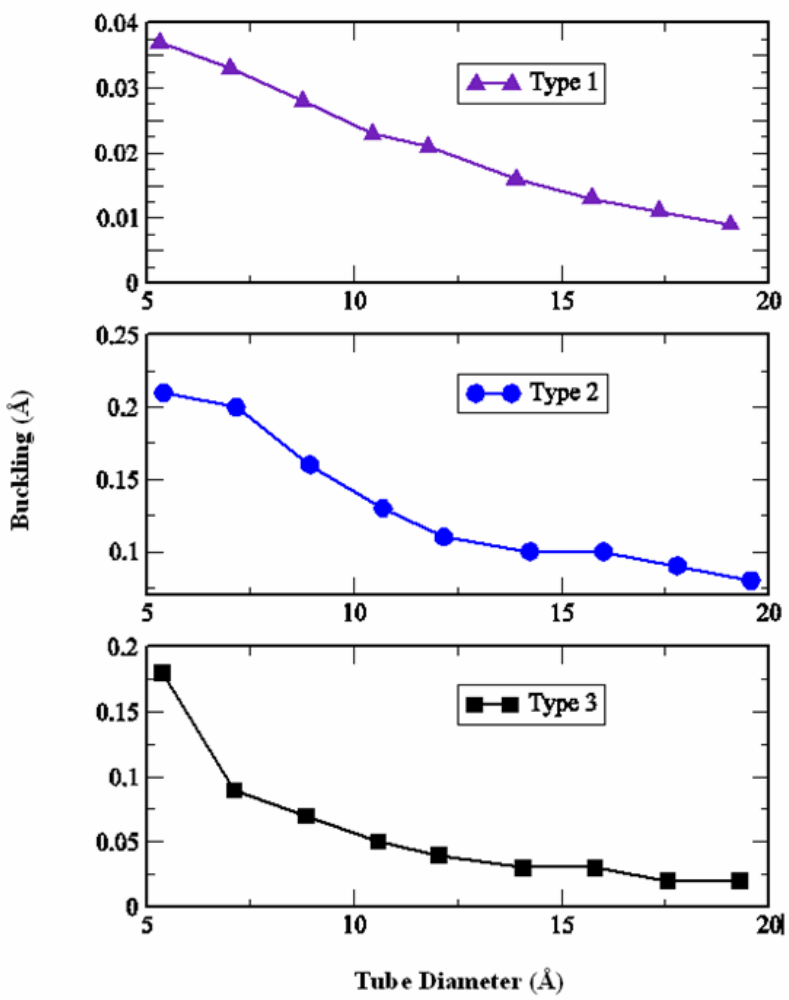

Fig. 3.6. Tube buckling (Å) vs. tube diameter (Å) for three types of armchair SiC nanotubes.

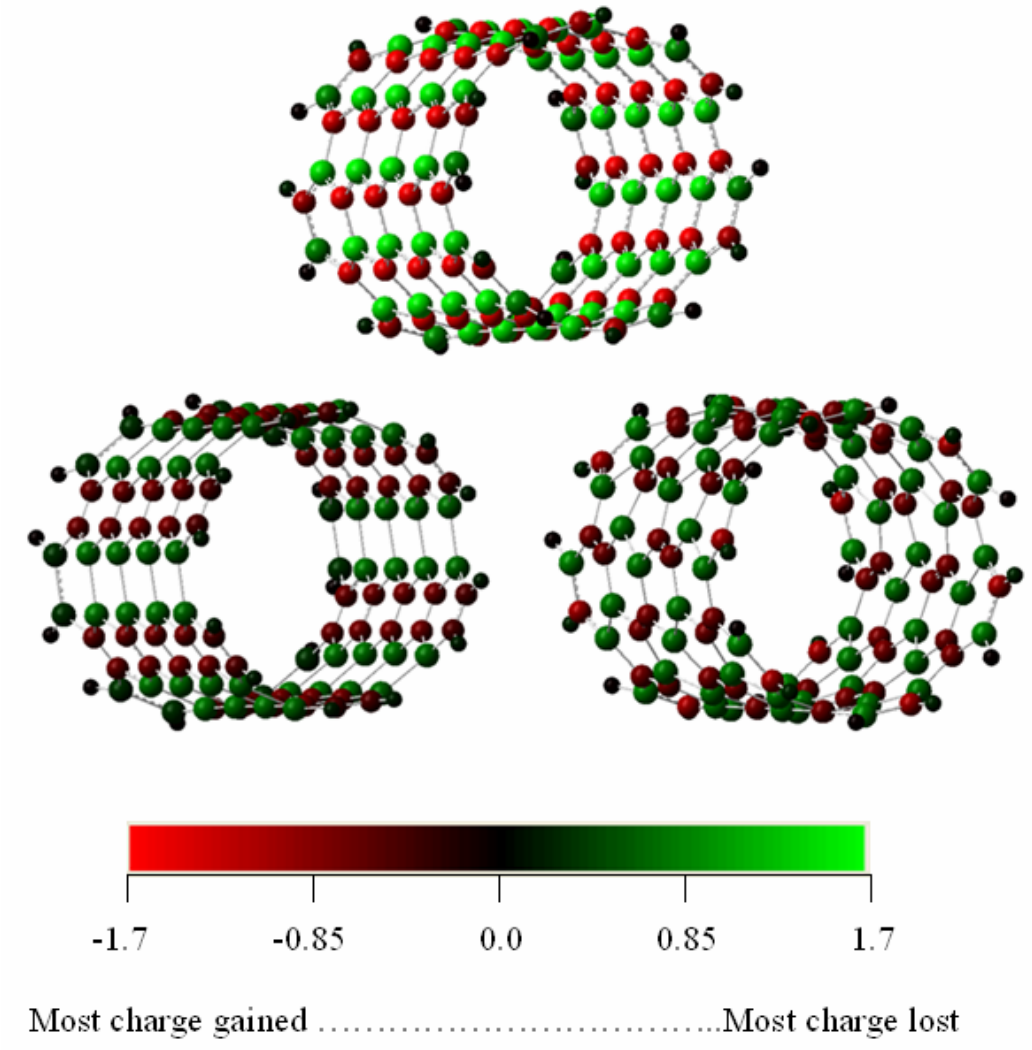

Fig. 3.7. Mulliken charge distributions for (8, 8) nanotubes. Top (type 1), bottom left (type 2) and bottom right (type 3). Carbon atoms gained and silicon atoms lost charge.

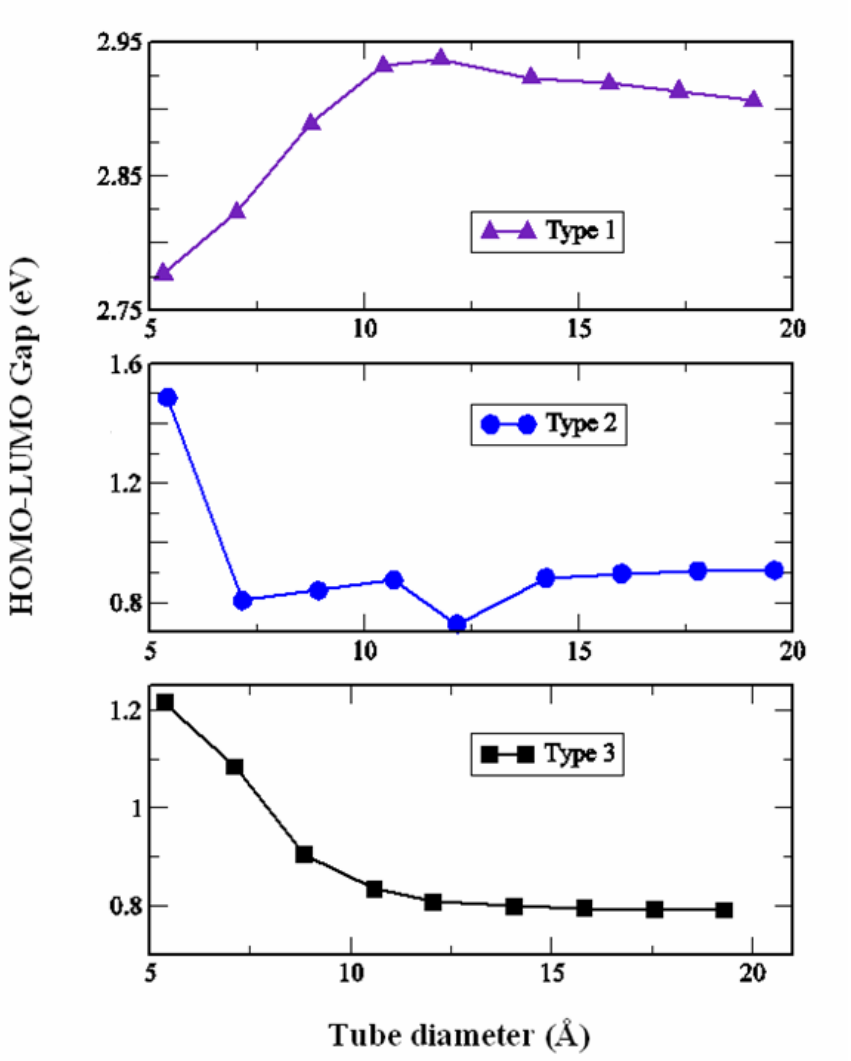

Fig. 3.8. HOMO-LUMO gap (eV) vs. tube diameter (Å) for all three types of armchair nanotubes.

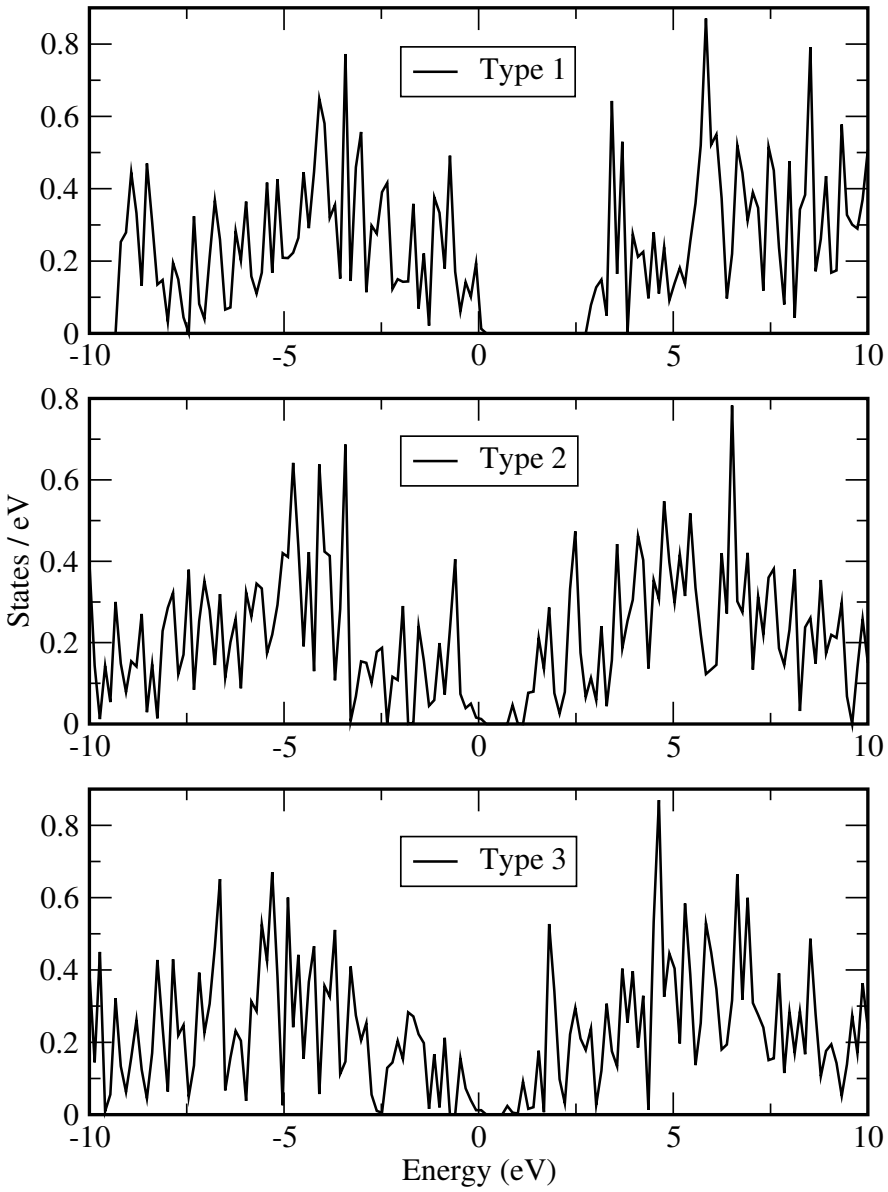

Fig. 3.9. Density of states for three types of armchair (11, 11) SiC nanotubes. E = 0 is the HOMO.

CHAPTER 4

ZIGZAG SILICON CARBIDE NANOTUBES

4.1 Construction of different types of nanotubes

We have used the finite cluster-CNT based approach for single wall CNT to construct SiC nanotubes. This approach comprises of rolling a graphene-like sheet of Si and C to form a nanotube. This rolling up can be described in terms of the chiral vector C_h, which connects two sites of the two-dimensional graphene-like sheet that are crystallographically equivalent. This chiral vector maps an atom from the left hand border onto an atom on the right border line and is an integer multiple of the two basis vectors a_1 and a_2, i. e., $C_h = na_1 + ma_2$. So the geometry of any nanotube can be described by the integer pair (n, m) which determines the chiral vector. An armchair nanotube corresponds to the case of n = m with the chiral angle 30°, and a zigzag nanotube corresponds to the case of m = 0 with the chiral angle 0°. All other (n, m) chiral vectors correspond to chiral nanotubes with chiral angles intermediate between 0° and 30°.Here we are concerned about the armchair nanotube only. As mentioned before, in the type 1 arrangement, silicon and carbon atoms are placed alternatively without any adjacent Si or C atoms. In type 2 and type 3 arrangements, the nearest neighbors of each Si atom consist of two C atoms and another Si atom and vice versa. The difference between type 2 and type 3 lies in the relative spatial position of Si and C atoms. If we consider one layer perpendicular to the tube axis, in type 3, Si and C atoms are alternating while in type 2 each layer contains either Si or C atoms. Fig. 4.1 shows the relative positions of Si and C atoms, while figs. 4.3-4.5 show the top and side views of (4,0) and (10,0) of all three types of zigzag nanotubes.

4.2 Results and discussions

The cohesive energy or the binding energy per atom for each system was calculated according to the following formula:

$$E_b = \{[aE(Si)+bE(C)+cE(H)]-[E(Si_aC_bH_c)]\}/(a+b+c) \quad (1)$$

where *a, b,* and *c* are the number of Si, C, and H atoms respectively. *E (Si), (C)* and *E(H)* are the ground state total energies of Si, C and H atoms, respectively and $E(Si_aC_bH_c)$ is the total energy of the optimized clusters representing the nanotubes. Table 4.1 and figure 4.6 show the variations of the cohesive energies per atom with respect to the total number of Si and C atoms for all three types of nanotubes. It is evident that type 1 tubes are most stable while type 2 and 3 has almost the same binding energy, though type 3 nanotubes are slightly more stable than type 2 nanotubes. However the smallest type 1 and 2 nanotubes (3, 0) show an exception as type 2 has higher binding energy/atom than type 1. From figure 4.2, we see that type 2 (3, 0) tube is a highly distorted structure which might be a reason of its unusually higher binding energy. The energy differences are, however, quite small between all three types of zigzag SiC nanotubes and *we believe that suitable experimental conditions can design and produce all three types of nanotubes*. As the number of atoms increases, the cohesive energy per atom also increases and approaches saturation. This is a common trend for all types of nanotubes. For comparison the largest type 1 SiCNT studied (11, 0) has a cohesive energy of 4.804 eV/atom, about 70.09% of the bulk (3C-SiC) cohesive energy of 6.854 eV/atom. As Si-C bonds are stronger than Si-Si bonds, type 1 nanotubes are more stable than other two types. The overall symmetry is another reason for their higher binding energies. Table 4.2 summarizes the bond length distribution for all nanotubes studied. This bond length distribution rather than fixed bond length is reminiscent of our *ab initio* calculations performed on hydrogen passivated finite SiC clusters. Generalized tight binding molecular dynamics calculations performed on infinite nanotubes usually gives fixed bond lengths unlike *ab initio* calculations.[44] It is also noticeable that tubes with smaller diameter have a wider range of bond lengths for all Si-C, C-

C and Si-Si bonds. The highly distorted structure type 2 (3, 0) shows the widest range. As the diameter or total number of Si and C atoms increase, this bond alteration or the variation range tends to decrease. Tubes of higher curvature with smaller diameter have weaker bonds, resulting in a possible reduction of Young's modulus, similar to the cases of C and composite $B_xC_yN_z$ nanotubes.[93] Si-C bond lengths are more widely spread in type 3 than the other two types.

The nanotube surfaces were found to be slightly rippled after optimization. In our previous work[113] for type 1 armchair nanotubes, more electronegative C atoms moved outward and more electropositive Si moved inward resulting in two concentric cylinders which was in good agreement with other *ab initio* results.[42, 44, 94, 95] This surface reconstruction has similar feature observed for group-III nitride nanotubes, where N atoms move away from the tube axis and group III elements like Ga, Al, B move toward the axis.[96-98]. We also found[113] in type 2 and type 3 armchair nanotubes, the average radial distance of Si atoms were higher than that for C atoms, because in those structures in addition to Si-C bonds there are Si-Si and C-C covalent type bonds. In this work all three types of zigzag nanotubes have the common feature of having two concentric cylinders, where cylinders made of Si atoms have higher radius than that of C atoms. As mentioned before, figs. 4.3-4.5 show the views of three different types of nanotubes along the axis of symmetry and side views for the zigzag configurations. Tight binding studies[99, 100] and Monte Carlo simulations using semi-empirical potentials[101] gave an inward displacements of Si and C atoms by relaxation. In contrast to that, one *ab initio* study[102] on 3C SiC surface reported displacements of Si and C atoms into different directions. Those were the cases for bulk SiC surface. The outward radial displacement of Si atoms consistent with our zigzag nanotube calculations was also found in one first principles calculation based on density functional theory, where Si substitutional doping in CNT has been studied[51]. These radial bucking caused by bond bending will create surface dipole and modify the surface band structure, which may be relevant for piezoelectric applications of SiC nanotube. Table 4.3

shows the average tube diameter and the amount of radial buckling. Type 3 tubes have the maximum diameters, followed by type 2 and type 1 nanotubes. In the case of armchair nanotubes, the sequence was types 2, 3, and 1.[32] The radial buckling has been calculated by subtracting the mean Si radius from the mean C radius. The common feature for all types is that, the amount of buckling decreases as the tube diameter increases. This has been shown in figure 4.7. Similar trend was found for BN nanotubes[93] which has the same arrangement as type 1. The buckling direction for type 1 zigzag nanotubes did not match with other *ab initio* results. The reason for this reverse trend is attributed to the fact that we have first rolled up the unoptimized graphene like SiC sheet and then performed full optimization rather than rolling up the optimized sheet. We believe this is more reasonable since graphene like SiC sheets do not exit in nature and because typically in experimental works as mentioned here and reported in the literature, SiC nanotubes were synthesized using carbon nanotubes as templates.[33-41] In addition it is also known that neither optimized graphene sheet nor the optimized rolled up graphene (CNT) have this buckling type surface reconstruction. The reverse buckling phenomenon can also be attributed to different theoretical approaches. Nonetheless, the variation of these bucklings with diameter, namely the reduction of buckling with diameter increases, well matched with type 1 SiC[42, 113] and BN nanotube cases[93]. The buckling effect tends to be more pronounced in type 3, then type 2 followed by type 1.

We also performed Mulliken charge analysis for the nanotubes studied here. All the structures show significant electron transfer from Si to C atoms. Figure 4.8 implies type 1 zigzag structures are more ionic than type 2 and type 3 nanotubes, as they have only Si-C bonds. In fact, the Si-C bonds in type1 are fully ionic whereas in types 2 and 3, the bonds, Si-C, Si-Si, and C-C, are a mixture of ionic and covalent bonds. Similar results were found in case of armchair nanotubes[113]. The asymmetry in charge distribution in SiC nanotubes has been and can further be exploited to achieve different electronic properties by exterior-wall decoration at different adsorption sites.[103, 104] Depending on the adsorption sites and adsorbent

atoms or groups the tube may behave as a metal, semiconductor (p-type or n-type) or an insulator. The probable existence of more point charges on the wall of type 1 nanotubes might make them better hydrogen storage device than carbon nanotubes[105]. However, the same possibilities might also exist for type 2 and 3 nanotubes. The existence of ionic bonds in type 1 and mixture of ionic and covalent bonds in type 2 and 3 structures is expected to make the tubes highly reactive to the external elements and may provide conducive environment for hydrogen storage as well. Table 4.4 shows the calculated dipole moment for all three types of SiC nanotubes. We do not see any relation between the amount of dipole moment and size. But it is noticeable that type 1 (3, 0), type 2 (5, 0) and type 3 (4, 0) and (6, 0) have small moment which indicates their high charge symmetry. In an overall view type 3 nanotubes have comparatively lower dipole moments than the other two types. Type 1with all ionic bonds show the maximum average moment. The alternating arrangement of Si and C atoms in one layer perpendicular to the tube axis for type 3 nanotubes is responsible for their lower moments. On the other hand type 1 and 2 tubes have either Si or C atoms in one layer. Figures 4.3 and 4.4 show, type 1 and type 2 tube ends are populated by either Si or C atoms. This is the primary reason for their very high moment. In our previous calculations for armchair nanotubes only type 2 tubes stabilized with high dipole moment. This fact reveals that symmetric configurations of the zigzag nanotubes are characterized by a higher potential energy than the asymmetric configurations implying that zigzag symmetric nanotubes are less stable than asymmetric counterparts. This indicates that zigzag SiC nanotubes are likely to be found into bundles if experimentally synthesized.

The highest occupied molecular orbital (HOMO) and the lowest unoccupied molecular orbital (LUMO) gap gives a measure of the “band gap” for the infinite periodic SiC nanotubes. Table 4.5 and figure 4.9 provide the evolution of these gaps as a function of tube diameters for all the structures. The electronic states are also listed in table 4.5. All the ground state structures we have studied here are in triplet state, except type 1 (3, 0). In contrast all armchair

nanotubes have non-magnetic ground state[113]. Unlike type 1 armchair nanotubes[113] where the gap increases with increasing tube diameter, gap for type 1 zigzag nanotubes shows an oscillatory pattern from (3, 0) to (7, 0), then acquires very low values for (8, 0), (9, 0) and (10, 0) and finally increases sharply at (11, 0). Type 1 armchair nanotubes have larger band gap than bulk 3C-SiC (2.4eV) where type 1 zigzag nanotubes gaps were found less than 1 eV. In case of type 2, gap and tube diameter have an alternating relationship also but can be characterized by a predominant decreasing trend while for type 3, band gap decreases monotonically with increasing tube diameter and expected to approach small gap semiconducting to semi-metallic regime. The same relationship for type 3 was found in our previous work on armchair nanotube calculations. However unlike armchair case where SiC nanotubes were found with wide gap to very small gap semiconductors, zigzag nanotubes are all small gap semiconductors. On the other hand carbon nanotubes are metallic in armchair and semiconducting zigzag configuration. The existence of the covalent C-C bonds and Si-Si bonds in type 2 and type 3 zigzag nanotubes is the origin of their over all smaller gaps than type1 nanotubes. More ionic type bonding localizes the electronic states in type 1 nanotubes and consequently increases the band gap[42]. However we found some exceptions as mentioned earlier. The band gap variation with tube diameter indicates that type 2 and specifically type 3 tubes might exhibit metallic behavior at higher diameter. The evolution of band gap with the tube diameter can be analyzed by the curvature induced σ-π hybridization[35]. For the newly proposed type 3, curvature induced σ-π hybridization has the effect of uplifting the conduction bands, resulting in higher band gaps with decreasing diameters. Figure 4.10 demonstrates energy density of states (DOS) for largest nanotubes we studied in three different configurations. The DOS is built by fitting a Gaussian function in each eigenvalue and then summing them up. The comparatively large gap of type 1 to the gaps in the other two types is clearly visible. Also, type2 (3, 0) which became highly distorted after optimization has an unusually high gap.

Band gap tailoring of semiconductors is an important task and challenging endeavor in molecular electronics as it facilitates the integration of devices and systems for performing a specific work. Among all three types of SiC nanotubes we studied, type 1 which is the most stable one, has valence charge density strongly accumulated around C atoms. Significant electron transfer from Si to C atoms results in charge accumulation which makes the nanotube wall highly reactive to the external atom or group of atoms. This asymmetry has been exploited to band structure modification by side wall decoration with H, CH_3, SiH_3, N, NH, NH_2[103, 104, 110] and Si or C substitution by N atom.[110] Although our previous armchair calculations show a wider variation of band gaps for all three types[113], in this work it has also been shown that by changing the relative positions of C and Si atoms it is possible to have nanotubes with different band gaps for a specific diameter. In nanotube based technology Schottky barriers form at the metal/nanotube junctions, through which carriers (electrons and holes) must tunnel.[111] These barriers have a profound effect on the function and performance of nanotube based transistors. In general the charge transfer takes place at the metal nanotube interface that leads to band-bending and the creation of Schottky barrier.[112] Its height depends on workfunction difference and some other factors like interface quality. Carrier tunneling through Schottky barriers in one dimension is a dominant conduction mechanism[114]. The newly proposed type 3 single wall SiC zigzag nanotube gap is inversely proportional to tube diameter, as is the effective mass, for electrons and holes. Thus, at a given temperature, larger diameter nanotube will have a larger free carrier concentration than smaller diameter nanotube, and they will have a lower effective mass. Consequently, because of the smaller band gap of large diameter nanotubes, the band line-up at the metal/nanotube interface will result in lower Schottky barriers at the transistor source and drain. Because of the smaller effective mass tunneling through these barriers will be facilitated. Though type 2 nanotubes do not show any continuous gap decrease with the increasing diameter, the relationship between HOMO-LUMO gap with the diameter shows they might possess smaller gap at the larger diameters. Type 1 (8, 0), (9, 0) and (10, 0) tubes have

fairly large diameter and very low gap too, though (11, 0) gap increased drastically. These indicate that in SiCNT based junctions, type 3 and type 2 might play important role at the nanoscale molecular electronic networks, where SiC nanotubes are desirable over carbon nanotubes for some specific reasons. For example, one of the limitations of CNTs is their inability to survive in high-temperature, harsh-environment applications. Silicon carbide nanotubes (SiCNTs) are preferred for their superior material properties under such conditions.

Table 4.1 Cohesive Energies/atom (in eV) for Zigzag SiC Nanotubes.

Nanotube	Stoichiometry	Total number of atoms	Cohesive energy per atom (eV)		
			Type1	Type2	Type3
SiC (3, 0)	$Si_{33}C_{33}H_6$	72	4.071	4.183	
SiC (4, 0)	$Si_{44}C_{44}H_8$	96	4.357	4.292	4.337
SiC (5, 0)	$Si_{55}C_{55}H_{10}$	120	4.536	4.366	
SiC (6, 0)	$Si_{66}C_{66}H_{12}$	144	4.634	4.441	4.481
SiC (7, 0)	$Si_{77}C_{77}H_{14}$	168	4.696	4.492	
SiC (8, 0)	$Si_{88}C_{88}H_{16}$	192	4.735	4.532	4.551
SiC (9, 0)	$Si_{99}C_{99}H_{18}$	216	4.768	4.551	
SiC (10, 0)	$Si_{110}C_{110}H_{20}$	240	4.785	4.571	4.591
SiC (11, 0)	$Si_{121}C_{121}H_{22}$	264	4.804	4.586	

Table 4.2. Bond Length Distributions (Å) for Zigzag SiC Nanotubes.

Nanotube	Type 1	Type 2			Type 3		
	Si-C (Å)	Si-C (Å)	Si-Si (Å)	C-C (Å)	Si-C (Å)	Si-Si (Å)	C-C (Å)
SiC (3, 0)	1.78-1.89	1.85-1.96	2.32-2.47	1.37-1.61			
SiC (4, 0)	1.78-1.86	1.83-1.90	2.27-2.31	1.39-1.41	1.81-1.90	2.34-2.43	1.42-1.46
SiC (5, 0)	1.79-1.83	1.80-1.90	2.27-2.31	1.40-1.42			
SiC (6, 0)	1.80-1.83	1.79-1.87	2.22-2.30	1.42-1.43	1.82-1.86	2.28-2.30	1.42-1.45
SiC (7, 0)	1.80-1.85	1.82-1.85	2.24-2.27	1.43-1.45			
SiC (8, 0)	1.80-1.82	1.82-1.85	2.22-2.30	1.42-1.45	1.81-1.86	2.25-2.26	1.42-1.45
SiC (9, 0)	1.80-1.83	1.82-1.84	2.22-2.27	1.41-1.44			
SiC(10, 0)	1.80-1.82	1.82-1.84	2.23-2.28	1.41-1.44	1.81-1.85	2.23-2.25	1.42-1.45
SiC(11, 0)	1.80-1.82	1.82-1.84	2.23-2.26	1.42-1.44			

Table 4.3. Tube Diameters (Å) and Radial Buckling (Å) for Zigzag SiC Nanotubes.

Nanotube	Type 1		Type 2		Type 3	
	Tube diameter (Å)	Radial buckling (Å)	Tube diameter (Å)	Radial buckling (Å)	Tube diameter (Å)	Radial buckling (Å)
SiC (3, 0)	3.340	0.106	3.738	0.162		
SiC (4, 0)	4.249	0.037	4.303	0.094	4.319	0.372
SiC (5, 0)	5.175	0.016	5.237	0.093		
SiC (6, 0)	6.127	0.008	6.189	0.070	6.244	0.245
SiC (7, 0)	7.098	0.007	7.152	0.065		
SiC (8, 0)	8.074	0.005	8.136	0.060	8.201	0.173
SiC (9, 0)	9.050	0.005	9.128	0.048		
SiC(10, 0)	10.047	0.004	10.121	0.035	10.164	0.056
SiC(11, 0)	11.025	0.003	11.113	0.026		

Table 4.4 Dipole Moments of Zigzag SiC Nanotubes (in Debye).

Nanotube	Type 1 (Debye)	Type 2 (Debye)	Type 3 (Debye)
SiC (3, 0)	1.156	4.187	
SiC (4, 0)	7.438	2.117	0.559
SiC (5, 0)	5.899	1.861	
SiC (6, 0)	20.970	12.550	0.549
SiC (7, 0)	36.598	14.921	
SiC (8, 0)	50.381	2.885	6.088
SiC (9, 0)	67.539	17.134	
SiC (10, 0)	19.489	9.011	4.407
SiC (11, 0)	42.708	23.031	

Table 4.5. HOMO-LUMO Gaps (in eV) and Electronic States for Zigzag SiC nanotubes.

SiC Nanotube	Type 1 Zigzag		Type 2 Zigzag		Type 3 Zigzag	
	HOMO-LUMO gap	Electronic State	HOMO-LUMO gap	Electronic State	HOMO-LUMO gap	Electronic State
SiC (3, 0)	0.751	^1A	1.303	^3A		
SiC (4, 0)	0.662	$^3A_1$	0.539	^3A	0.661	^3B
SiC (5, 0)	0.881	^3A	0.426	^3A		
SiC (6, 0)	0.669	^3A	0.436	^3A	0.505	^3A
SiC (7, 0)	0.799	^3A	0.500	^3A		
SiC (8, 0)	0.287	^3A	0.537	^3A	0.388	^3A
SiC (9, 0)	0.109	^3A	0.389	^3A		
SiC(10, 0)	0.129	$^3B_1$	0.163	$^3A_2$	0.285	^3A
SiC(11, 0)	0.834	^3A	0.345	^3A		

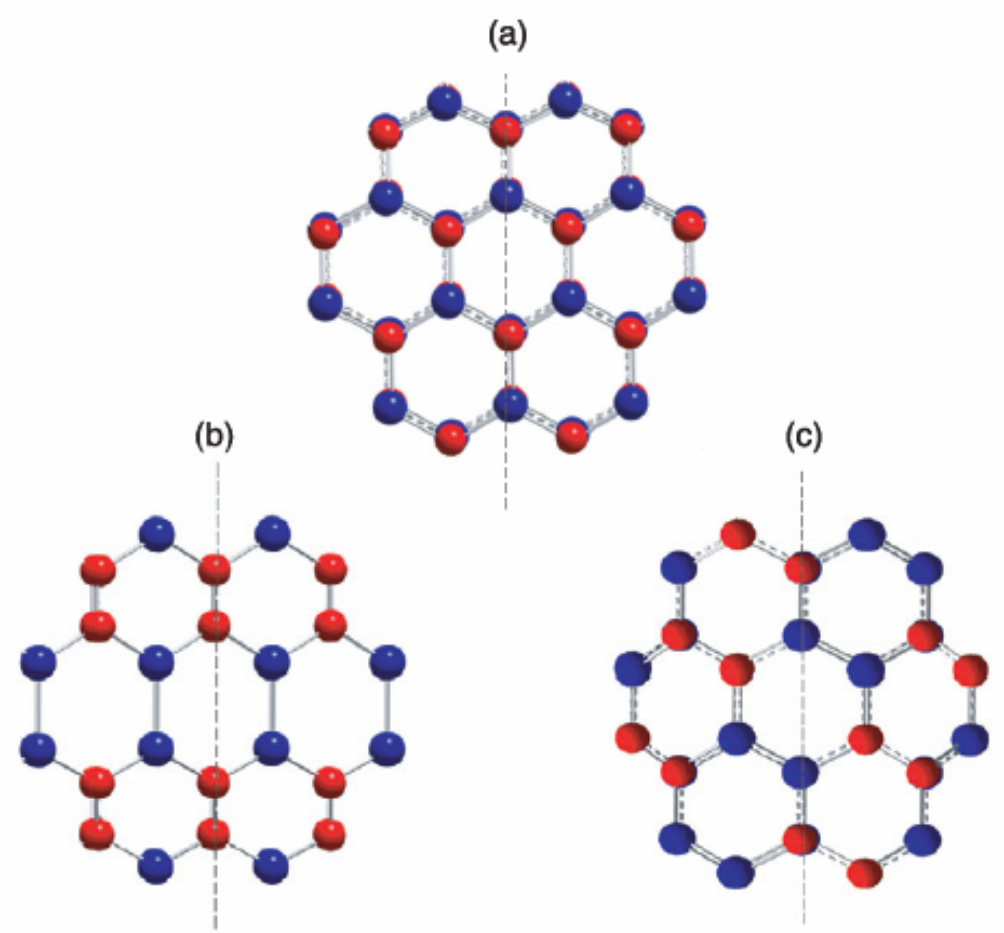

Fig. 4.1. Atomic arrangements for (a) type 1, (b) type 2 and (c) type 3 zigzag nanotubes. The carbon atoms are red and silicon atoms are blue. The dashed lines represent the orientation of tube axis.

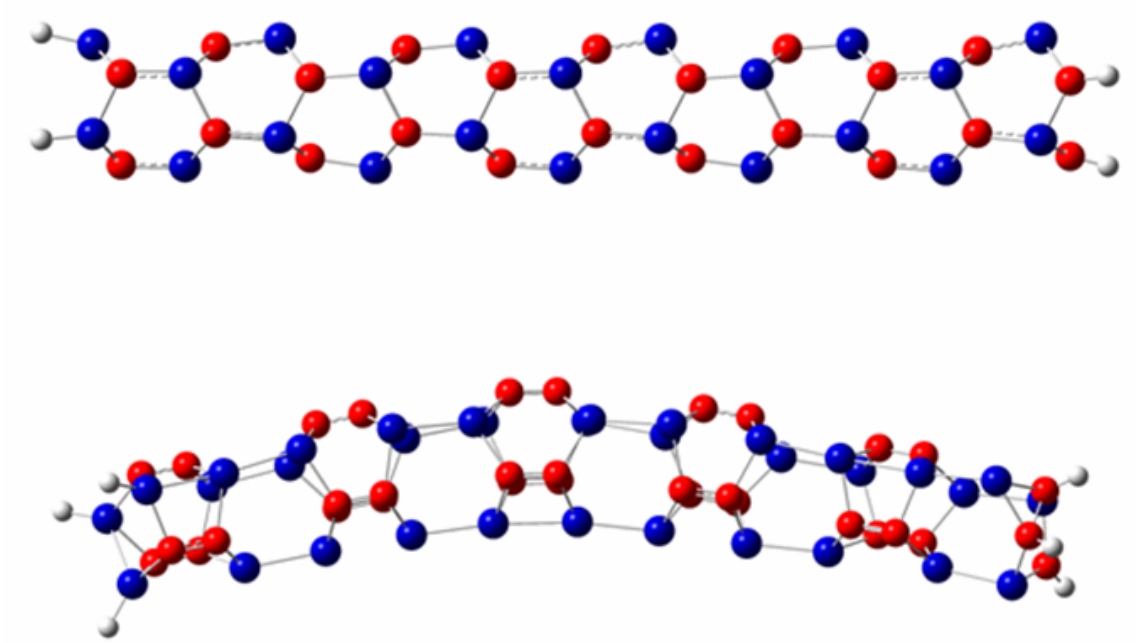

Fig. 4.2. Side views of single wall (3, 0) nanotubes. Top (type 1) and bottom (type 2) structures, the latter showing remarkable distortions. Red atoms are carbon and blue atoms are Si.

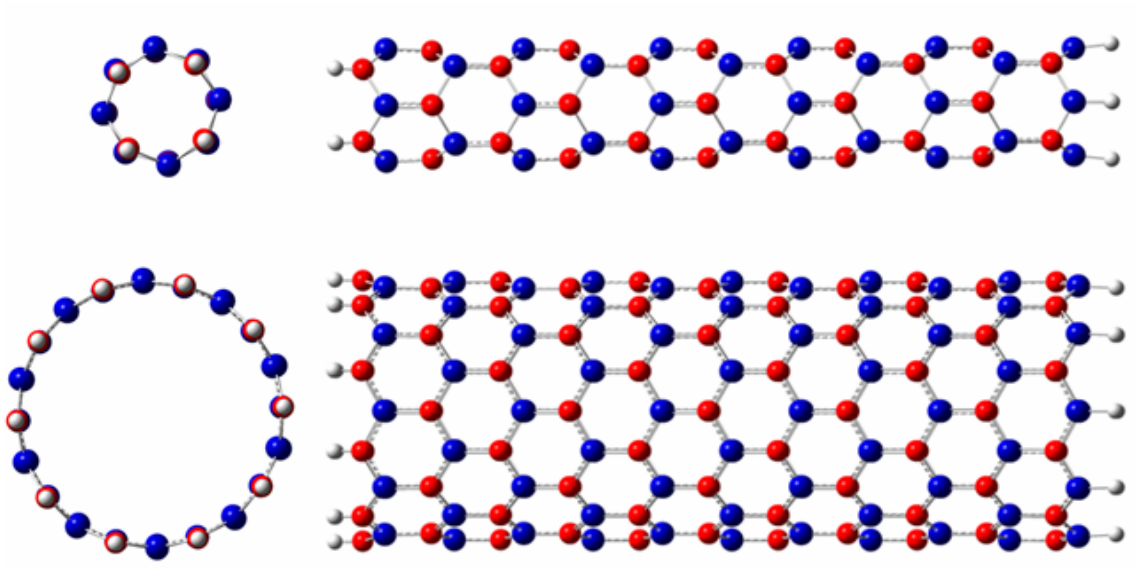

Fig. 4.3. Top and side views of single wall type 1 (4, 0) and (10, 0) SiC nanotubes. Red atoms are carbon and blue atoms are Si.

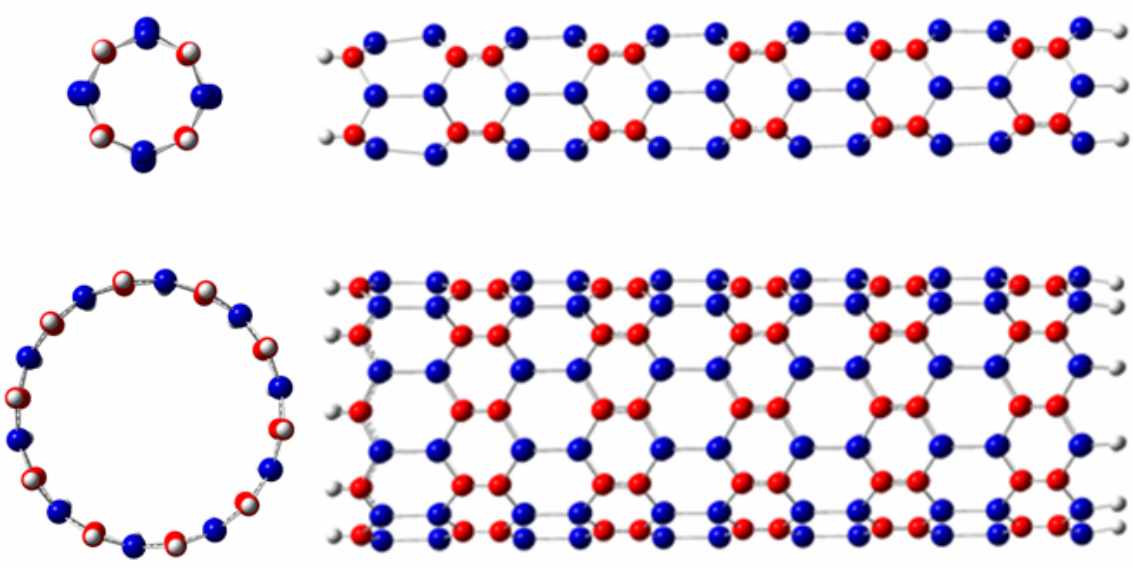

Fig. 4.4. Top and side views of single wall type 2 (4, 0) and (10, 0) SiC nanotubes. Red atoms are carbon and blue atoms are Si.

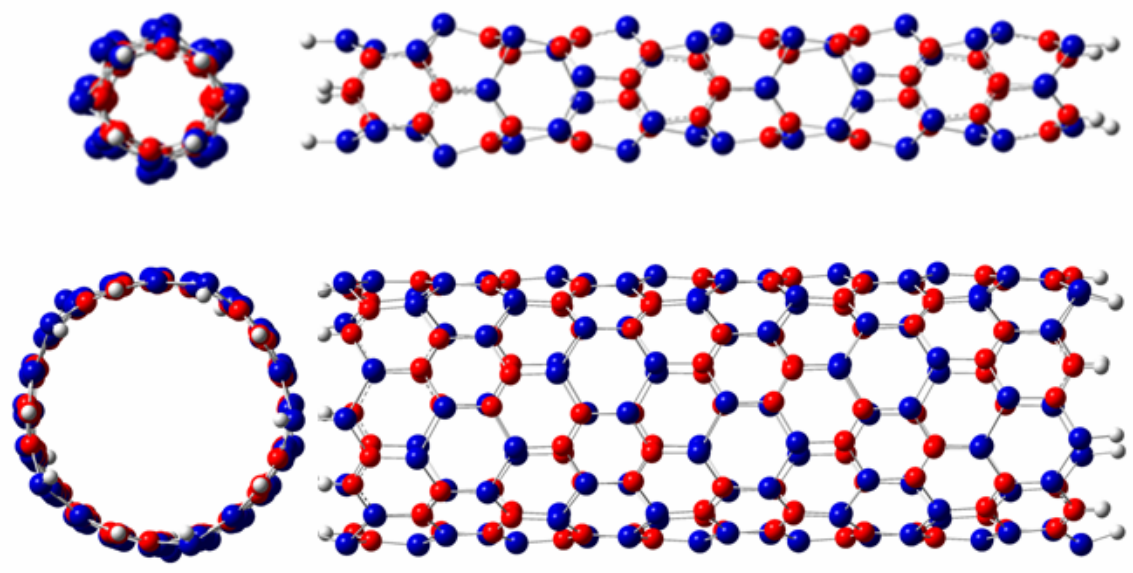

Fig. 4.5. Top and side views of single wall type 3 (4, 0) and (10, 0) SiC nanotubes. Red atoms are carbon and blue atoms are Si.

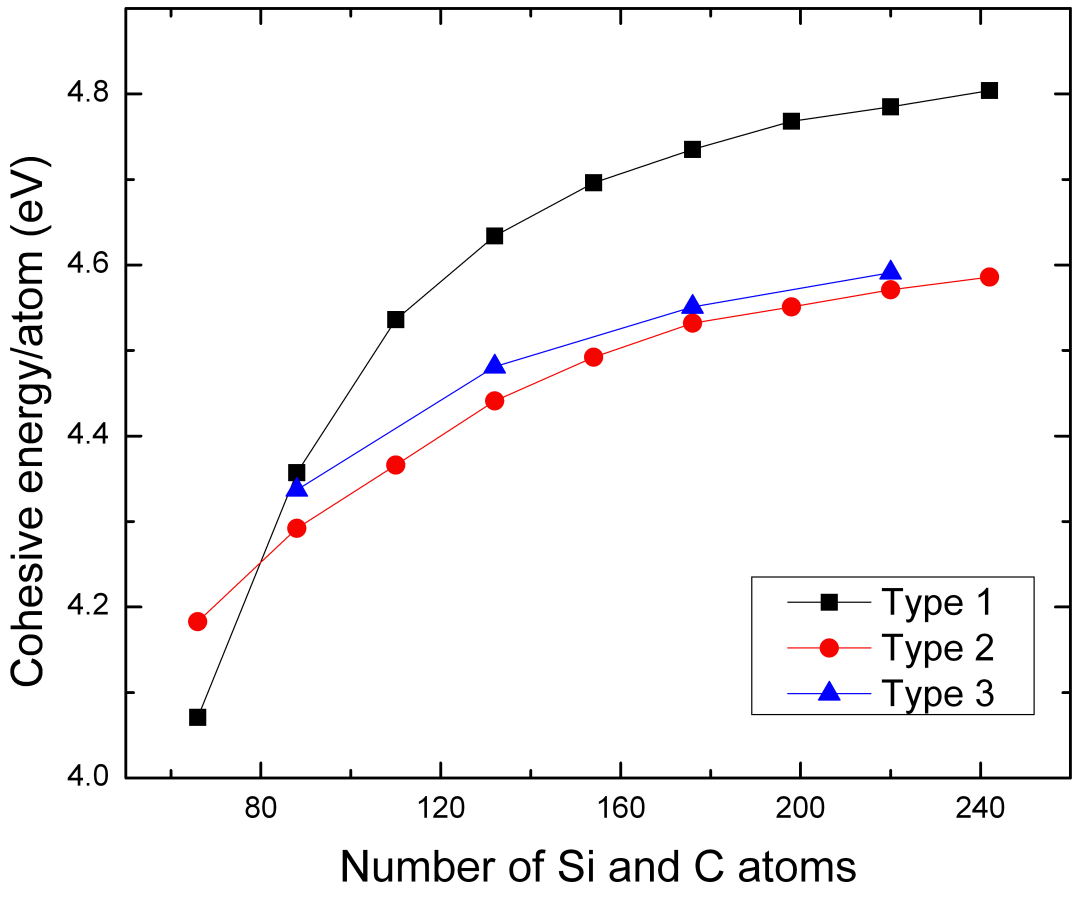

Fig. 4.6. Cohesive energy/atom vs. total number of Si and C atoms.

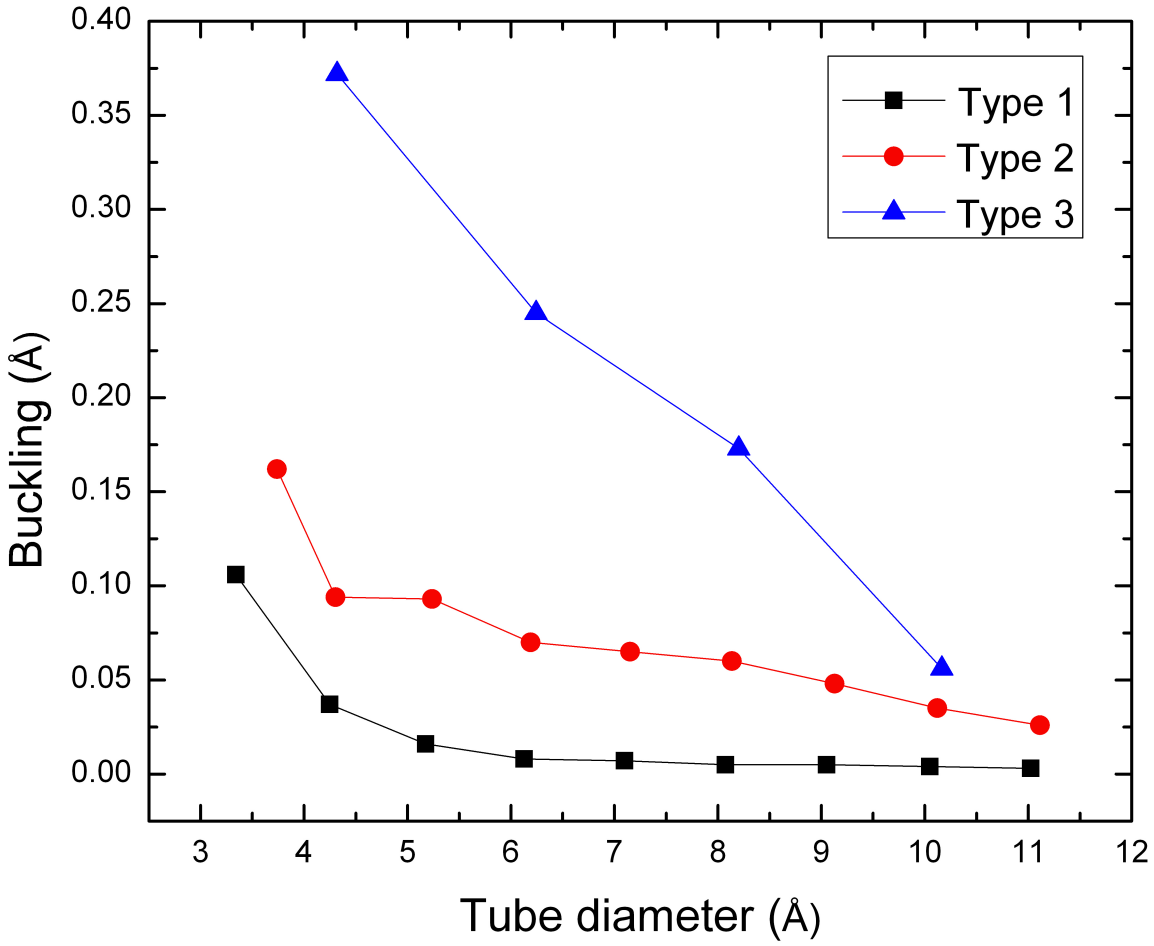

Fig. 4.7. Tube buckling (Å) vs. tube diameter (Å) for three types of zigzag SiC nanotubes.

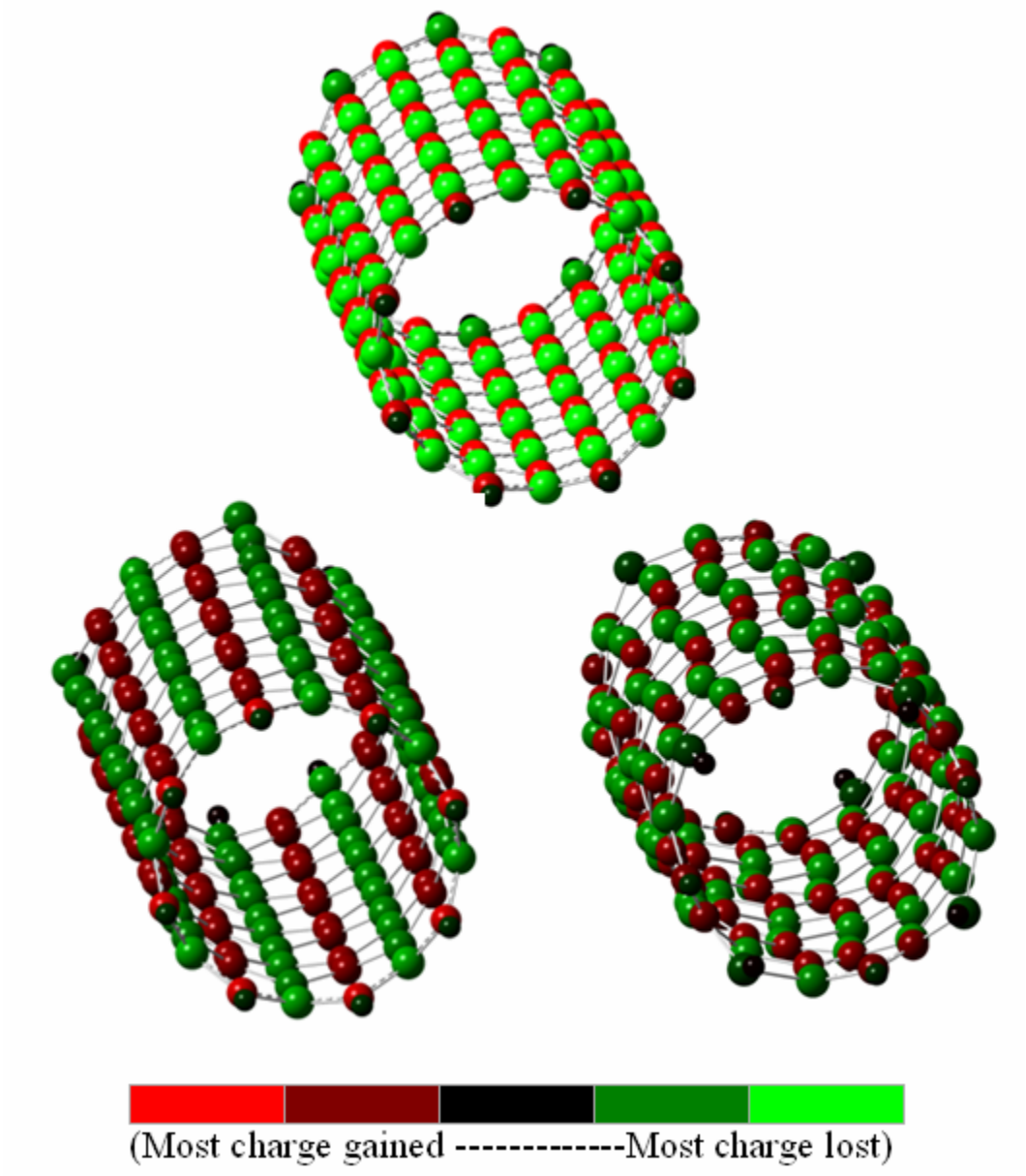

Fig. 4.8. Mulliken charge distributions for (8, 0) nanotubes. Top (type 1), bottom left (type 2) and bottom right (type 3). Carbon atoms gained and silicon atoms lost charge.

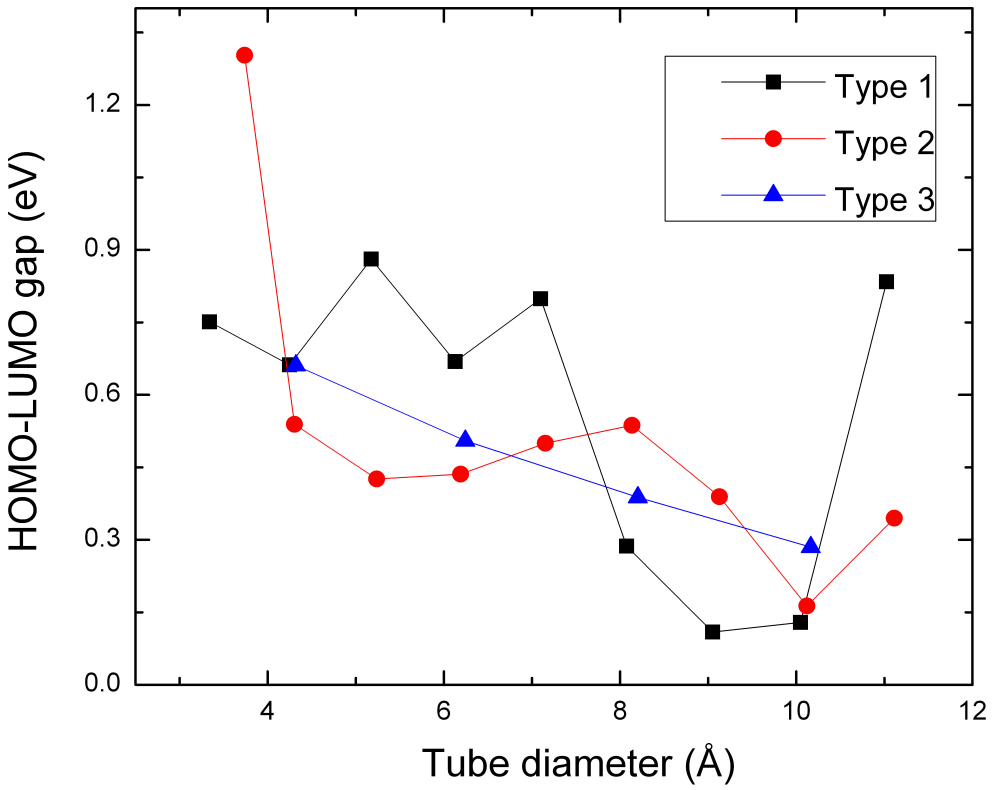

Fig. 4.9. HOMO-LUMO gap (eV) vs. tube diameter (Å) for all three types of zigzag nanotubes.

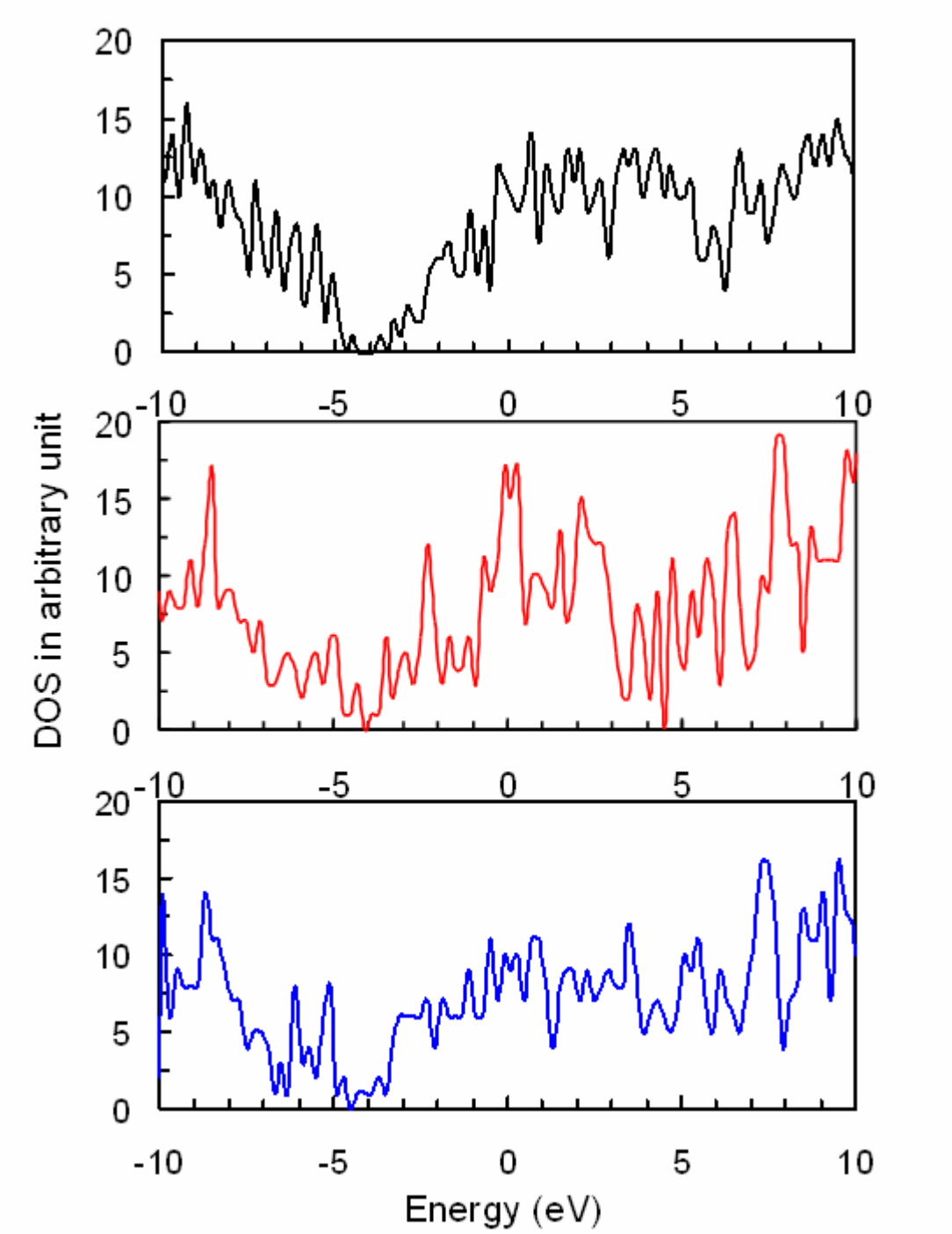

Fig. 4.10. Density of states for type 1 (11, 0) (top), type 2 (11, 0) (middle), and type 3 (10, 0) (bottom) zigzag nanotubes.

CHAPTER 5

INTERACTIONS OF Fe ATOM WITH ARMCHAIR SiC NANOTUBES

5.1 Different sites of nanotubes

In this study, a Fe atom is placed at the center of each type of nanotubes from (3, 3) to (6, 6) with the aim of exploring comparative evolution and modification of geometric and electronic properties from bare nanotubes along with the relative binding energies of Fe atoms inside those nanotubes. Placing a Fe atom inside nanotubes with higher diameters beyond (6, 6) would not provide significant information due to negligible interaction with the tube wall. In our previous work[113], we have noted that as the size of the nanotubes increased from (3, 3) to (11, 11), binding energies tended to saturate for all three types of nanotubes. From (3, 3) to (6, 6), the increase in binding energies was more prominent and then a slow variation continues up to (11, 11). For this reason and for obvious severe demand on computational resources, we opted to concentrate on Fe adsorption at different sites of (3, 3) and (6, 6) for all three types of nanotubes. Fig. 5.1 shows the relative positions of Si and C atoms in different types of nanotubes. In the type 1 arrangement, with only Si-C bonds, silicon and carbon atoms are placed alternatively without any adjacent Si or C atoms. In types 2 and 3 arrangements with Si-C, Si-Si, and C-C bonds, the nearest neighbors of each Si atom consist of two C atoms and another Si atom and vice versa. The difference between type 2 and type 3 lies in the relative spatial positions of the Si and C atoms. If we consider one layer perpendicular to the tube axis, in type 3, Si and C atoms are alternating while in type 2 each layer contains either Si or C atoms. Fig. 5.1 also shows the different adsorption sites, five for type 1 and seven for types 2 and 3 nanotubes. There are three major adsorption sites: top, bridge, and hollow. C top and Si top refer to the positions directly perpendicular to the tube wall along the C and Si atoms

respectively. There are two major bridge sites named as normal and zigzag bridge. The relative orientation of those two sites with respect to the tube axis is clearly visible in the figures. Those two bridge sites are named according to their terminal atoms. Hollow sites are at the middle of the hexagons. In types 1 and 3 only one type of hexagon is present and there is only one hollow site. In type 2, two different hexagons are present and this gives rise to two different hollow sites. The first hollow site is associated with the hexagon containing four C and two Si atoms, whereas the second hollow site is positioned along the center perpendicular to hexagon containing two C and four Si atoms.

5.2 Results and discussions

The binding energy for the encapsulated or adsorbed Fe atom is obtained from the expression below.

$$E_b = E\,(SiCNT) + E\,(Fe) - E\,(Fe+SiCNT) \quad (1)$$

where *E (SiCNT)* and *E (Fe)* are the ground state energies of the bare nanotube and Fe atom respectively. *E (Fe + SiCNT)* represent the ground state energy of the Fe encapsulated or adsorbed SiCNT. Table 5.1 shows the stoichiometry and the binding energies of the Fe atom inside the nanotube from (3, 3) to (6, 6) for all types. Though type 1 bare nanotubes were found to be most stable in our previous work[113], we note from table 1 that type 2 tubes have the strongest interactions with Fe atoms followed by type 3 and then type 1. As the diameter or the tube size increases, interactions between Fe atom and tube wall decrease for all types. Fig. 5.2 shows this variation of binding energy/atom with respect to tube diameter. After optimization Fe atoms were found to retain their initial positions (center of the tube) with negligible deviation along the tube axis. The diameters did not change upon Fe atom encapsulation, from that of bare nanotubes. The Mulliken charges on the Fe atom are shown in table 2. For the smallest nanotubes, charge transfers occur from the tube to the Fe atom. This direction of charge transfer continues for all type 1 larger nanotubes but for the other two types the direction is reversed as we increase the tube diameter. From (4, 4) to (6, 6) tubes, Fe atom transfers

charge to the tube in case of type 2 and type 3 tubes. We believe that this is due to the presence of two other types of bonds, namely Si-C and C-C in types 2 and 3 nanotubes and since both Si and C atoms are more electronegative compared to Fe. Figure 5.3 demonstrates how the highest occupied molecular orbital (HOMO) is localized to the Fe atom in type 1 (3, 3). The undoped tube HOMO was uniformly distributed. Similar behavior was observed for the other two types. The total charge density for the smallest tube (3, 3) is shown in figure 5.4. We note that for type 2, there is significant overlap between the charge of the Fe atom with the SiCNT, followed by that for type 3 and type 1. The more lateral expansion of the blue region for types 2 and 3 relative to type 1 is reminiscent of our previous observation of buckling effect, where buckling was almost negligible in type 1 nanotubes.[113]

Tables 5.3 through 5.8 show Fe atom adsorption energies, distances of Fe atom from the tube wall, nearest C-Fe and Si-Fe distances, and the Mulliken charges of Fe atom for (3, 3) and (6, 6) nanotubes of three types. Only (3, 3) and (6, 6) tubes were considered here since no significantly new results were expected by studying the (4, 4) and (5, 5) tubes and also because we are interested in the curvature effects of the tubes. There are five possible sites for type 1 and seven sites for other two types described earlier. For type 1 (3, 3), Si-C normal bridge site is the most stable and Si top is the least stable sites, with a difference in adsorption energy of 0.67 eV. The corresponding sites for type 2 (3, 3) are second hollow and C-C normal bridge, with a difference in adsorption energy of 1.09 eV. In case of type 3 (3, 3), they are hollow and C-C zigzag bridge, with the corresponding difference being 1.42 eV. The Si-C zigzag bridge for type 1 (6, 6) and C top for types 2 and 3 (6, 6) are the most stable Fe adsorption sites. The difference in adsorption energies between the most and least favored sites for type 1 (6, 6) is about 0.62eV. These values are 0.90 eV and 0.41 eV for type 2 (6, 6) and type 3 (6, 6), respectively. Another noticeable observation is that Fe prefers to bond with C than with Si, a common feature for all types for both (3, 3) and (6, 6) consistent with our Fe-C and Fe-Si dimer calculations, where the binding energies/atom are 1.81 eV and 1.26 eV, respectively. Using the

DMol3 suite of software, for Ti adsorption on type 1 (5, 5) SiCNT, Meng *et al.*[53] found the most favorable site to be the C top site. We also note that Fe adsorption energy decreases with increasing radius (or decreasing curvature) of the tube. Therefore by creating regions of different curvature on a single SiCNT by radial deformation or be designing different types of tubes, it is possible to get different values of adsorption energies. The average adsorption energy on a type 1 (3, 3) is 1.515eV and that on a (6, 6) is 1.100eV. For type 2, the corresponding numbers are 2.658eV and 1.350eV and for type 3, 2.564eV and 1.581eV. So type 2 and type 3 nanotubes have better Fe adsorption capacity as a whole; in other words, complete Fe coating is predicted to be more facile for these two types of SiC nanotubes. Despite possessing highest binding energy/atom for the bare tube, type 1 tubes have the least possibility of being coated with Fe atoms. This implies Fe-Fe interaction can dominate over Fe-nanotube interaction which might result in forming isolated Fe clusters than complete Fe coating.

Mulliken charge analysis shows electron transfer occurs from Fe atom to the nanotube for all sites of all types except for second hollow site of type 2 (6, 6) and (3, 3) and Si-Si normal bridge of type 2 (3, 3) where Fe atom gains 0.275e, 0.652e and 0.135e from the tube, respectively. No trend between amount of charge transfer and adsorption energy of the site was found here, suggesting the local structure as a whole determines the amount and direction of charge transfer as well as the binding strength of the adsorbent. From adsorption energies, it can be inferred that the most favorable sites for the three types of (6, 6) nanotubes C top site of type 2 has the maximum adsorption energy, followed by C top of type 3 and Si-C zigzag bridge site of type 1. The corresponding order of the sites for (3, 3) is hollow of type 3, second hollow of type 2 and Si-C normal bridge site of type 1. When Fe atom was placed on C top and Si top sites of (6, 6) SiCNT, the atom slightly migrated toward the neighboring normal or zigzag bridge sites but did not deviate completely from the initial positions. This slight migration was observed towards the hollow sites in case of (3, 3) nanotubes. This is the reason we see slight differences

between the distances of Fe atom from the tube wall and the Fe-C and Fe-Si distances for the C top and Si top sites. Figures 5.5, 5.6, and 5.7 show the HOMO localizations for the most and the least preferred sites for all three types (6, 6) nanotubes with Fe atom adsorbed on them. The more localization of the “negative” and “positive” values of the wave function is found for the most preferred sites. The difference in localization is not much perspicuous for the type 3 sites. The reason is attributed to the fact that the difference in adsorption energies between the most and least preferred sites for type 3 configuration is small compared to those for the other two types.

In nanotube and fullerene based technology, molecular electronic structures are required with a wide variety of mechanical, electronic, optical and magnetic properties. Band gap tailoring is an important issue for different purposes especially when coupling of nanostructures is concerned in a complex network. Tables 5.9-5.11 show the HOMO-LUMO gaps of the (Fe+SiCNT) system and the change of the gaps with respect to the bare nanotube gaps.[113] In our previous calculation for bare nanotubes, band gaps for type 1 nanotubes were found to be larger than bulk 3C-SiC gap, while type 2 and type 3 nanotubes had significantly lower band gaps. Unlike the other two types, band gap for type 3 nanotubes showed a monotonous decreasing trend with increasing tube diameter. Table 5.9 and figure 5.8 show the variation of these gaps with tube diameter for the Fe atom encapsulated in type 1 nanotube. There is a continuous decrease in gap with increasing tube diameter for the Fe encapsulated tube. This trend is reversed from the bare tube gap variation. There is a significant decrease in gap upon Fe atom encapsulation for type 1 nanotubes. In case of types 2 and 3 only small tubes show this reduction while it remains almost unchanged for the tubes with smaller curvature or higher diameter. These results indicate that band gaps can be tuned by Fe doping inside the type 1 tubes only. Table 5.10 and figure 5.9 show the variation of gaps with tube diameter for the Fe atom encapsulation in type 2 nanotubes. This variation for type 3 is shown in table 5.11 and figure 5.10. The HOMO-LUMO gaps and the corresponding changes in gaps

from the bare nanotubes for different adsorption sites of three types of SiCNTs have been presented in tables 5.12-5.17. Our previous results showed the bare nanotube (6, 6) gaps to be 2.932eV, 0.876eV, and 0.835eV for types 1, 2 and 3, respectively. These gaps were 2.776eV, 1.487eV and 1.216eV for the (3, 3) tubes in three configurations. For (6, 6) we observe the same trends as in the encapsulation case, as gap change is significant for type 1 only. For all the five sites the reduction in band gap is close to 1eV with the maximum decrease occurred for C top site. Adsorbing Fe atom can slightly decrease the gap when it is at the either C top or first hollow site of type 2 (6, 6) nanotube. All other sites do not show any significant change. It is interesting to notice that type 3 sites do not show any remarkable gap modification upon Fe adsorption on any of the seven sites. Unlike all other sites Si top and Si-Si zigzag bridge sites show a very small gap increase upon Fe atom adsorption. In case of (3, 3) type 1 sites also showed the maximum reduction of gaps upon Fe adsorption. However unlike (6, 6), type 2 and type 3 (3, 3) tubes show noticeable band gap modification. All these results suggest that band gap tuning upon single Fe atom interaction with armchair SiC nanotubes is mostly feasible for type 1 structures. Figure 5.11 demonstrates energy density of states (DOS) for pristine type 1 (6, 6) nanotube and the corresponding Fe atom adsorbed nanotube that has the maximum adsorption energy (Si-C zigzag bridge site). The DOS is built by fitting a Gaussian function in each eigenvalue and then summing them up. The Gaussian width used to broaden the eigenvalues is 0.05 eV and E=0 refers to the HOMO. It is worth noting that there are very few isolated extra created states near the HOMO within the pseudogap in case of the adsorbed nanotube. Similar observation was found for the other sites of type 1 nanotubes. This significant decrease in band gap for type 1 nanotubes upon Fe atom interaction might play important role at the metal nanotube junction in molecular electronic networks or other potential applied areas of band gap engineering.

All the (Fe + SiCNT) systems we studied here have magnetic ground states. Because a bare SiCNT has a nonmagnetic ground state[113], the net spin of (Fe + SiCNT) system originates

from the magnetic moment of the encapsulated and adsorbed Fe atom. Tables 5.12-5.17 show the electronic states and the spin magnetic moments of Fe atom inside and outside the tube. It is evident that encapsulated Fe atom loses its magnetic moment more inside the smaller tubes where interaction is stronger. Mulliken population analysis shows that the more 4s electron migration to 4p and 3d orbitals of Fe atom is responsible for this quenching of magnetic moment in case of smaller diameter nanotubes. Magnetic moment of Fe atom placed at the center inside (8, 0) carbon nanotube [48] was found to be 2.36 μ_B. These values were 2.46 for (3, 3) CNT [115] and 2.3 for (4, 4) CNT[116]. From table 5.9-5.11 we see these values are higher for all tubes of all types which indicate that Fe atom retains its magnetic moment inside SiCNT more than it does inside CNT. From the values of the magnetic moments of Fe atom for different adsorption sites of three types of tubes, it is obvious that Fe atom magnetic moment are more quenched on type 2 and 3 sites than type 1 sites for (3, 3) and (6, 6), consistent with higher adsorption energy of Fe atom for those sites discussed earlier. The high magnetic moments generated upon encapsulation and adsorption of Fe atom in single wall SiCNT should have important implications in magnetic device applications.

Table 5.1. Cohesive Energies/atom (in eV) for Fe Atom Encapsulated in Armchair SiC Nanotubes.

Nanotube	Stoichiometry	Total number of atoms	Binding energy of Fe atom (eV) inside the nanotube		
			Type1	Type2	Type3
SiC (3, 3)	$Si_{30}C_{30}H_{12}Fe_1$	73	1.712	3.149	2.634
SiC (4, 4)	$Si_{40}C_{40}H_{16}Fe_1$	97	0.557	1.104	0.833
SiC (5, 5)	$Si_{50}C_{50}H_{20}Fe_1$	121	0.535	0.632	0.634
SiC (6, 6)	$Si_{60}C_{60}H_{24}Fe_1$	145	0.491	0.561	0.553

Table 5.2. Tube Diameters (in Å) and Mulliken Charges of Encapsulated Fe atoms.

Nanotube	Tube diameter (Å)			Mulliken charge of Fe atom		
	Type1	Type2	Type3	Type1	Type2	Type3
SiC (3, 3)	5.313	5.412	5.375	-0.296	-0.294	-0.172
SiC (4, 4)	7.022	7.162	7.116	-0.140	0.529	0.411
SiC (5, 5)	8.760	8.936	8.841	-0.071	0.217	0.152
SiC (6, 6)	10.451	10.694	10.582	-0.049	0.081	0.058

Table 5.3. Adsorption Energies of Fe Atoms (eV), Distances of Fe Atoms from Tube Walls (Å), Nearest C-Fe Distances (Å), Nearest Si-Fe distances (Å), and Mulliken Charges of Fe Atoms Adsorbed on Type 1 (3, 3) Armchair SiC Nanotube.

Site	Adsorption energy of Fe atom (eV)	Distance of Fe atom from tube wall (Å)	Nearest C-Fe distance (Å)	Nearest Si-Fe distance (Å)	Mulliken charge of Fe atom
C top	1.527	1.738	1.930	2.492	0.195
Si top	1.201	2.134	2.826	2.415	0.236
Hollow	1.567	1.350	2.219	2.552	0.281
Si-C normal Bridge	1.871	1.763	2.068	2.380	0.248
Si-C zigzag bridge	1.410	1.997	2.101	2.425	0.252

Table 5.4. Adsorption Energies of Fe Atoms (eV), Distances of Fe Atoms from Tube Walls (Å), Nearest C-Fe Distances (Å), Nearest Si-Fe distances (Å), and Mulliken Charges of Fe Atoms Adsorbed on Type 1 (6, 6) Armchair SiC Nanotube.

Site	Adsorption energy of Fe atom (eV)	Distance of Fe atom from tube wall (Å)	Nearest C-Fe distance (Å)	Nearest Si-Fe distance (Å)	Mulliken charge of Fe atom
C top	1.237	2.234	2.330	2.675	0.022
Si top	0.928	2.476	3.189	2.518	0.139
Hollow	0.714	1.544	2.505	2.420	0.126
Si-C normal Bridge	1.289	2.117	2.168	2.441	0.113
Si-C zigzag bridge	1.333	2.167	2.191	2.493	0.094

Table 5.5. Adsorption Energies of Fe Atoms (eV), Distances of Fe Atoms from Tube Walls (Å), Nearest C-Fe Distances (Å), Nearest Si-Fe distances (Å), and Mulliken Charges of Fe Atoms Adsorbed on Type 2 (3, 3) Armchair SiC Nanotube.

Site	Adsorption energy of Fe atom (eV)	Distance of Fe atom from tube wall (Å)	Nearest C-Fe distance (Å)	Nearest Si-Fe distance (Å)	Mulliken charge of Fe atom
C top	2.983	2.275	2.963	2.456	0.134
Si top	2.836	2.244	2.914	2.451	0.160
First hollow	2.028	1.005	2.155	2.638	0.465
Second hollow	3.116	1.153	2.020	2.415	-0.652
C-C normal bridge	2.022	1.933	2.250	2.332	0.151
Si-Si normal bridge	2.745	2.124	3.261	2.349	-0.135
Si-C zigzag bridge	2.875	2.265	2.874	2.461	0.155

Table 5.6. Adsorption Energies of Fe Atoms (eV), Distances of Fe Atoms from Tube Walls (Å), Nearest C-Fe Distances (Å), Nearest Si-Fe distances (Å), and Mulliken Charges of Fe Atoms Adsorbed on Type 2 (6, 6) Armchair SiC Nanotube.

Site	Adsorption energy of Fe atom (eV)	Distance of Fe atom from tube wall (Å)	Nearest C-Fe distance (Å)	Nearest Si-Fe distance (Å)	Mulliken charge of Fe atom
C top	1.765	2.137	2.255	2.376	0.182
Si top	1.489	2.447	3.517	2.618	0.159
First hollow	0.866	1.641	2.502	2.600	0.254
Second hollow	0.932	1.749	2.960	2.391	-0.275
C-C normal bridge	1.237	1.618	2.145	2.582	0.200
Si-Si normal bridge	1.446	2.021	3.514	2.428	0.047
Si-C zigzag bridge	1.717	2.337	2.722	2.469	0.133

Table 5.7. Adsorption Energies of Fe Atoms (eV), Distances of Fe Atoms from Tube Walls (Å), Nearest C-Fe Distances (Å), Nearest Si-Fe distances (Å), and Mulliken Charges of Fe Atoms Adsorbed on Type 3 (3, 3) Armchair SiC Nanotube.

Site	Adsorption energy of Fe atom (eV)	Distance of Fe atom from tube wall (Å)	Average C-Fe distance (Å)	Average Si-Fe distance (Å)	Mulliken charge of Fe atom
C top	2.862	1.542	2.071	2.413	0.182
Si top	2.157	2.618	3.604	2.372	0.202
Hollow	3.241	1.638	2.158	2.448	0.232
Si-C normal bridge	2.867	1.625	2.167	2.419	0.212
Si-C zigzag bridge	2.860	1.604	2.132	2.434	0.193
C-C zigzag bridge	1.823	1.602	2.078	2.425	0.187
Si-Si zigzag bridge	2.139	2.098	3.496	2.412	0.082

Table 5.8. Adsorption Energies of Fe Atoms (eV), Distances of Fe Atoms from Tube Walls (Å), Nearest C-Fe Distances (Å), Nearest Si-Fe distances (Å), and Mulliken Charges of Fe Atoms Adsorbed on Type 3 (6, 6) Armchair SiC Nanotube.

Site	Adsorption energy of Fe atom (eV)	Distance of Fe atom from tube wall (Å)	Average C-Fe distance (Å)	Average Si-Fe distance (Å)	Mulliken charge of Fe atom
C top	1.745	1.969	2.392	2.551	0.233
Si top	1.434	2.430	3.577	2.583	0.132
Hollow	1.664	2.435	3.227	2.679	0.171
Si-C normal bridge	1.332	2.032	2.139	2.443	0.219
Si-C zigzag bridge	1.684	1.954	2.552	2.618	0.226
C-C zigzag bridge	1.647	1.785	2.101	2.434	0.225
Si-Si zigzag bridge	1.562	2.317	3.492	2.417	0.066

Table 5.9. HOMO-LUMO Gaps (in eV), Change in HOMO-LUMO Gaps (in eV) from Bare Nanotubes, Electronic States and Spin Magnetic Moments (μ_B) of Fe Atoms Encapsulated in Type 1 Armchair SiC Nanotubes.

Nanotube	HOMO-LUMO gap (eV)	Change in HOMO-LUMO gap (eV)	Electronic state	Spin magnetic moment (μ_B) of Fe atom
(3, 3)	1.764	1.012	^{5}A	3.054
(4, 4)	1.728	1.095	^{5}A	3.989
(5, 5)	1.521	1.368	^{5}A	3.995
(6, 6)	1.409	1.523	^{5}A	4.010

Table 5.10. HOMO-LUMO Gaps (in eV), Change in HOMO-LUMO Gaps (in eV) from Bare Nanotubes, Electronic States and Spin Magnetic Moments (μ_B) of Fe Atoms Encapsulated in Type 2 Armchair SiC Nanotubes.

Nanotube	HOMO-LUMO gap (eV)	Change in HOMO-LUMO gap (eV)	Electronic state	Spin magnetic moment (μ_B) of Fe atom
(3, 3)	1.012	0.475	^{5}A	2.917
(4, 4)	0.773	0.033	^{5}A	3.405
(5, 5)	0.821	0.018	^{5}A	4.023
(6, 6)	0.813	0.063	^{5}B	4.047

Table 5.11. HOMO-LUMO Gaps (in eV), Change in HOMO-LUMO Gaps (in eV) from Bare Nanotubes, Electronic States and Spin Magnetic Moments (μ_B) of Fe Atoms Encapsulated in Type 3 Armchair SiC Nanotubes.

Nanotube	HOMO-LUMO gap (eV)	Change in HOMO-LUMO gap (eV)	Electronic state	Spin magnetic moment (μ_B) of Fe atom
(3, 3)	0.573	0.643	^{5}A	3.040
(4, 4)	0.473	0.611	^{5}A	3.654
(5, 5)	0.865	0.040	^{5}A	3.995
(6, 6)	0.825	0.010	^{5}B	4.003

Table 5.12. HOMO-LUMO Gaps (in eV), Change in HOMO-LUMO Gaps (in eV) from Bare Nanotubes, Electronic States and Spin Magnetic Moments (μ_B) of Fe Atoms Adsorbed on Type 1 (3, 3) Armchair SiC Nanotube.

Site	HOMO-LUMO gap (eV)	Change in HOMO-LUMO gap (eV)	Electronic State	Spin magnetic moment (μ_B) of Fe atom
C top	2.129	0.647	^{3}A	2.602
Si top	2.212	0.564	^{5}A	3.851
Hollow	1.972	0.804	^{3}A	2.894
Si-C Normal bridge	1.942	0.834	^{5}A	3.731
Si-C Zigzag bridge	1.754	1.022	^{5}A	3.737

Table 5.13. HOMO-LUMO Gaps (in eV), Change in HOMO-LUMO Gaps (in eV) from Bare Nanotubes, Electronic States and Spin Magnetic Moments (μ_B) of Fe Atoms Adsorbed on Type 1 (6, 6) Armchair SiC Nanotube.

Site	HOMO-LUMO gap (eV)	Change in HOMO-LUMO gap (eV)	Electronic State	Spin magnetic moment (μ_B) of Fe atom
C top	1.807	1.125	^5A	3.968
Si top	2.158	0.774	^5A	3.926
Hollow	1.972	0.960	^3A	2.659
Si-C Normal bridge	1.998	0.934	^5A	3.919
Si-C Zigzag bridge	1.853	1.079	^5A	3.865

Table 5.14. HOMO-LUMO Gaps (in eV), Change in HOMO-LUMO Gaps (in eV) from Bare Nanotubes, Electronic States and Spin Magnetic Moments (μ_B) of Fe Atoms Adsorbed on Type 2 (3, 3) Armchair SiC Nanotube.

Site	HOMO-LUMO gap (eV)	Change in HOMO-LUMO gap (eV)	Electronic State	Spin magnetic moment (μ_B) of Fe atom
C top	1.110	0.377	^5A	3.071
Si top	1.092	0.395	^5A	3.074
First hollow	1.055	0.432	^5A	3.046
Second hollow	1.070	0.417	^5A	2.639
C-C normal bridge	0.762	0.725	^5A	2.918
Si-Si normal bridge	1.061	0.426	^5A	3.209
Si-C zigzag bridge	1.066	0.421	^3A	2.986

Table 5.15. HOMO-LUMO Gaps (in eV), Change in HOMO-LUMO Gaps (in eV) from Bare Nanotubes, Electronic States and Spin Magnetic Moments (μ_B) of Fe Atoms Adsorbed on Type 2 (6, 6) Armchair SiC Nanotube.

Site	HOMO-LUMO gap (eV)	Change in HOMO-LUMO gap (eV)	Electronic State	Spin magnetic moment (μ_B) of Fe atom
C top	0.752	0.124	^5A	3.337
Si top	0.860	0.016	^5A	3.266
First hollow	0.549	0.327	^5A	3.256
Second hollow	0.838	0.038	^3A	2.554
C-C normal bridge	0.824	0.052	^3A	2.830
Si-Si normal bridge	0.841	0.035	^5A	3.480
Si-C zigzag bridge	0.852	0.024	^3A	2.905

Table 5.16. HOMO-LUMO Gaps (in eV), Change in HOMO-LUMO Gaps (in eV) from Bare Nanotubes, Electronic States and Spin Magnetic Moments (μ_B) of Fe Atoms Adsorbed on Type 3 (3, 3) Armchair SiC Nanotube.

Site	HOMO-LUMO gap (eV)	Change in HOMO-LUMO gap (eV)	Electronic State	Spin magnetic moment (μ_B) of Fe atom
C top	0.858	0.358	^5A	3.148
Si top	0.843	0.373	^5A	3.155
Hollow	1.450	-0.234	^5A	3.373
Si-C Normal bridge	1.005	0.211	^5A	3.468
Si-C zigzag bridge	0.870	0.346	^5A	3.211
C-C zigzag bridge	0.614	0.602	^5A	2.868
Si-Si zigzag Bridge	0.987	0.229	^3A	2.853

Table 5.17. HOMO-LUMO Gaps (in eV), Change in HOMO-LUMO Gaps (in eV) from Bare Nanotubes, Electronic States and Spin Magnetic Moments (μ_B) of Fe Atoms Adsorbed on Type 3 (6, 6) Armchair SiC Nanotube.

Site	HOMO-LUMO gap (eV)	Change in HOMO-LUMO gap (eV)	Electronic State	Spin magnetic moment (μ_B) of Fe atom
C top	0.786	0.049	^5A	3.680
Si top	0.885	-0.050	^5A	3.217
Hollow	0.773	0.062	^5A	3.203
Si-C Normal bridge	0.779	0.056	^3A	2.659
Si-C zigzag bridge	0.780	0.055	^5A	3.744
C-C zigzag bridge	0.774	0.061	^3A	2.762
Si-Si zigzag Bridge	0.868	-0.033	^3A	2.783

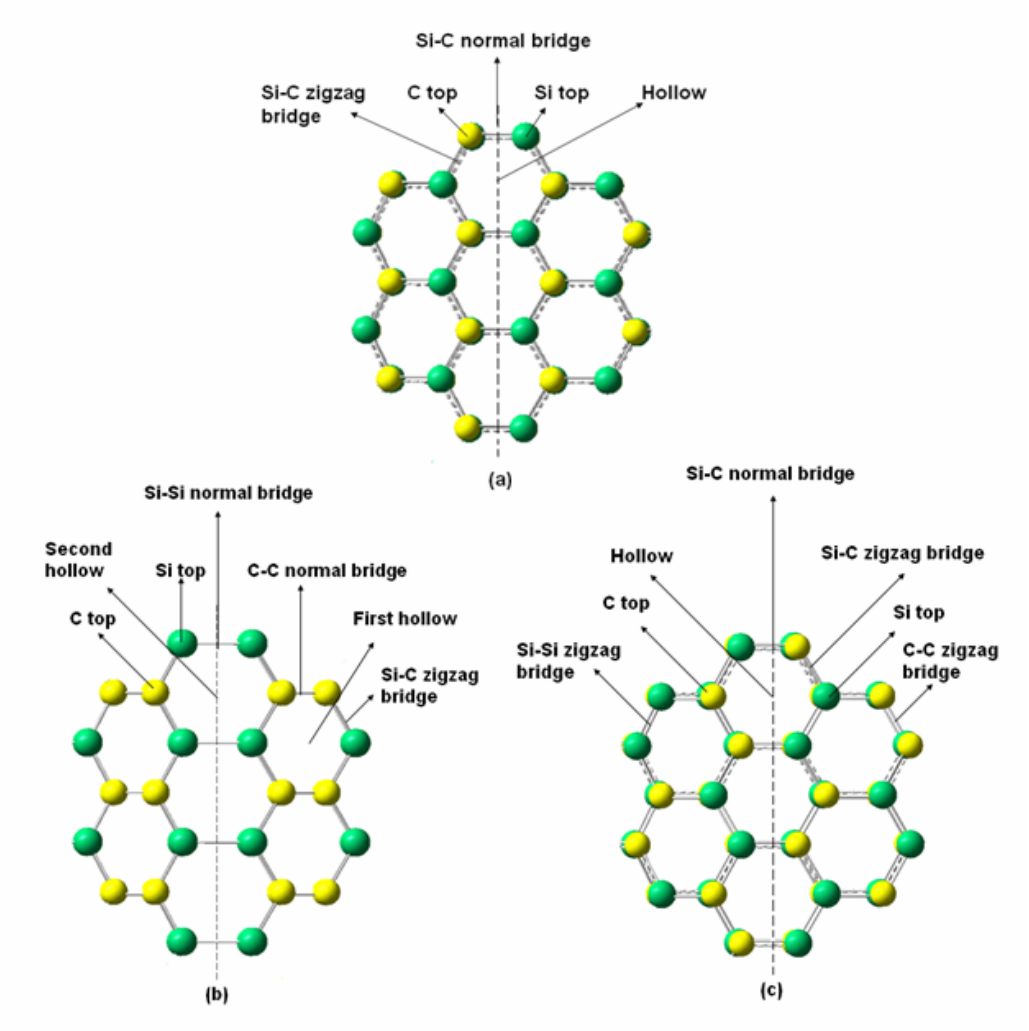

Fig. 5.1. Atomic arrangements and different adsorption sites for (a) type 1, (b) type 2 and (c) type 3 armchair nanotubes. The carbon atoms are yellow and silicon atoms are green. The dashed lines represent the orientation of tube axis.

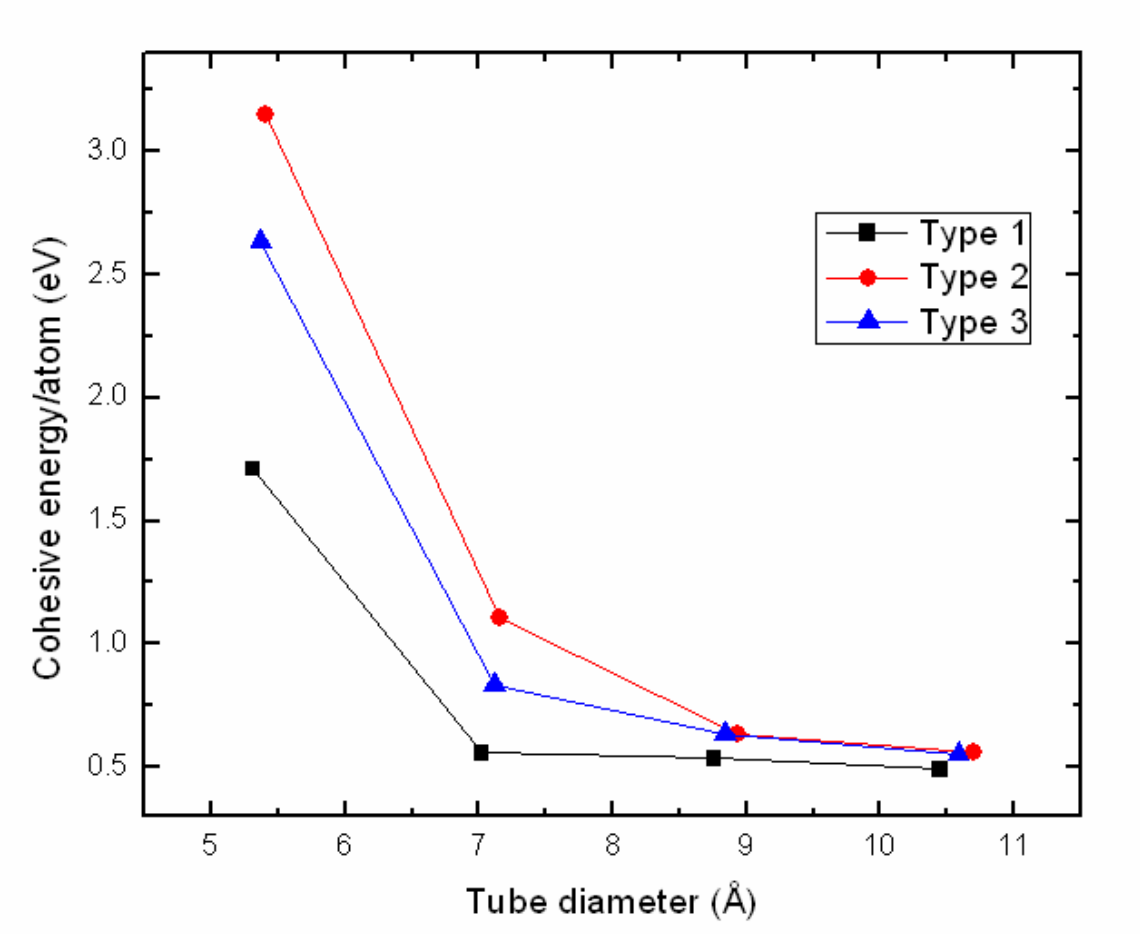

Fig. 5.2. Cohesive energy/atom (eV) vs. tube diameter (Å) for all three types of Fe atom doped armchair nanotubes.

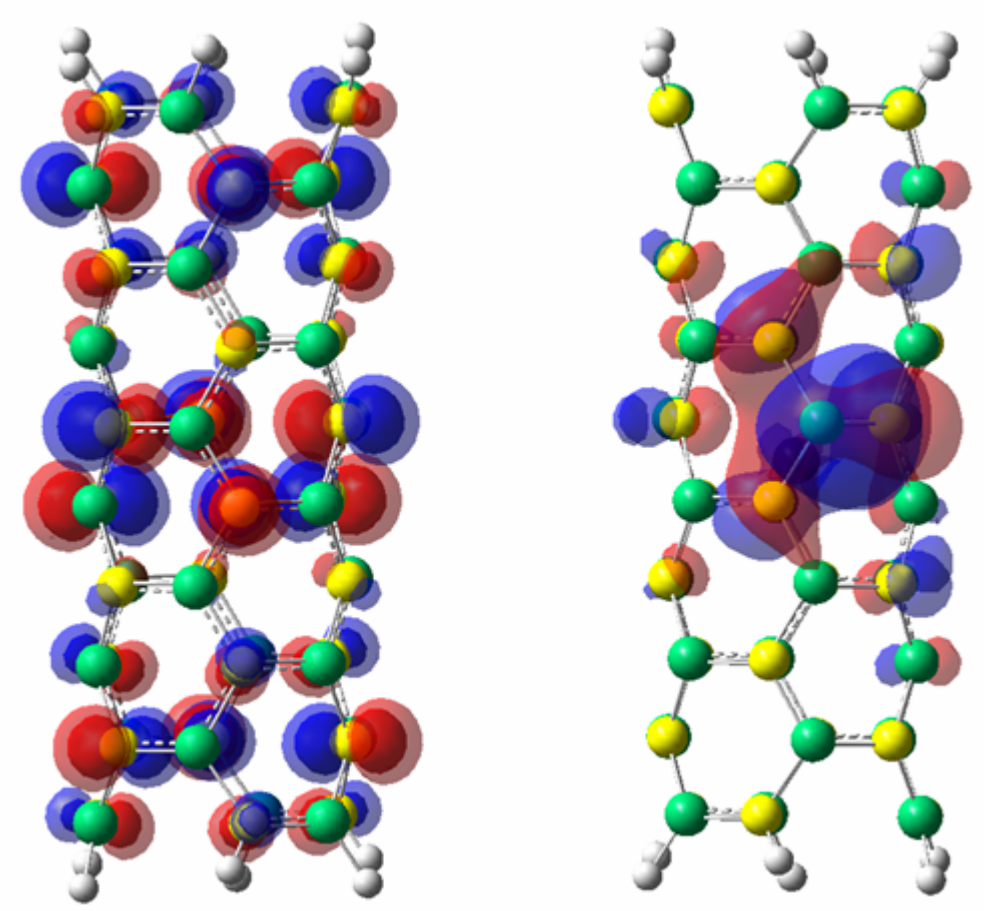

Fig. 5.3. The localization of highest occupied level for type 1 (3, 3) bare (left) and Fe atom doped (right) nanotubes. The green, yellow and black atoms are Si, C and Fe respectively. Red transparent lobes show the positive and blue transparent lobes show the negative values of the wave function.

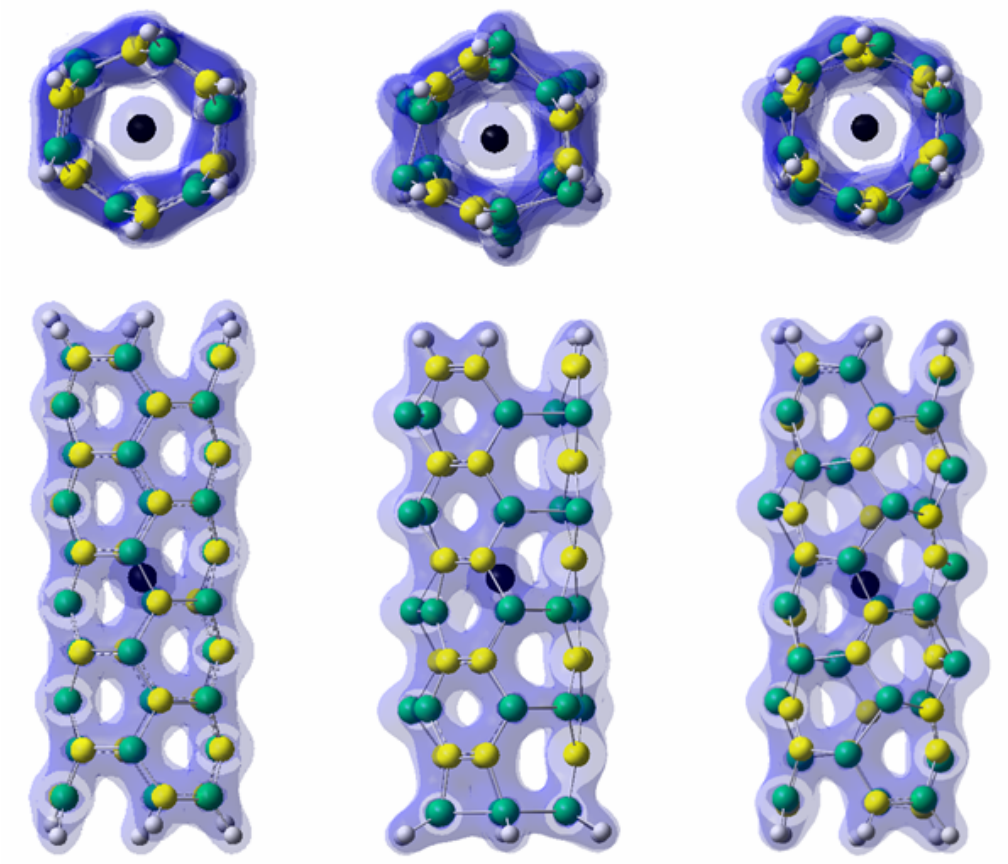

Fig. 5.4. Top and side views of the calculated total charge density (blue color) of Fe encapsulated (3, 3) for type 1 (left), type 2 (middle) and type 3 (right) nanotubes. The green, yellow and black atoms are C, Si and Fe respectively.

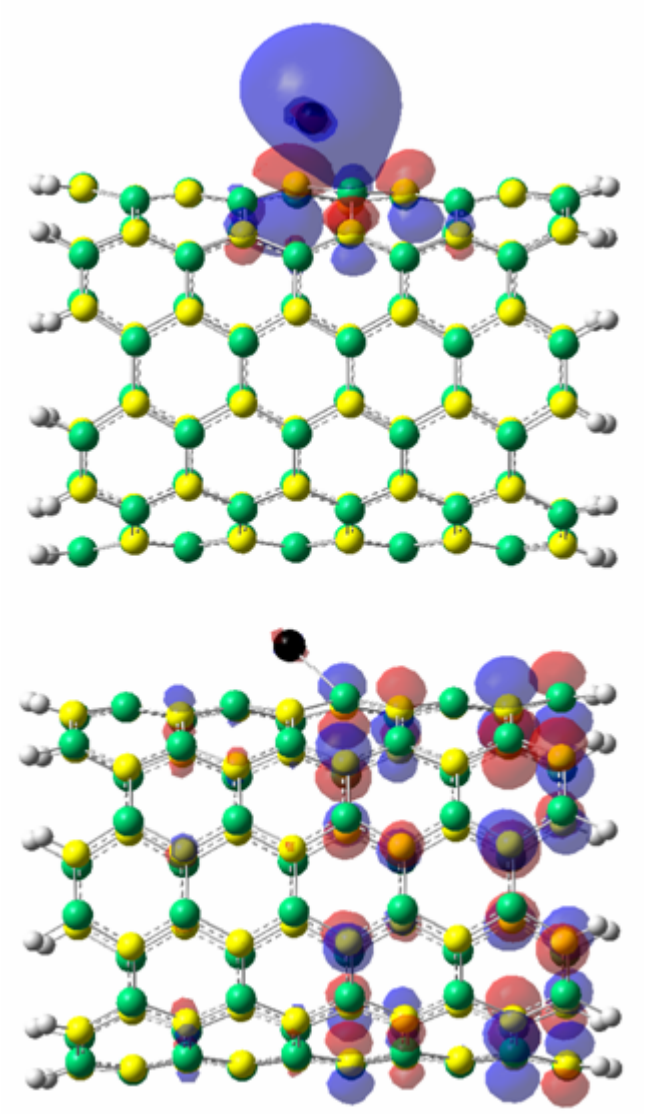

Fig. 5.5. The localization of highest occupied level for Fe atom adsorbed on type 1 (6, 6) nanotube. The most preferred Si-C zigzag bridge site (top) and least preferred hollow site (bottom). The green, yellow and black atoms are Si, C and Fe respectively. Red transparent lobes show the positive and blue transparent lobes show the negative values of the wave function.

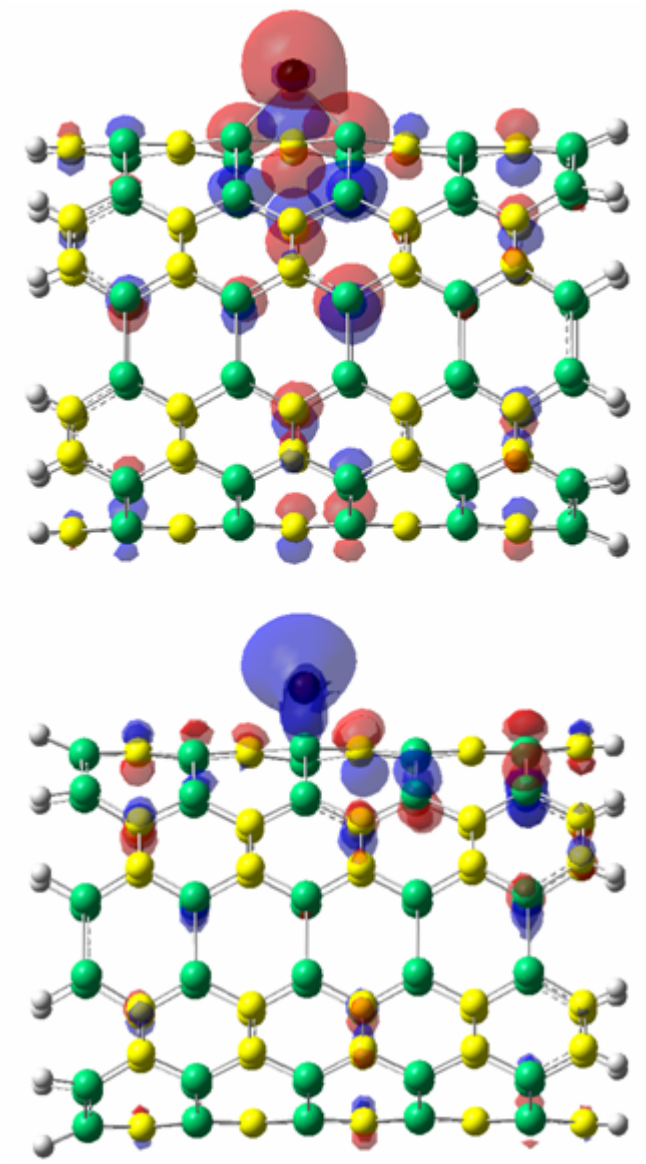

Fig. 5.6. The localization of highest occupied level for Fe atom adsorbed on type 2 (6, 6) nanotube. The most preferred C top site (top) and least preferred first hollow site (bottom). The green, yellow and black atoms are Si, C and Fe respectively. Red transparent lobes show the positive and blue transparent lobes show the negative values of the wave function.

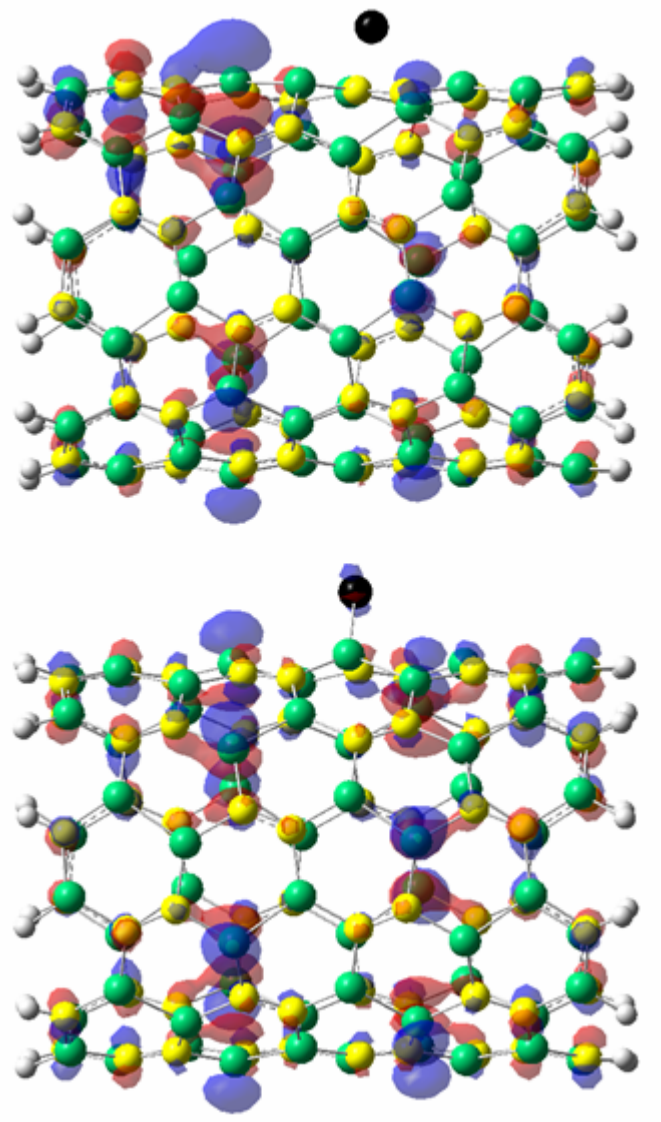

Fig. 5.7. The localization of highest occupied level for Fe atom adsorbed on type 3 (6, 6) nanotube. The most preferred C top site (top) and least preferred Si-C normal bridge site (bottom). The green, yellow and black atoms are Si, C and Fe respectively. Red transparent lobes show the positive and blue transparent lobes show the negative values of the wave function.

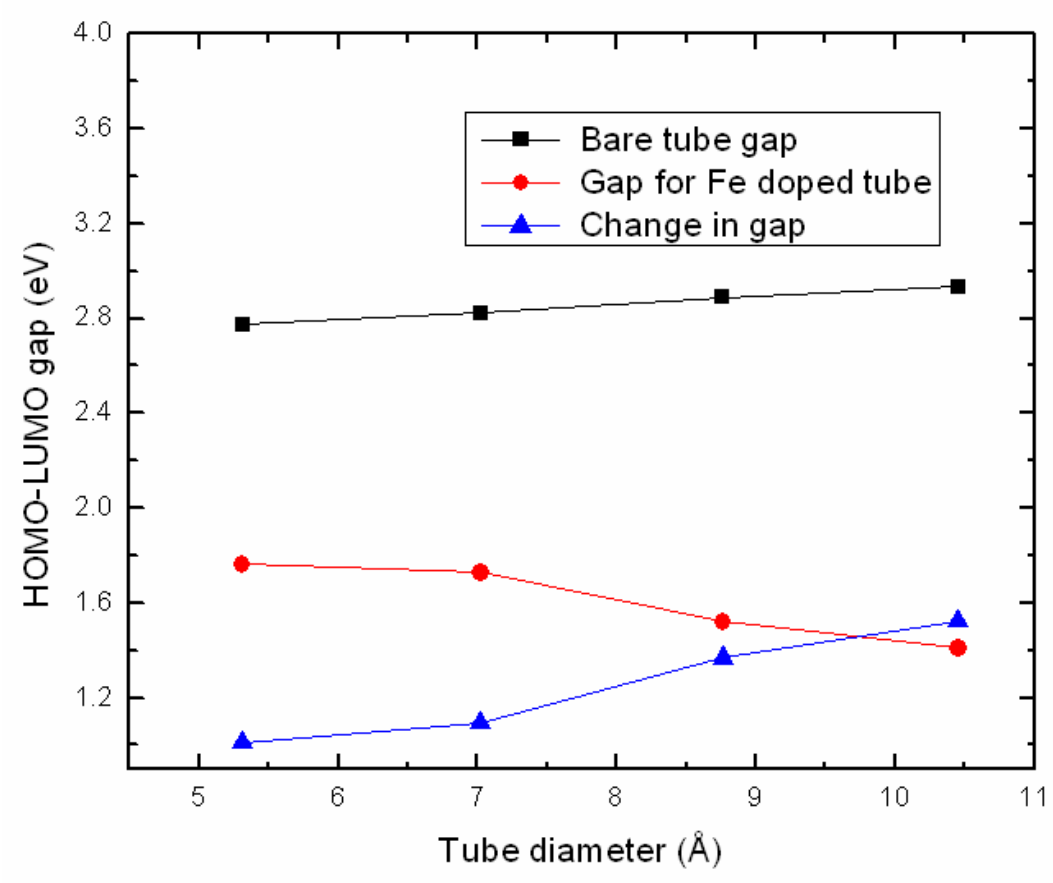

Fig 5.8. Bare nanotube HOMO-LUMO gap (eV), gap for the Fe doped tube and change (decrease) in gap of the doped tube with respect to the bare tube gap vs. tube diameter (Å) for type 1 nanotubes.

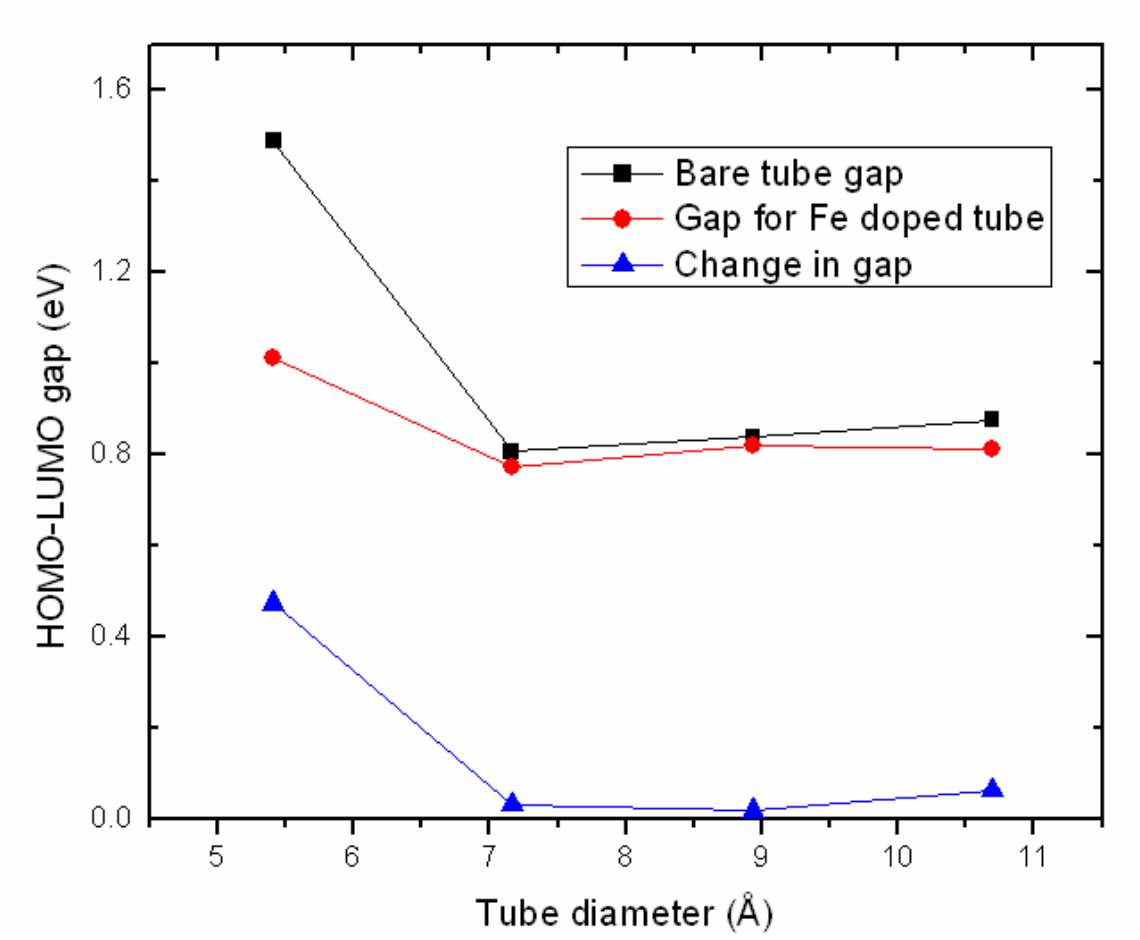

Fig. 5.9. Bare nanotube HOMO-LUMO gap (eV), gap for the Fe doped tube and change (decrease) in gap of the doped tube with respect to the bare tube gap vs. tube diameter (Å) for type 2 nanotubes.

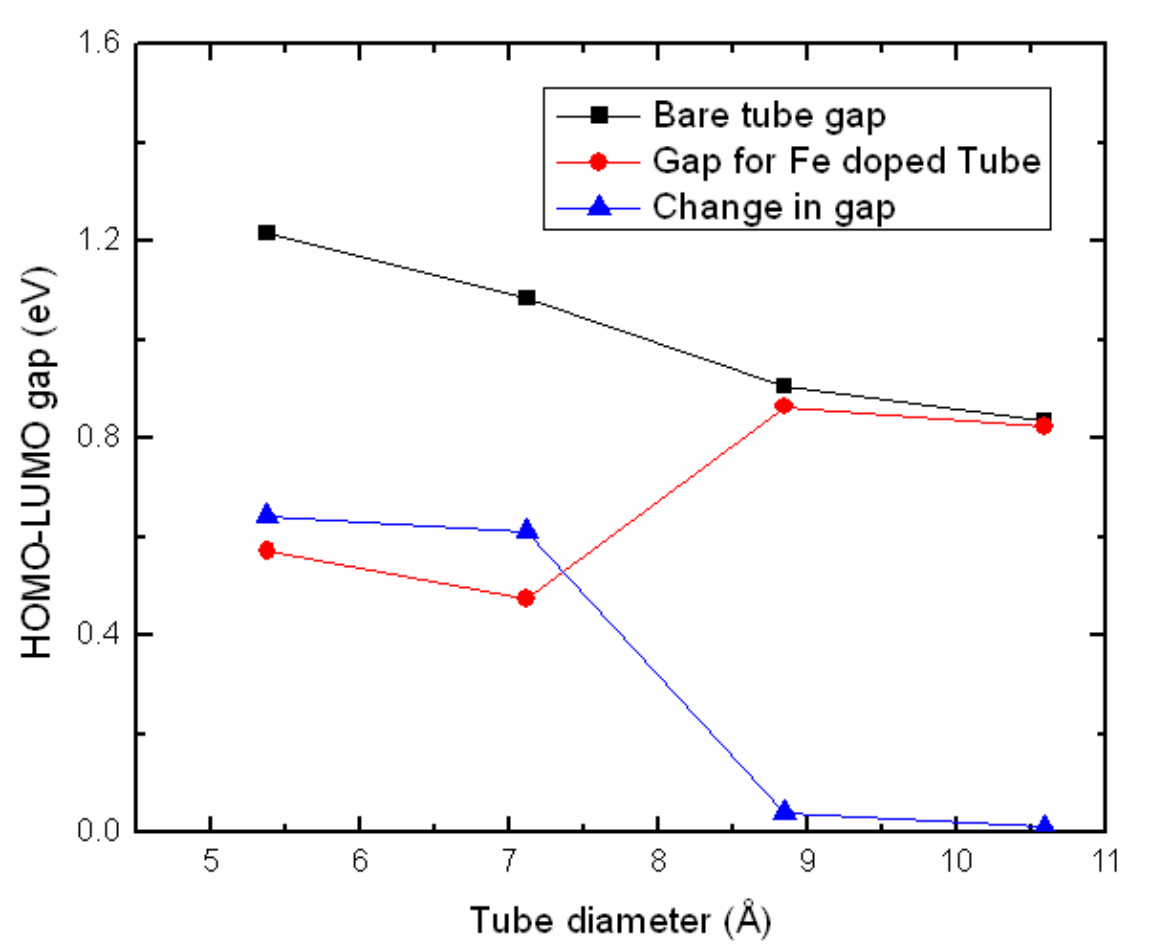

Fig 5.10. Bare nanotube HOMO-LUMO gap (eV), gap for the Fe doped tube and change (decrease) in gap of the doped tube with respect to the bare tube gap vs. tube diameter (Å) for type 3 nanotubes.

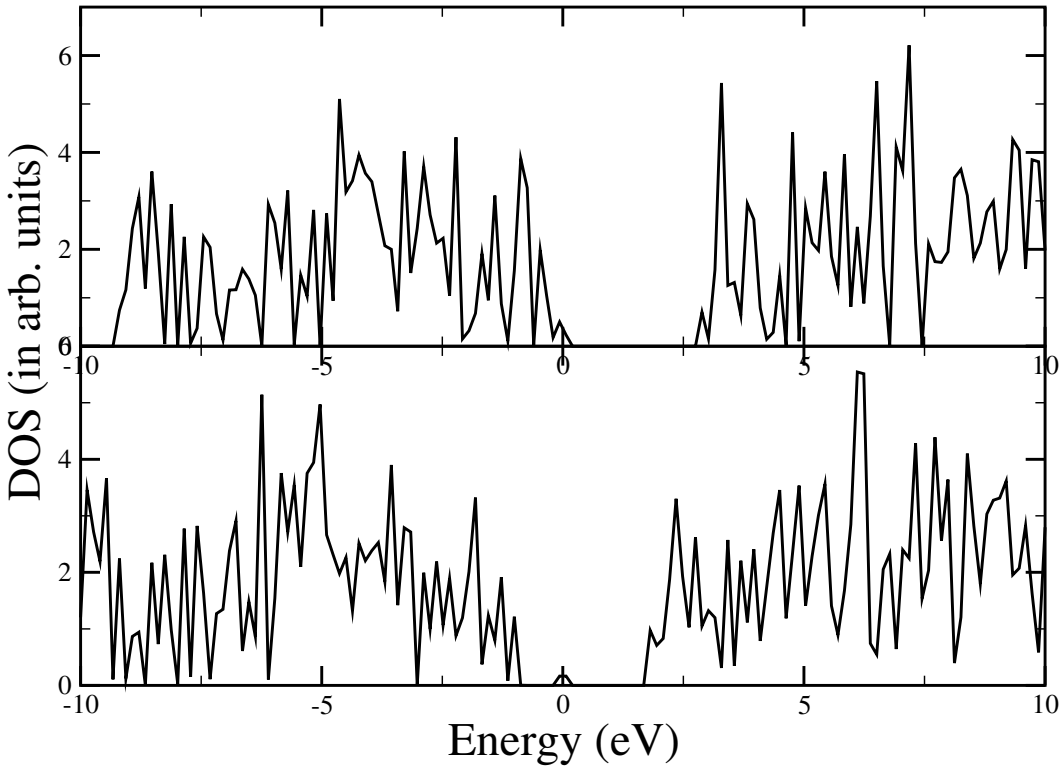

Fig. 5.11. Density of states for type 1 (6, 6) bare (top) and the corresponding Fe adsorbed (for the most stable Si-C zigzag bridge site) (bottom) nanotubes.

CHAPTER 6

INTERACTIONS OF Fe ATOM WITH ZIGZAG SiC NANOTUBES

6.1 Different sites of nanotubes

In this study, a Fe atom is placed at the center of each type of nanotubes from (4, 0) to (8, 0) with the aim of exploring comparative evolution and modification of geometric, electronic and magnetic properties from bare nanotubes along with the relative binding energies of Fe atoms inside those nanotubes. Placing a Fe atom inside nanotubes with higher diameters beyond (8, 0) would not provide significant information due to negligible interaction with the tube wall. In our previous work[113], we have noted that as the size of the nanotubes increased from (3, 0) to (11, 0), binding energies tended to saturate for all three types of nanotubes. From (3, 0) to (6, 0), the increase in binding energies was more prominent and then a slow variation continues up to (11, 0). For this reason and for obvious severe demand on computational resources, we opted to concentrate on Fe adsorption at different sites of (4, 0), (6, 0) and (10, 0) for all three types of nanotubes. Since smallest type 3 zigzag nanotube is (4, 0), we chose (4, 0) instead of (3, 0) as the smallest tube. Fig. 1 shows the relative positions of Si and C atoms in different types of nanotubes. In the type 1 arrangement, with only Si-C bonds, silicon and carbon atoms are placed alternatively without any adjacent Si or C atoms. In types 2 and 3 arrangements with Si-C, Si-Si, and C-C bonds, the nearest neighbors of each Si atom consist of two C atoms and another Si atom and vice versa. The difference between type 2 and type 3 lies in the relative spatial positions of the Si and C atoms. If we consider one layer perpendicular to the tube axis, in type 3, Si and C atoms are alternating while in type 2 each layer contains either Si or C atoms. Fig. 1 also shows the different adsorption sites, five for type 1, seven for types 2 and eight for type 3 nanotubes. There are three major adsorption sites: top, bridge, and hollow. C top and Si top refer to the positions directly perpendicular to the tube wall along the C and Si

atoms respectively. There are two major bridge sites named as normal and zigzag bridge. The relative orientation of those two sites with respect to the tube axis is clearly visible in the figures. Normal bridges are all parallel to the tube axis. Those two bridge sites are named according to their terminal atoms. Hollow sites are at the middle of the hexagons. In type 1 only one type of hexagon is present and there is only one hollow site. In type 2 and 3, two different hexagons are present and this gives rise to two different hollow sites. The first hollow site is associated with the hexagon containing four C and two Si atoms, whereas the second hollow site is positioned along the center perpendicular to hexagon containing two C and four Si atoms.

6.2 Results and discussions

The binding energy for the encapsulated or adsorbed Fe atom is obtained from the expression below.

$$E_b = E\,(SiCNT) + E\,(Fe) - E\,(Fe+SiCNT) \quad (1)$$

where *E (SiCNT)* and *E (Fe)* are the ground state energies of the bare nanotube and Fe atom respectively. *E (Fe + SiCNT)* represent the ground state energy of the Fe encapsulated or adsorbed SiCNT. Table 6.1 shows the stoichiometry and the binding energies of the Fe atom inside the nanotube from (4, 0) to (8, 0) for all types. Though type 1 bare nanotubes were found to be most stable[113], we observed in our previous work on armchair SiCNT[117] that type 2 tubes have the strongest interactions with Fe atoms followed by type 3 and then type 1. Here from table 1 we notice that in type 1 zigzag SiCNTs Fe atom has the maximum binding energy then type 2 followed by type 3. As the diameter or the tube size increases, interactions between Fe atom and tube wall decrease for all types. After optimization Fe atoms were found to retain their initial positions (center of the tube) with negligible deviation along the tube axis. The diameters did not change upon Fe atom encapsulation, from that of bare nanotubes. It is predicted that for higher diameter type 3 tubes will not bind Fe atom as from table 6.1 we see a negative binding energy for Fe atom when encapsulated in (8, 0). The Mulliken charges on the Fe atom are shown in table 6.2. In general charge transfer occurs from the tube to the Fe atom. This

direction of charge transfer is reversed for (6, 0) of all types, (7, 0) for type 2 and (8, 0) for type 2 and 3. Figure 6.2 demonstrates how the highest occupied molecular orbital (HOMO) is localized in type 1 and 3 (4, 0). The undoped tube HOMO was uniformly distributed in type 3 and localized to one side of the tube in both type 1 type 2. This is attributed to the fact that type 1 and 2 SiCNTs have either C or Si atoms at the end unlike in type 3. Figure 6.2 also shows that upon Fe atom encapsulation in type 1 tubes HOMO is redistributed uniformly through the entire tube with a higher concentration around the Fe atom. Similar behavior was found for type 2. However Fe atom doping inside type 3 tubes redistributed the HOMO in a reverse way, changing from uniform to localized distribution. This HOMO localization is indicative of the shift of more reactive regions of the nanotube upon Fe atom encapsulation. The total charge density for the smallest type 1 and 2 nanotubes (4, 0) is shown in figure 6.3. We note that for type 1, there is significant overlap between the charge of the Fe atom with the SiCNT than that of type 2.

Tables 6.3 through 6.11 show Fe atom adsorption energies, distances of Fe atom from the tube wall, nearest C-Fe and Si-Fe distances, and the Mulliken charges of Fe atom for (4, 0), (6, 0) and (10, 0) nanotubes of three types. Only (4, 0), (6, 0) and (10, 0) tubes were considered here since no significantly new results were expected by studying the tubes with other diameters and also because we are interested in the curvature effects of the tubes. There are five possible sites for type 1, seven sites for type 2 and eight sites for type 3 described earlier. For type 1 (4, 0), C top site is the most stable and hollow site is the least stable sites, with a difference in adsorption energy of 0.937 eV. The corresponding sites for type 2 (4, 0) are first hollow and second hollow, with a difference in adsorption energy of 1.837 eV. In case of type 3 (4, 0), they are Si-Si zigzag bridge and second hollow, with the corresponding difference being 1.054 eV. The C top for type 1 and type 3 (6, 0) and first hollow for type 2 (6, 0) are the most stable Fe adsorption sites. The difference in adsorption energies between the most and least favored sites for type 1 (6, 0) is about 0.618eV. These values are 4.232 eV and 1.318 eV for

type 2 (6, 0) and type 3 (6, 0), respectively. In case of type 1 (10, 0) the most preferred site is hollow and least preferred site is Si-C normal bridge with an energy difference of 1.371eV. The corresponding sites for type 2 (10, 0) and type 3 (10, 0) are first hollow, Si-C zigzag bridge and Si-Si zigzag bridge, Si top respectively. It is interesting to note that with the tube curvature change most preferred sites are changed for type 1 and type 3 nanotubes whereas type 2 nanotubes retain their most stable site as the first hollow. Another noticeable observation is that in general Fe prefers to bond with C than with Si, consistent with our Fe-C and Fe-Si dimer calculations, where the binding energies/atom are 1.81 eV and 1.26 eV, respectively. Using the DMol3 suite of software, for Ti adsorption on type 1 (5, 5) SiCNT, Meng *et al.*[53] found the most favorable site to be the C top site. Using periodic boundary conditions and the Dmol3 suite of software, Zhao and Ding have also found the same trend in (8, 0) for Fe adsorption.[54] We also note that Fe adsorption energy decreases with increasing radius (or decreasing curvature) of the tube for all types with some exceptions. Therefore by creating regions of different curvature on a single SiCNT by radial deformation or by designing different types of tubes, it is possible to get different values of adsorption energies. The average adsorption energy of Fe atom on a type 1 (4, 0), (6, 0) and (10, 0) are 2.712eV, 1.341eV and 1.548eV. For type 2, the corresponding numbers are 3.372eV, 3.365eV and 1.964eV and for type 3, 3.180eV, 2.532eV and 1.810eV. So type 2 and type 3 nanotubes have better Fe adsorption capacity as a whole; in other words, complete Fe coating is predicted to be more facile for these two types of SiC nanotubes. Despite possessing highest binding energy/atom for the bare tube, type 1 tubes have the least possibility of being coated with Fe atoms. This implies Fe-Fe interaction can dominate over Fe-nanotube interaction which might result in forming isolated Fe clusters than complete Fe coating. Similar conclusion was drawn for armchair SiC nanotubes in our previous calculations.[117] However type 1 nanotubes retain their shape after Fe atom adsorption unlike other types that undergo some degree of structural distortions for all sites and for some cases even bond breakings. Both (4, 0) and (6, 0) type 1 nanotubes were found to maintain original

shape after adsorption. Figure 6.4 showing (4, 0) nanotubes for all types. The breakings of bonds are marked in red lines. We did not observe any other bond breaking in any other nanotubes, but structural deformation is more pronounced in both types 2 and 3 nanotubes. These distortions from bare tube, upon Fe atom adsorption might degenerate ballistic conduction properties of the nanotubes. However this deformation was not observed for the (10, 0) nanotubes.

Mulliken charge analysis shows electron transfer occurs from Fe atom to the nanotube for all sites of all types except for second hollow site of type 3 (4, 0), Si-Si zigzag bridge site of type 3 (6, 0) and C top site of type 1 (10, 0) where Fe atom gains 0.792e, 0.018e and 0.108e from the tube, respectively. No trend between amount of charge transfer and adsorption energy of the site was found here, suggesting the local structure as a whole determines the amount and direction of charge transfer as well as the binding strength of the adsorbent. From adsorption energies, it can be inferred that the most favorable sites for the three types of (6, 0) nanotubes first hollow site of type 2 has the maximum adsorption energy, followed by Si-C zigzag bridge and Si-Si normal bridge sites of the same. The corresponding order of the sites for (4, 0) is again first hollow, Si-Si normal bridge and Si-C zigzag bridge site of type 2 respectively. When Fe atom was placed on C top and Si top sites of (6, 0) and (4, 0) SiCNTs, the adatom slightly migrated toward the neighboring normal, zigzag bridge or hollow sites but did not deviate completely from the initial positions. This is the reason we see slight differences between the distances of Fe atom from the tube wall and the Fe-C and Fe-Si distances for the C top and Si top sites. Figures 6.5, 6.6, and 6.7 show the HOMO localizations for the most and the least preferred sites for all three types (6, 0) nanotubes with Fe atom adsorbed on them. The more localization of the “negative” and “positive” values of the wave function is found for the most preferred sites for type 2 and 3. The difference in localization is not visible for the type 1 sites. The reason is attributed to the fact that the difference in adsorption energies between

the most and least preferred sites for type 1 configuration is small compared to those for the other two types.

In nanotube and fullerene based technology, molecular electronic structures are required with a wide variety of mechanical, electronic, optical and magnetic properties. Band gap tailoring is an important issue for different purposes especially when coupling of nanostructures is concerned in a complex network. Tables 6.12-6.23 show the HOMO-LUMO gaps of the (Fe+SiCNT) system and the change of the gaps with respect to the bare nanotube gaps.[113] In our previous calculation for bare nanotubes, band gaps for type 1 nanotubes were found to be larger than type 2 and type 3 nanotubes in average. Unlike the other two types, band gap for type 3 nanotubes showed a monotonous decreasing trend with increasing tube diameter. Table 6.12 and figure 6.8 show the variation of these gaps with tube diameter for the Fe atom encapsulated in type 1 nanotube. In our previous study on armchair nanotubes[117] there was a continuous decrease in gap with increasing tube diameter for the Fe encapsulated tube. This trend was reversed from the bare tube gap variation. Here we see that Fe atom doped tubes have same zigzag trend in band gaps like pristine zigzag tubes. The reduction in band gap is not significant upon Fe atom encapsulation for type 1 zigzag nanotubes unlike armchair case.[117] Table 6.13 and figure 6.9 show the variation of gaps with tube diameter for the Fe atom encapsulation in type 2 nanotubes. This variation for type 3 is shown in table 6.14 and figure 6.10. In case of types 2 and 3 this band gap remains almost unchanged. Type 2 (5, 0) and type 3 (6, 0) show an increase of gaps. These results indicate that band gaps tuning by Fe doping inside the zigzag tubes is not very promising for SiC nanotubes in zigzag configuration. The HOMO-LUMO gaps and the corresponding changes in gaps from the bare nanotubes for different adsorption sites of three types of zigzag SiCNTs have been presented in tables 6.15-6.23. Our previous results[113] showed the bare nanotube (6, 0) gaps to be 0.669eV, 0.436eV, and 0.505eV for types 1, 2 and 3, respectively. These gaps were 0.662eV, 0.539eV and 0.661eV for the (4, 0) tubes in three configurations. Bare (10, 0) nanotube gaps were 0.129eV,

0.163eV and 0.285eV respectively for type 1, type 2 and type 3. For (6, 0) we observe the gap change is more significant for type 1 only. Among all the five sites the reduction in band gap is 0.369eV and 0.272eV for C top and Si-C normal bridge sites respectively. There is small gap increase for the other sites of this structure. Adsorbing Fe atom can slightly decrease the gap when it is at the Si top site of type 2 (6, 0) nanotube. All other sites of type 2 (6, 0) show very small gap increase. Type 3 (6, 0) sites also do not show any remarkable gap modification upon Fe adsorption on any of the seven sites. Unlike all other sites Si top, Si-C normal bridge and Si-Si zigzag bridge sites show a very small gap increase upon Fe atom adsorption. The other sites show negligible gap decrease except C top and second hollow site where we see gap decrease values are comparatively higher, 0.139eV and 0.154eV respectively. In case of (4, 0) type 1 sites also showed the minimum reduction of gaps upon Fe adsorption. However unlike type 1 (4, 0), type 2 and type 3 (4, 0) tubes show higher band gap modification. Most of the sites of (10, 0) nanotubes show significant band gap increase for all types. All these results show that band gap tailoring is feasible for higher diameter nanotubes. Figure 6.11 demonstrates energy density of states (DOS) for pristine type 1 (6, 0) nanotube, the corresponding Fe atom adsorbed nanotube that has the maximum adsorption energy (Si-C zigzag bridge site) and minimum adsorption energy (Si top site). The DOS is built by fitting a Gaussian function in each eigenvalue and then summing them up. The Gaussian width used to broaden the eigenvalues is 0.05 eV and E=0 refers to the HOMO. It is interesting to notice that for the most stable C top site band gap decrease is highest and for the least stable Si top site band gap increase is highest among all the five sites of type 1 (6, 0) nanotube. These observations on band gap decrease and increase in zigzag SiCNTs which are highly site dependent might play important role at the metal nanotube junction in molecular electronic networks or other potential applied areas of band gap engineering.

All the (Fe + SiCNT) systems we studied here have magnetic ground states. A bare zigzag SiCNT has a magnetic ground state too[113] but with a smaller value of net magnetic

moment. This high spin of (Fe + SiCNT) system originates from the magnetic moment of the encapsulated and adsorbed Fe atom. Tables 6.12-6.17 show the electronic states and the spin magnetic moments of Fe atom inside and outside the tube. It is evident from the tables that encapsulated Fe atom loses its magnetic moment more inside the smaller tubes where interaction is stronger. This fact is common for all three types of SiCNTs. Mulliken population analysis shows that the more 4s electron migration to 4p and 3d orbitals of Fe atom is responsible for this quenching of magnetic moment in case of smaller diameter nanotubes where Fe atom and nanotube interaction is stronger. Magnetic moment of Fe atom placed at the center inside (8, 0) carbon nanotube [48] was found to be 2.36 μ_B. These values were 2.46 for (3, 3) CNT [115] and 2.3 for (4, 4) CNT[116]. In our previous work[117] on armchair and from table 12-14 we see these values are higher for zigzag tubes of all types which indicate that Fe atom retains its magnetic moment inside SiCNT more than it does inside CNT. From the values of the magnetic moments of Fe atom for different adsorption sites of three types of tubes, it is obvious that Fe atom magnetic moments have more site dependence on type 2 and 3 than type 1 sites. This site dependence also changes with diameter of the tubes. In type 3 (4, 0) and (6, 0) Fe atom magnetic moments are almost completely quenched for first hollow and Si-Si zigzag bridge sites. This variation was not observed in our previous calculations on armchair (SiCNT + Fe) system.[117] The high magnetic moments generated upon encapsulation and adsorption of Fe atom in single wall both armchair and zigzag SiCNTs should have important implications in spintronics applications.

Table 6.1. Cohesive Energies/atom (in eV) for Fe Atom Encapsulated in Zigzag SiC Nanotubes.

Nanotube	Stoichiometry	Total number of atoms	Binding energy of Fe atom (eV) inside the nanotube		
			Type1	Type2	Type3
SiC (4, 0)	$Si_{44}C_{44}H_8Fe_1$	97	4.548	3.798	3.594
SiC (5, 0)	$Si_{55}C_{55}H_{10}Fe_1$	121	2.877	2.827	
SiC (6, 0)	$Si_{66}C_{66}H_{12}Fe_1$	145	1.615	1.439	1.650
SiC (7, 0)	$Si_{77}C_{77}H_{14}Fe_1$	169	0.811	0.259	
SiC (8, 0)	$Si_{88}C_{88}H_{16}Fe_1$	193	0.629	0.097	-0.532

Table 6.2. Tube Diameters (in Å) and Mulliken Charges of Encapsulated Fe Atoms.

Nanotube	Tube diameter (Å)			Mulliken charge of Fe atom		
	Type1	Type2	Type3	Type1	Type2	Type3
SiC (4, 0)	4.249	4.303	4.319	-0.873	-1.880	-0.752
SiC (5, 0)	5.175	5.237		-0.326	-0.851	
SiC (6, 0)	6.127	6.189	6.244	0.070	0.436	0.496
SiC (7, 0)	7.098	7.152		-0.084	0.462	
SiC (8, 0)	8.074	8.136	8.201	-0.039	0.411	0.418

Table 6.3. Adsorption Energies of Fe Atoms (eV), Distances of Fe Atoms from Tube Walls (Å), Nearest C-Fe Distances (Å), Nearest Si-Fe Distances (Å), and Mulliken Charges of Fe Atoms Adsorbed on Type 1 (4, 0) Zigzag SiC Nanotube.

Site	Adsorption energy of Fe atom (eV)	Distance of Fe atom from tube wall (Å)	Nearest C-Fe distance (Å)	Nearest Si-Fe distance (Å)	Mulliken charge of Fe atom
C top	3.101	1.921	1.939	2.649	0.427
Si top	2.986	2.024	2.153	2.581	0.443
Hollow	2.164	1.204	2.043	2.278	0.426
Si-C normal Bridge	2.713	1.996	2.104	2.639	0.439
Si-C zigzag bridge	2.598	1.637	2.005	2.648	0.396

Table 6.4. Adsorption Energies of Fe Atoms (eV), Distances of Fe Atoms from Tube Walls (Å), Nearest C-Fe Distances (Å), Nearest Si-Fe Distances (Å), and Mulliken Charges of Fe Atoms Adsorbed on Type 1 (6, 0) Zigzag SiC Nanotube.

Site	Adsorption energy of Fe atom (eV)	Distance of Fe atom from tube wall (Å)	Nearest C-Fe distance (Å)	Nearest Si-Fe distance (Å)	Mulliken charge of Fe atom
C top	1.577	2.089	2.104	2.488	0.060
Si top	0.959	2.455	3.049	2.480	0.223
Hollow	1.215	1.648	2.155	2.453	0.269
Si-C normal Bridge	1.410	2.015	2.157	2.579	0.301
Si-C zigzag bridge	1.542	1.952	2.086	2.432	0.276

Table 6.5. Adsorption Energies of Fe Atoms (eV), Distances of Fe Atoms from Tube Walls (Å), Nearest C-Fe Distances (Å), Nearest Si-Fe Distances (Å), and Mulliken Charges of Fe Atoms Adsorbed on Type 1 (10, 0) Zigzag SiC Nanotube.

Site	Adsorption energy of Fe atom (eV)	Distance of Fe atom from tube wall (Å)	Nearest C-Fe distance (Å)	Nearest Si-Fe distance (Å)	Mulliken charge of Fe atom
C top	1.473	2.133	2.154	2.698	-0.108
Si top	1.616	2.524	3.376	2.668	0.193
Hollow	2.054	1.796	2.306	2.450	0.188
Si-C normal Bridge	0.683	2.177	2.315	2.461	0.226
Si-C zigzag bridge	1.915	2.056	2.155	2.373	0.128

Table 6.6. Adsorption Energies of Fe Atoms (eV), Distances of Fe Atoms from Tube Walls (Å), Nearest C-Fe Distances (Å), Nearest Si-Fe Distances (Å), and Mulliken Charges of Fe Atoms Adsorbed on Type 2 (4, 0) Zigzag SiC Nanotube.

Site	Adsorption energy of Fe atom (eV)	Distance of Fe atom from tube wall (Å)	Nearest C-Fe distance (Å)	Nearest Si-Fe distance (Å)	Mulliken charge of Fe atom
C top	2.833	1.652	1.985	3.119	0.581
Si top	3.187	2.294	3.410	2.467	0.178
First hollow	4.592	1.853	3.152	2.391	0.226
Second hollow	2.755	1.054	2.167	2.474	0.471
C-C normal bridge	2.757	1.693	2.005	3.156	0.572
Si-Si normal bridge	3.814	2.123	3.937	2.402	0.222
Si-C zigzag bridge	3.669	1.987	2.105	2.337	0.288

Table 6.7. Adsorption Energies of Fe Atoms (eV), Distances of Fe Atoms from Tube Walls (Å), Nearest C-Fe Distances (Å), Nearest Si-Fe Distances (Å), and Mulliken Charges of Fe Atoms Adsorbed on Type 2 (6, 0) Zigzag SiC Nanotube.

Site	Adsorption energy of Fe atom (eV)	Distance of Fe atom from tube wall (Å)	Nearest C-Fe distance (Å)	Nearest Si-Fe distance (Å)	Mulliken charge of Fe atom
C top	3.696	1.895	2.116	2.436	0.236
Si top	2.005	2.261	3.610	2.411	0.217
First hollow	5.370	2.341	3.294	2.477	0.219
Second hollow	1.138	1.820	2.413	2.499	0.209
C-C normal bridge	2.348	1.943	2.080	3.087	0.402
Si-Si normal bridge	4.060	2.065	3.910	2.453	0.139
Si-C zigzag bridge	4.937	1.847	2.203	2.439	0.181

Table 6.8. Adsorption Energies of Fe Atoms (eV), Distances of Fe Atoms from Tube Walls (Å), Nearest C-Fe Distances (Å), Nearest Si-Fe Distances (Å), and Mulliken Charges of Fe Atoms Adsorbed on Type 2 (10, 0) Zigzag SiC Nanotube.

Site	Adsorption energy of Fe atom (eV)	Distance of Fe atom from tube wall (Å)	Nearest C-Fe distance (Å)	Nearest Si-Fe distance (Å)	Mulliken charge of Fe atom
C top	2.211	1.926	2.071	2.611	0.238
Si top	2.056	2.389	3.463	2.604	0.209
First hollow	2.856	2.241	3.270	2.478	0.137
Second hollow	1.636	1.695	2.790	2.801	0.207
C-C normal bridge	1.579	1.952	2.030	2.780	0.276
Si-Si normal bridge	2.108	2.410	3.805	2.647	0.191
Si-C zigzag bridge	1.302	2.019	2.192	2.454	0.156

Table 6.9. Adsorption Energies of Fe Atoms (eV), Distances of Fe Atoms from Tube Walls (Å), Nearest C-Fe Distances (Å), Nearest Si-Fe Distances (Å), and Mulliken Charges of Fe Atoms Adsorbed on Type 3 (4, 0) Zigzag SiC Nanotube.

Site	Adsorption energy of Fe atom (eV)	Distance of Fe atom from tube wall (Å)	Nearest C-Fe distance (Å)	Nearest Si-Fe distance (Å)	Mulliken charge of Fe atom
C top	3.044	1.731	2.065	2.449	0.171
Si top	2.329	2.492	3.574	2.446	0.219
First hollow	2.864	1.706	2.180	2.480	0.194
Si-C normal bridge	2.522	2.663	3.531	2.394	0.269
Si-C zigzag bridge	3.134	1.786	2.111	2.496	0.203
C-C zigzag bridge	3.028	1.871	2.032	2.470	0.234
Si-Si zigzag Bridge	3.195	1.955	3.574	2.446	0.162
Second hollow	2.141	0.655	2.578	2.361	-0.792

Table 6.10. Adsorption Energies of Fe Atoms (eV), Distances of Fe Atoms from Tube Walls (Å), Nearest C-Fe Distances (Å), Nearest Si-Fe Distances (Å), and Mulliken Charges of Fe Atoms Adsorbed on Type 3 (6, 0) Zigzag SiC Nanotube.

Site	Adsorption energy of Fe atom (eV)	Distance of Fe atom from tube wall (Å)	Nearest C-Fe distance (Å)	Nearest Si-Fe distance (Å)	Mulliken charge of Fe atom
C top	2.816	2.074	2.183	2.431	0.083
Si top	2.769	2.141	3.315	2.343	0.142
First hollow	1.498	1.610	2.462	2.456	0.159
Si-C normal bridge	1.707	2.343	2.492	2.401	0.259
Si-C zigzag bridge	2.477	2.098	2.198	2.432	0.226
C-C zigzag bridge	2.075	1.786	2.073	2.483	0.170
Si-Si zigzag Bridge	2.344	2.024	3.376	2.318	-0.018
Second hollow	2.039	2.332	3.413	2.492	0.148

Table 6.11. Adsorption Energies of Fe Atoms (eV), Distances of Fe Atoms from Tube Walls (Å), Nearest C-Fe Distances (Å), Nearest Si-Fe Distances (Å), and Mulliken Charges of Fe Atoms Adsorbed on Type 3 (10, 0) Zigzag SiC Nanotube.

Site	Adsorption energy of Fe atom (eV)	Distance of Fe atom from tube wall (Å)	Nearest C-Fe distance (Å)	Nearest Si-Fe distance (Å)	Mulliken charge of Fe atom
C top	2.036	2.103	2.062	2.428	0.240
Si top	0.794	2.397	3.563	2.447	0.221
First hollow	1.824	1.608	2.381	2.405	0.208
Si-C normal bridge	1.859	2.150	2.170	2.471	0.199
Si-C zigzag bridge	2.022	2.123	2.195	2.352	0.221
C-C zigzag bridge	1.667	1.917	1.985	2.570	0.195
Si-Si zigzag Bridge	2.200	2.363	3.551	2.411	0.089
Second hollow	2.080	2.135	3.160	2.510	0.156

Table 6.12. HOMO-LUMO Gaps (in eV), Change in HOMO-LUMO Gaps (in eV) from Bare Nanotubes, Electronic States and Spin Magnetic Moments (μ_B) of Fe Atoms Encapsulated in type 1 Zigzag SiC Nanotubes.

Nanotube	HOMO-LUMO gap (eV)	Change in HOMO-LUMO gap (eV)	Electronic state	Spin magnetic moment (μ_B) of Fe atom
(4, 0)	0.659	0.003	^{5}A	1.873
(5, 0)	0.840	0.041	^{5}A	2.843
(6, 0)	0.296	0.373	^{5}B	2.968
(7, 0)	0.554	0.245	^{5}A	3.964
(8, 0)	0.177	0.110	^{5}A	3.988

Table 6.13. HOMO-LUMO Gaps (in eV), Change in HOMO-LUMO Gaps (in eV) from Bare Nanotubes, Electronic States and Spin Magnetic Moments (μ_B) of Fe Atoms Encapsulated in type 2 Zigzag SiC Nanotubes.

Nanotube	HOMO-LUMO gap (eV)	Change in HOMO-LUMO gap (eV)	Electronic state	Spin magnetic moment (μ_B) of Fe atom
(4, 0)	0.536	0.003	^{5}A	1.774
(5, 0)	0.534	-0.108	^{5}A	2.069
(6, 0)	0.416	0.020	^{5}B	3.139
(7, 0)	0.363	0.137	^{5}A	4.285
(8, 0)	0.362	0.175	^{5}A	4.108

Table 6.14. HOMO-LUMO Gaps (in eV), Change in HOMO-LUMO Gaps (in eV) from Bare Nanotubes, Electronic States and Spin Magnetic Moments (μ_B) of Fe Atoms Encapsulated in type 3 Zigzag SiC Nanotubes.

Nanotube	HOMO-LUMO gap (eV)	Change in HOMO-LUMO gap (eV)	Electronic state	Spin magnetic moment (μ_B) of Fe atom
(4, 0)	0.594	0.067	^{5}A	2.725
(6, 0)	0.523	-0.018	^{5}A	3.115
(8, 0)	0.255	0.133	^{5}A	4.187

Table 6.15. HOMO-LUMO Gaps (in eV), Change in HOMO-LUMO Gaps (in eV) from Bare Nanotubes, Electronic States and Spin Magnetic Moments (μ_B) of Fe Atoms Adsorbed on Type 1 (4, 0) Zigzag SiC Nanotube.

Site	HOMO-LUMO gap (eV)	Change in HOMO-LUMO gap (eV)	Electronic State	Spin magnetic moment (μ_B) of Fe atom
C top	0.582	0.080	^5A	3.120
Si top	0.651	0.011	^3A	3.128
Hollow	0.698	0.036	^5A	3.207
Si-C Normal bridge	0.649	0.013	^3A	3.165
Si-C Zigzag bridge	0.603	0.059	^3A	3.042

Table 6.16. HOMO-LUMO Gaps (in eV), Change in HOMO-LUMO Gaps (in eV) from Bare Nanotubes, Electronic States and Spin Magnetic Moments (μ_B) of Fe Atoms Adsorbed on Type 1 (6, 0) Zigzag SiC Nanotube.

Site	HOMO-LUMO gap (eV)	Change in HOMO-LUMO gap (eV)	Electronic State	Spin magnetic moment (μ_B) of Fe atom
C top	0.300	0.369	^5A	2.708
Si top	0.839	-0.170	^5A	3.668
Hollow	0.766	-0.097	^3A	2.750
Si-C Normal bridge	0.397	0.272	^5A	2.995
Si-C Zigzag bridge	0.710	-0.041	^5A	2.776

Table 6.17. HOMO-LUMO Gaps (in eV), Change in HOMO-LUMO Gaps (in eV) from Bare Nanotubes, Electronic States and Spin Magnetic Moments (μ_B) of Fe Atoms Adsorbed on Type 1 (10, 0) Zigzag SiC Nanotube.

Site	HOMO-LUMO gap (eV)	Change in HOMO-LUMO gap (eV)	Electronic State	Spin magnetic moment (μ_B) of Fe atom
C top	0.168	-0.039	^5A	3.922
Si top	0.640	-0.511	^3A	3.901
Hollow	0.966	-0.837	^5A	2.710
Si-C Normal bridge	0.256	-0.127	^3A	2.642
Si-C Zigzag bridge	0.918	-0.789	^3A	2.499

Table 6.18. HOMO-LUMO Gaps (in eV), Change in HOMO-LUMO Gaps (in eV) from Bare Nanotubes, Electronic States and Spin Magnetic Moments (μ_B) of Fe Atoms Adsorbed on Type 2 (4, 0) Zigzag SiC Nanotube.

Site	HOMO-LUMO gap (eV)	Change in HOMO-LUMO gap (eV)	Electronic State	Spin magnetic moment (μ_B) of Fe atom
C top	0.715	-0.176	^3A	3.093
Si top	0.631	-0.092	^5A	1.217
First hollow	0.471	0.068	^5A	2.870
Second hollow	0.847	-0.308	^3A	3.057
C-C normal bridge	0.696	-0.157	^5A	3.071
Si-Si normal bridge	0.748	-0.209	^5A	2.934
Si-C zigzag bridge	0.925	-0.386	^3A	3.057

Table 6.19. HOMO-LUMO Gaps (in eV), Change in HOMO-LUMO Gaps (in eV) from Bare Nanotubes, Electronic States and Spin Magnetic Moments (μ_B) of Fe Atoms Adsorbed on Type 2 (6, 0) Zigzag SiC Nanotube.

Site	HOMO-LUMO gap (eV)	Change in HOMO-LUMO gap (eV)	Electronic State	Spin magnetic moment (μ_B) of Fe atom
C top	0.459	-0.023	^5A	1.660
Si top	0.365	0.071	^3A	3.093
First hollow	0.525	-0.089	^5A	3.013
Second hollow	0.497	-0.061	^5A	2.912
C-C normal bridge	0.472	-0.036	^5A	2.850
Si-Si normal bridge	0.462	-0.026	^5A	2.819
Si-C zigzag bridge	0.529	-0.093	^3A	1.053

Table 6.20. HOMO-LUMO Gaps (in eV), Change in HOMO-LUMO Gaps (in eV) from Bare Nanotubes, Electronic States and Spin Magnetic Moments (μ_B) of Fe Atoms Adsorbed on Type 2 (10, 0) Zigzag SiC Nanotube.

Site	HOMO-LUMO gap (eV)	Change in HOMO-LUMO gap (eV)	Electronic State	Spin magnetic moment (μ_B) of Fe atom
C top	0.535	-0.372	^5A	2.577
Si top	0.418	-0.255	^3A	3.034
First hollow	0.344	-0.181	^5A	3.252
Second hollow	0.484	-0.321	^5A	2.926
C-C normal bridge	0.391	-0.228	^3A	2.738
Si-Si normal bridge	0.318	-0.155	^3A	3.390
Si-C zigzag bridge	0.133	0.030	^5A	1.395

Table 6.21. HOMO-LUMO Gaps (in eV), Change in HOMO-LUMO Gaps (in eV) from Bare Nanotubes, Electronic States and Spin Magnetic Moments (μ_B) of Fe Atoms Adsorbed on Type 3 (4, 0) Zigzag SiC Nanotube.

Site	HOMO-LUMO gap (eV)	Change in HOMO-LUMO gap (eV)	Electronic State	Spin magnetic moment (μ_B) of Fe atom
C top	0.482	0.179	^3A	2.756
Si top	0.675	-0.014	^5A	3.129
First hollow	0.490	0.171	^3A	0.566
Si-C Normal bridge	0.563	0.098	^5A	3.155
Si-C zigzag bridge	0.618	0.043	^5A	2.918
C-C zigzag bridge	0.621	0.040	^3A	1.013
Si-Si zigzag Bridge	0.629	0.032	^5A	2.877
Second hollow	0.684	-0.023	^5A	2.964

Table 6.22. HOMO-LUMO Gaps (in eV), Change in HOMO-LUMO Gaps (in eV) from Bare Nanotubes, Electronic States and Spin Magnetic Moments (μ_B) of Fe Atoms Adsorbed on Type 3 (6, 0) Zigzag SiC Nanotube.

Site	HOMO-LUMO gap (eV)	Change in HOMO-LUMO gap (eV)	Electronic State	Spin magnetic moment (μ_B) of Fe atom
C top	0.365	-0.080	^5A	3.134
Si top	0.706	-0.421	^3A	1.163
First hollow	0.913	-0.628	^3A	2.682
Si-C normal bridge	0.608	-0.323	^3A	2.931
Si-C zigzag bridge	0.893	-0.608	^3A	2.661
C-C zigzag bridge	0.717	-0.432	^5A	2.647
Si-Si zigzag Bridge	0.808	-0.523	^5A	2.770
Second hollow	0.601	-0.316	^5A	2.907

Table 6.23. HOMO-LUMO Gaps (in eV), Change in HOMO-LUMO Gaps (in eV) from Bare Nanotubes, Electronic States and Spin Magnetic Moments (μ_B) of Fe Atoms Adsorbed on Type 3 (10, 0) Zigzag SiC Nanotube.

Site	HOMO-LUMO gap (eV)	Change in HOMO-LUMO gap (eV)	Electronic State	Spin magnetic moment (μ_B) of Fe atom
C top	0.375	0.130	^{3}A	1.772
Si top	0.557	-0.052	^{3}A	3.056
First hollow	0.570	0.065	^{5}A	2.844
Si-C normal bridge	0.571	-0.066	^{5}A	3.061
Si-C zigzag bridge	0.498	0.007	^{3}A	2.845
C-C zigzag bridge	0.606	-0.101	^{5}A	2.978
Si-Si zigzag Bridge	0.501	0.004	^{3}A	0.216
Second hollow	0.351	0.154	^{3}A	2.937

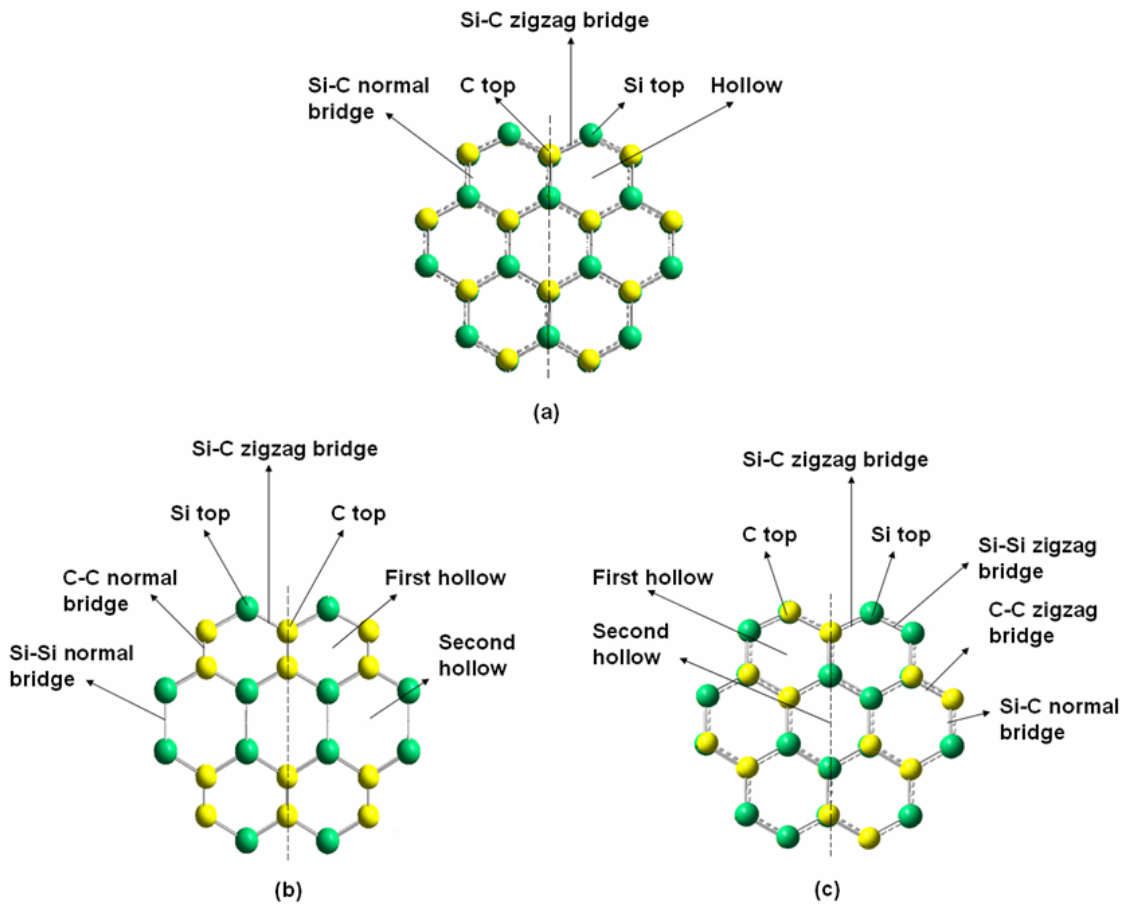

Fig. 6.1. Atomic arrangements and different adsorption sites for (a) type 1, (b) type 2 and (c) type 3 zigzag nanotubes. The carbon atoms are yellow and silicon atoms are green. The lines represent the orientation of tube axis.

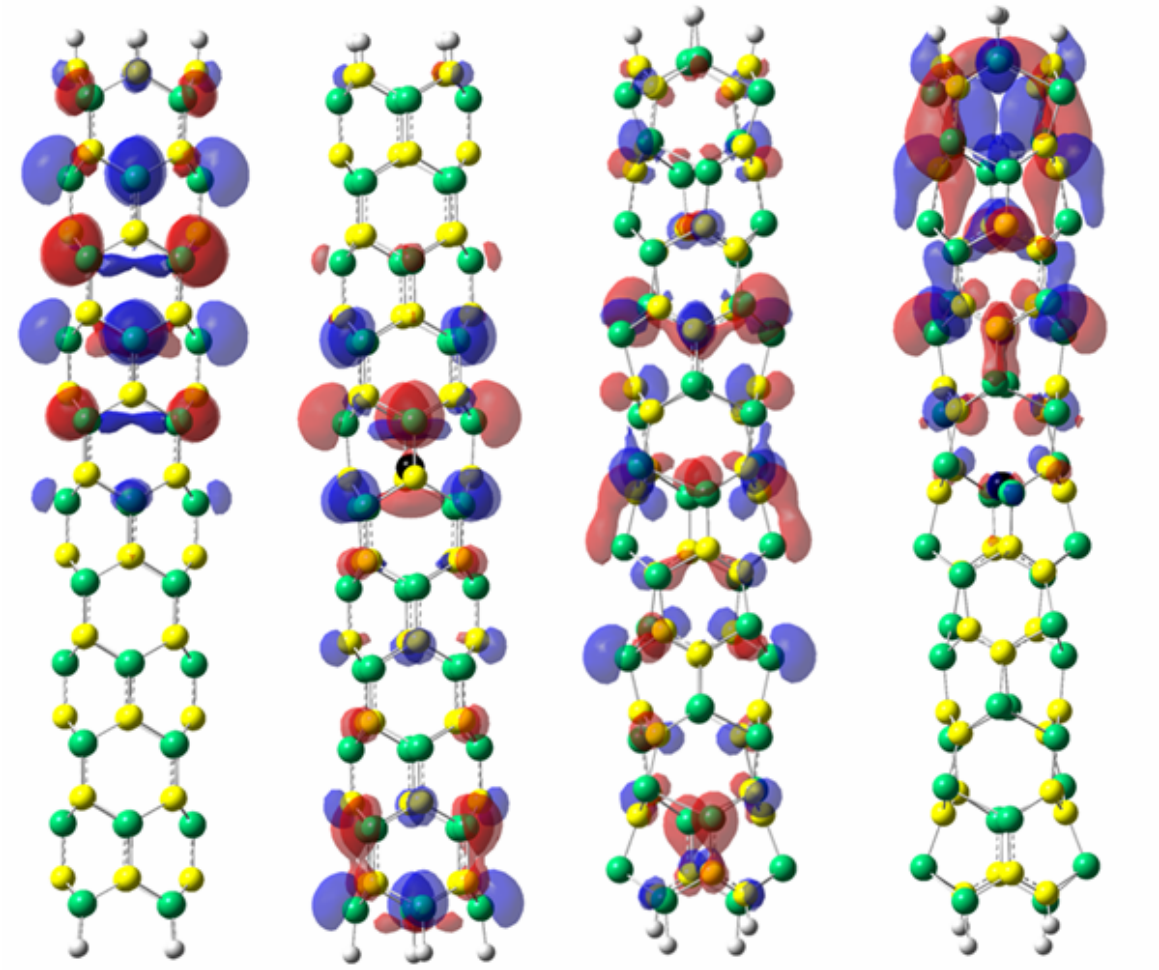

Fig. 6.2. The localization of highest occupied level for type 1 (4, 0) bare (a) Fe atom doped (b), type 3 (4, 0) bare (c) and Fe atom doped (d) nanotubes. The green, yellow and black atoms are Si, C and Fe respectively. Red transparent lobes show the positive and blue transparent lobes show the negative values of the wave function.

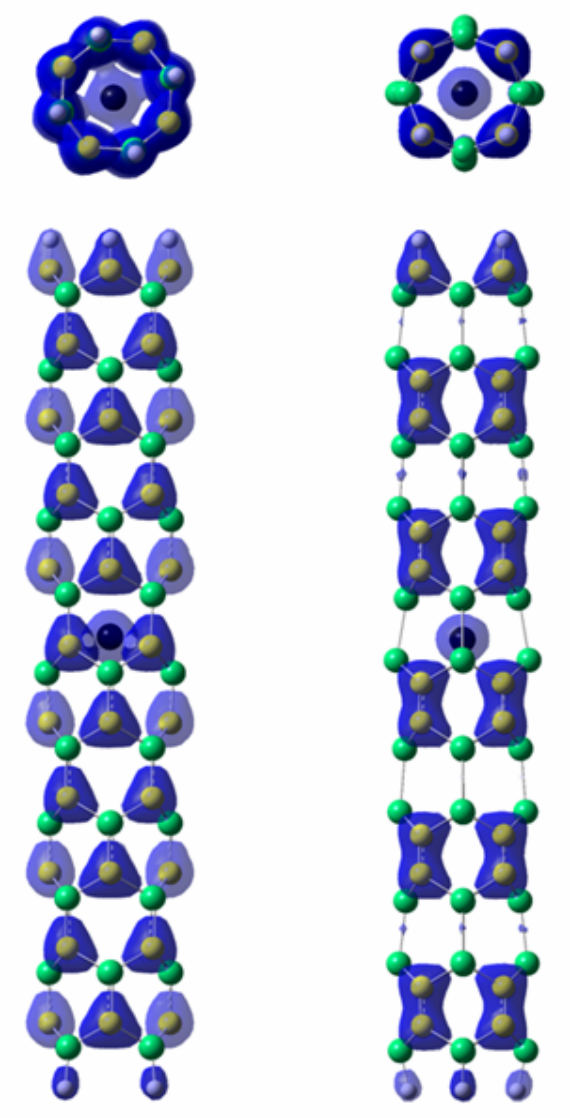

Fig. 6.3. Top and side views of the calculated total charge density (blue color) of Fe encapsulated (4, 0) for type 1 (left) and type 2 (right) nanotubes. The green, yellow and black atoms are C, Si and Fe respectively.

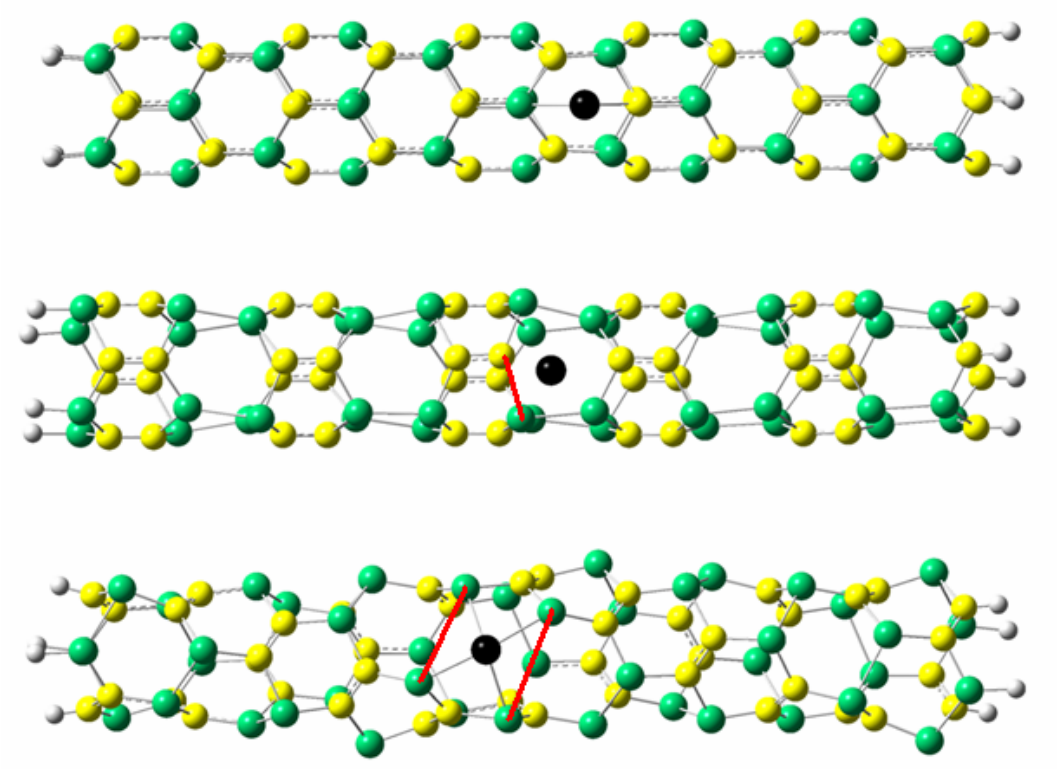

Fig. 6.4. Fe atom adsorption on the smallest single-wall (4, 0) nanotubes. Top (type 1, hollow site), middle (type 2, second hollow site) and bottom (type 3, second hollow site). The last two structures showing bond breaking and distortions of the nanotubes upon Fe atom adsorption. The green, yellow and black atoms are C, Si and Fe respectively. The red lines are marked where bond breaking occurs.

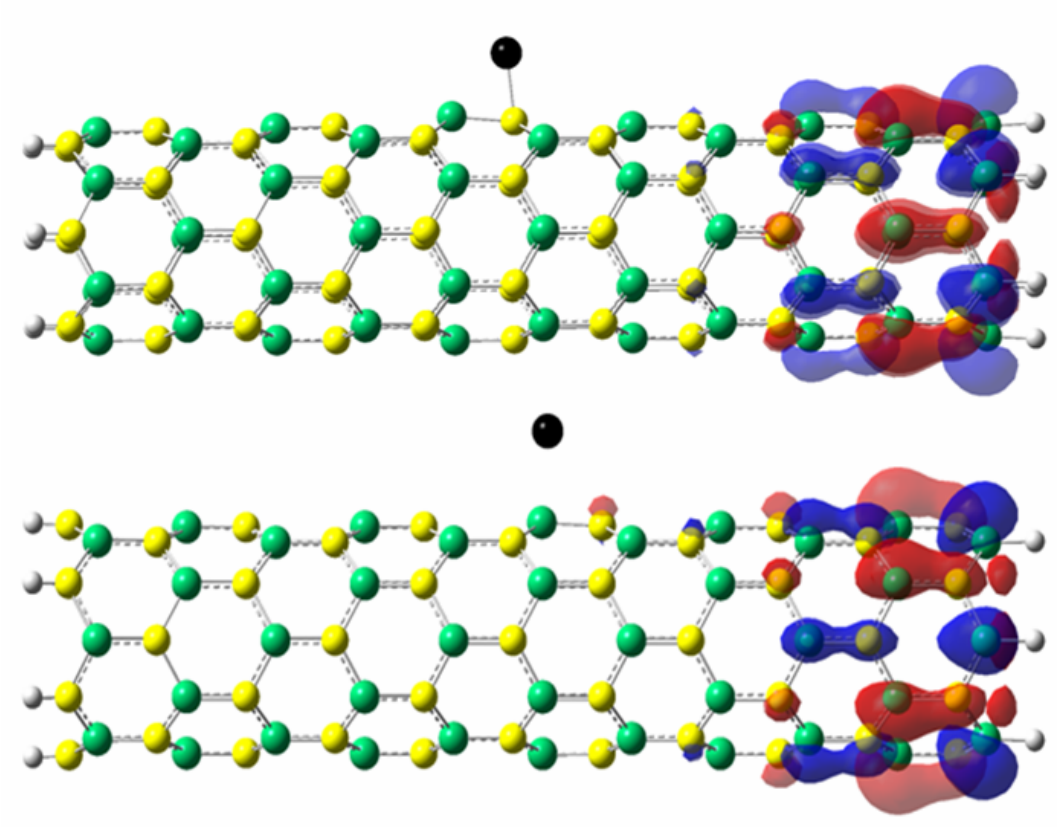

Fig. 6.5. The localization of highest occupied level for Fe atom adsorbed on type 1 (6, 0) nanotube. The most preferred C top site (top) and least preferred Si top site (bottom). The green, yellow and black atoms are Si, C and Fe respectively. Red transparent lobes show the positive and blue transparent lobes show the negative values of the wave function.

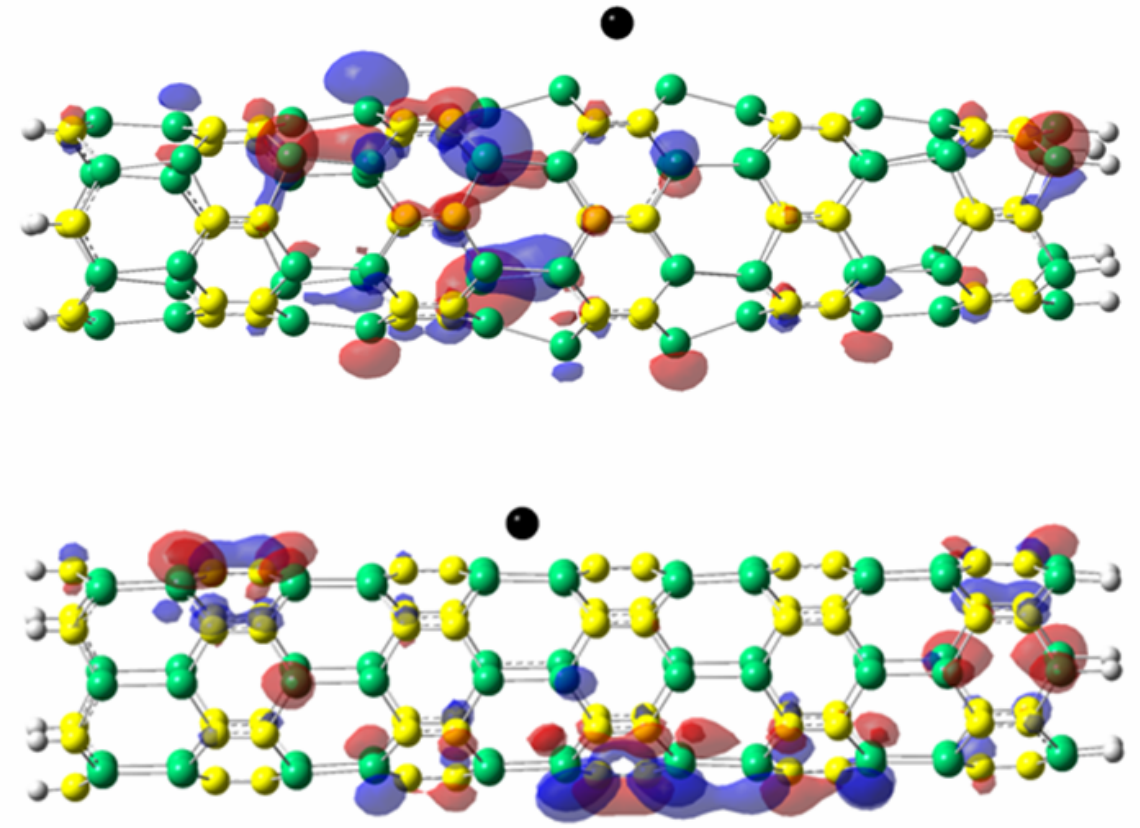

Fig. 6.6. The localization of highest occupied level for Fe atom adsorbed on type 2 (6, 0) nanotube. The most preferred first hollow site (top) and least preferred second hollow site (bottom). The green, yellow and black atoms are Si, C and Fe respectively. Red transparent lobes show the positive and blue transparent lobes show the negative values of the wave function.

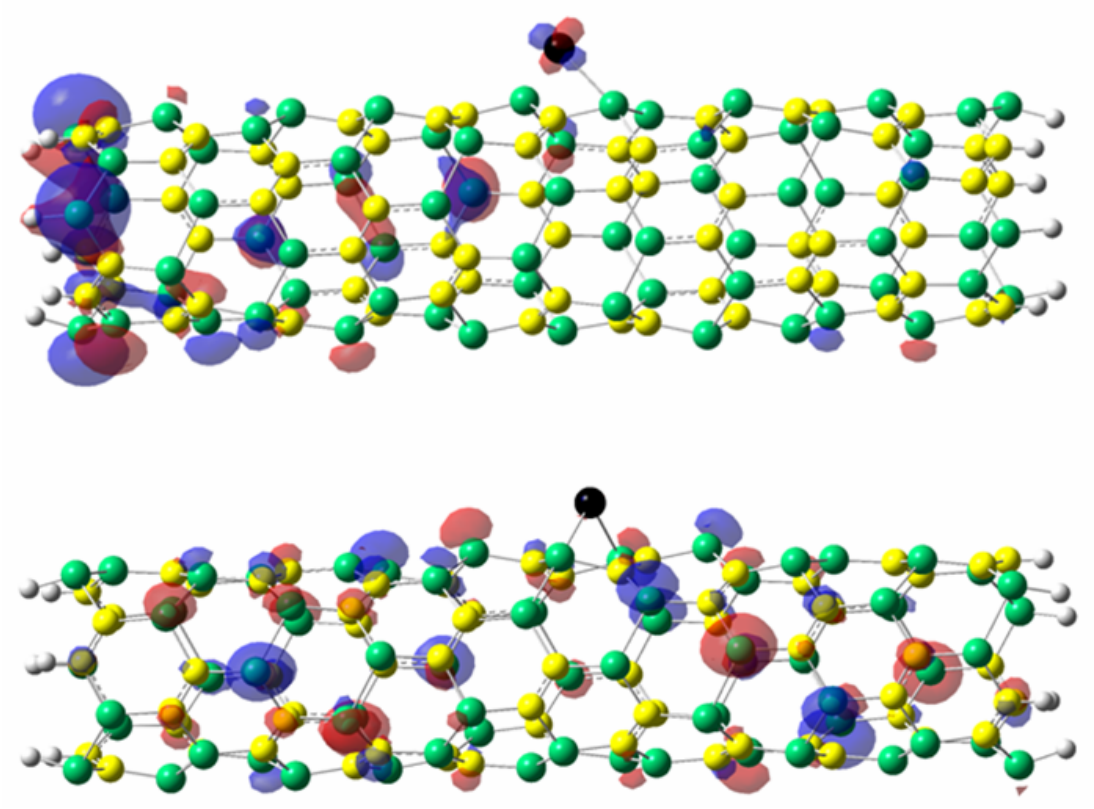

Fig. 6.7. The localization of highest occupied level for Fe atom adsorbed on type 3 (6, 0) nanotube. The most preferred C top site (top) and least preferred first hollow site (bottom). The green, yellow and black atoms are Si, C and Fe respectively. Red transparent lobes show the positive and blue transparent lobes show the negative values of the wave function.

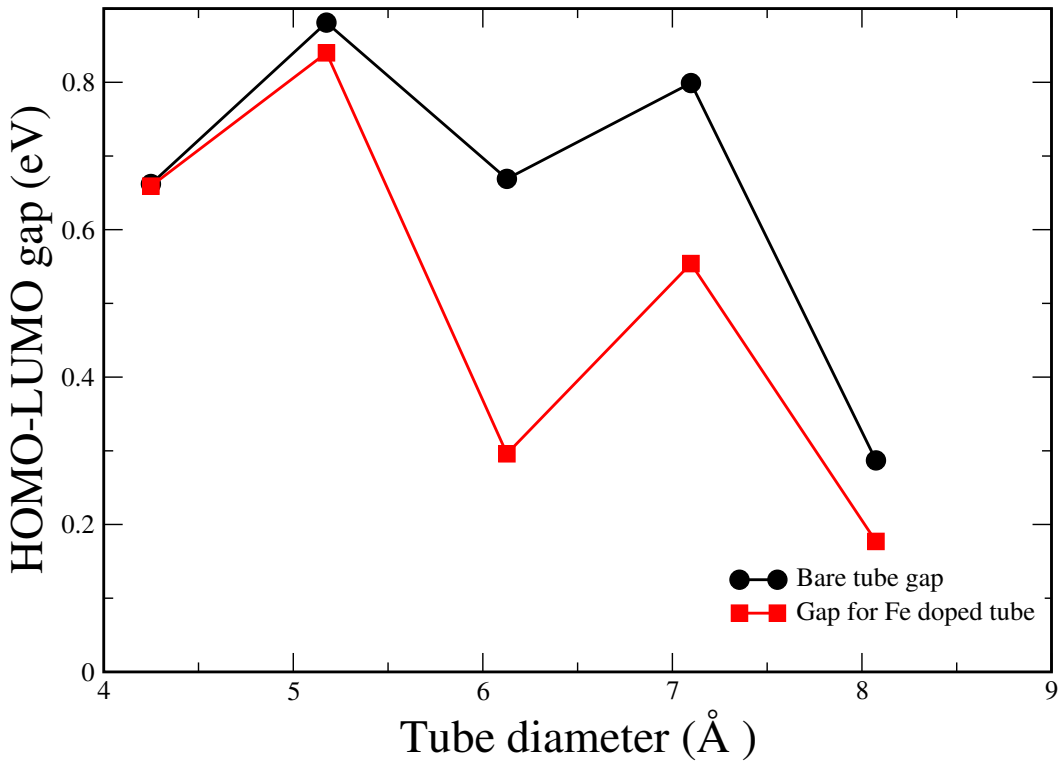

Fig. 6.8. Bare nanotube HOMO-LUMO gap (eV) and gap for the Fe encapsulated tube vs. tube diameter (Å) for type 1 zigzag nanotubes.

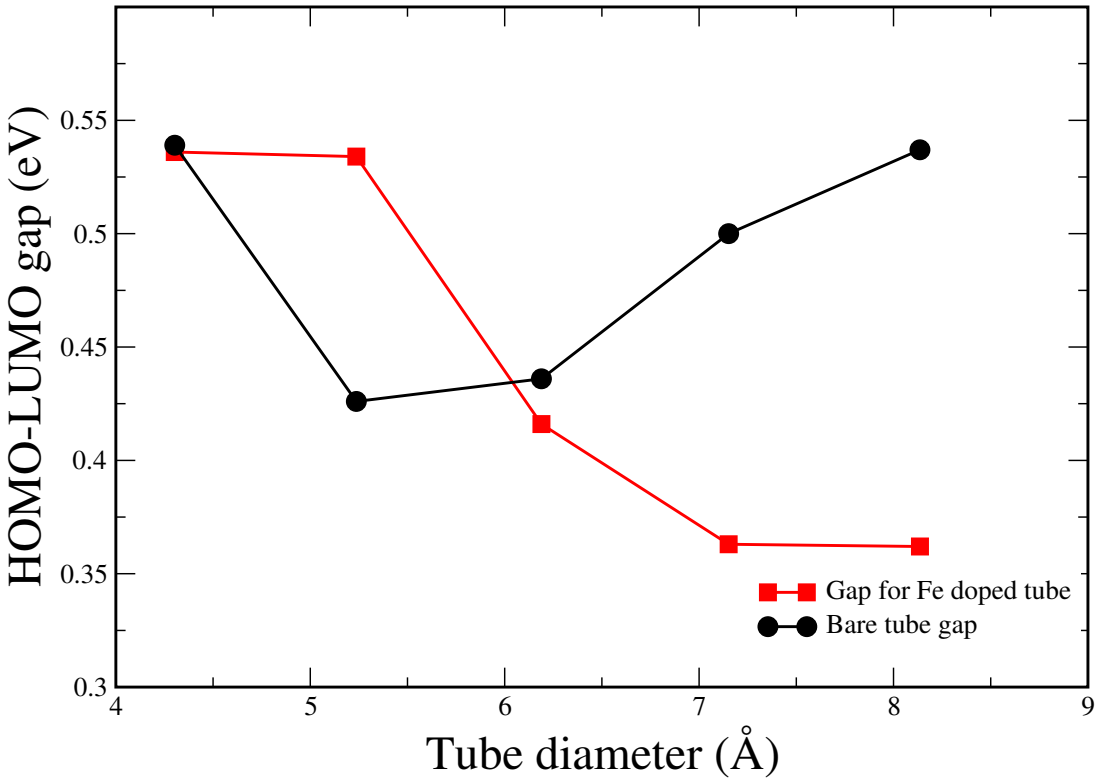

Fig. 6.9. Bare nanotube HOMO-LUMO gap (eV) and gap for the Fe encapsulated tube vs. tube diameter (Å) for type 2 zigzag nanotubes.

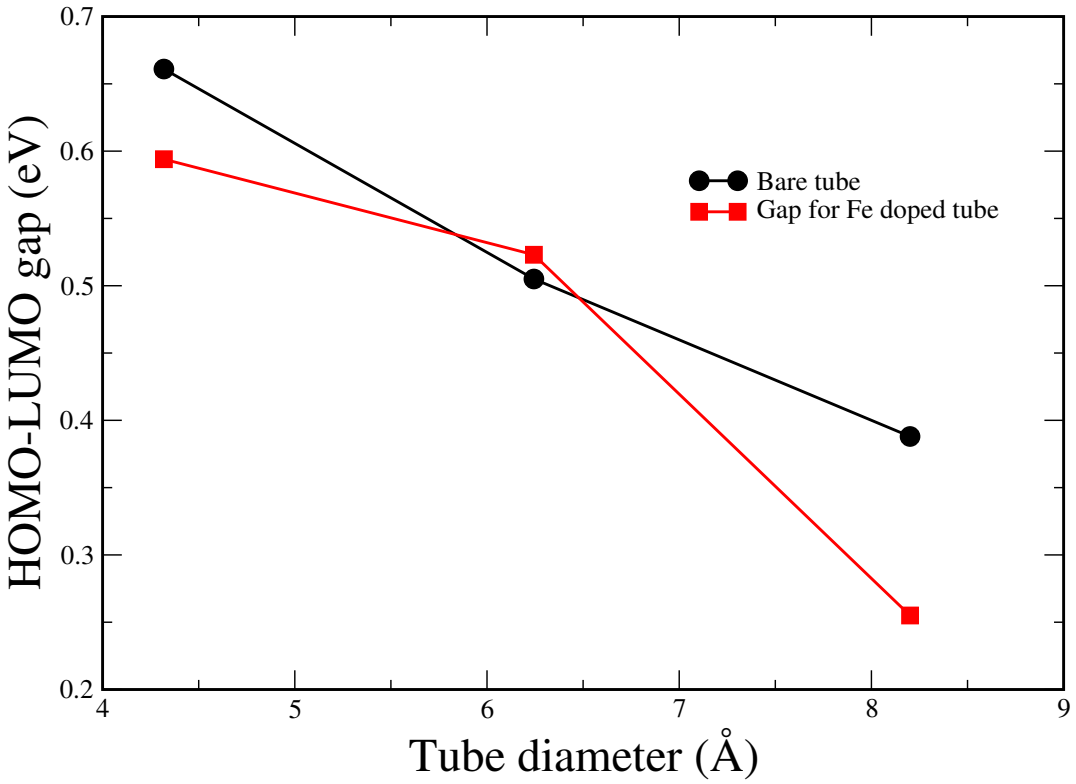

Fig. 6.10. Bare nanotube HOMO-LUMO gap (eV) and gap for the Fe encapsulated tube vs. tube diameter (Å) for type 3 zigzag nanotubes.

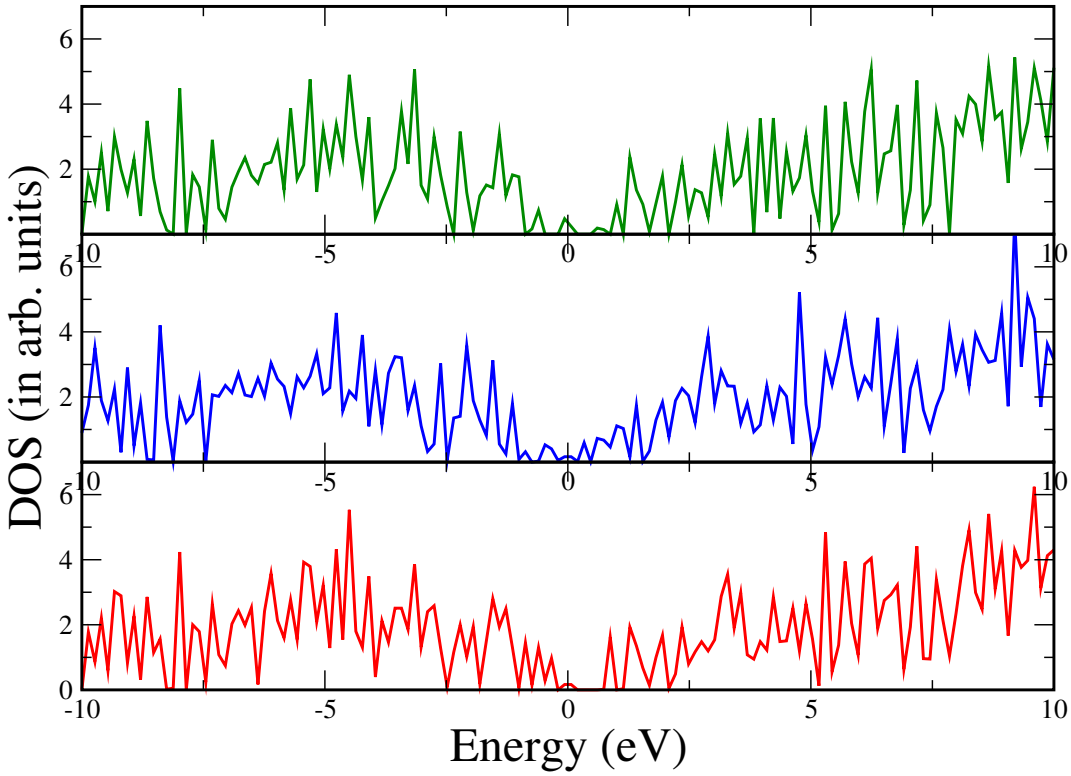

Fig. 6.11. Density of states for type 1 (6, 0) nanotubes. Bare (top), Fe atom adsorbed (for the most stable C top site) (middle) and (for the least stable Si top site) (bottom).

CHAPTER 7

CONCLUSIONS

7.1 Armchair and zigzag SiC nanotubes

We have studied three different types of single wall SiC nanotubes in armchair and zigzag configuration. Detailed analysis and comparison for stability and geometry have been performed along with the evolution of electronic properties with the tube diameters. Within the same helicity and under the constraint of Si to C ratio as 1:1, the dominant factor in deciding the stability, tube morphology and electronic behavior is the relative position of Si and C atoms, and consequently the nature of chemical bonds. As the number of atoms increases, the cohesive energy of nanotubes increases and approaches saturation. This is a common feature for all types of nanotubes. Three armchair and zigzag nanotubes are close in energy, with type 1 predicted to be most stable. Slight difference in hybridization of Si and C atoms on the tube surface causes radial buckling and surface dipoles forming from these bucklings may have potential applications at the nanoscale regime. The Mulliken charge analysis shows that type 1 structures are more ionic than type 2 and 3 structures. Unlike carbon nanotubes which are metallic in armchair configuration, all three types of armchair SiC nanotubes are semiconductors, where type 1 tubes have the largest band gaps. Like carbon nanotubes which are mostly semiconductors in zigzag configuration, all three types of SiC zigzag nanotubes are semiconductors, where type 1 tubes have largest band gaps in average. Strong ionic type bonding localizes the electronic states which results in wide band gap for the type 1 nanotubes. Type 2 and 3 nanotubes have significantly lower gaps in armchair configuration. While armchair type 2 and zigzag type 1 and type 2 nanotubes exhibit a zigzag type trend in gap and diameter relationship, there is a monotonous decrease in band gap with increasing tube diameter for type 3 in both helicities. The smaller band gaps of some SiC nanotubes with

larger diameters can open a new road to reduce Schottky barrier at the nanotube metal junction as they are expected to facilitate carrier tunneling with smaller effective mass. They might even exhibit metallic behavior at higher diameter. In this work it has been demonstrated that by changing relative positions of Si and C atoms one can have SiC nanotubes with a wide range of band gaps which obviate any side wall decoration. Our binding energy calculations reveal that all three types of armchair and zigzag nanotubes are stable and close in energy. Thus if they are synthesized under special experimental set up, it is possible to design molecular electronic system with SiC nanotubes only where wide to small gap semiconducting tubes and semimetallic to metallic tubes would perform as active devices and current carrying conductors respectively.

7.2 Fe atom encapsulation and adsorption in SiC nanotubes

We have studied the interactions of a Fe atom with single wall armchair and zigzag SiCNT in three different configurations. Our results show that interesting properties can be obtained by Fe atom doping inside and adsorbing on the surface of the SiC nanotubes. In case of armchair, encapsulated Fe atom at the center of the tube has maximum stability in type 2, then type 3, followed by type 1 nanotubes. For type 1 (6, 6), Si-C zigzag bridge, type 2 (6, 6) C top and type 3 (6, 6) C top sites are the most preferred sites for Fe atom adsorption. Si-C normal bridge, second hollow and the hollow sites are the most stable sites for type 1 (3, 3), type 2 (3, 3) and type 3 (3, 3) nanotubes when outer wall Fe atom adsorption is concerned. Type 2 and 3 nanotubes are predicted to be better candidates for coating with Fe than the most stable type 1 nanotubes. For all the adsorption sites Fe atom transferred charge to the nanotube with some exceptions. There is an obvious relationship between most and least preferred sites and the associated HOMO localization as HOMO localization is more prominent for the most preferred sites. Type 1 nanotubes are most sensitive to band gap modification upon encapsulation and adsorption of adatoms than the other two types. The gaps remain almost unaffected for the other two types when metal atom is placed inside the tube. As the

tube size (diameter) increases or in other words curvature decreases gap remains unchanged from the bare tube gap, in response to Fe atom adsorption for type 2 and 3. Encapsulated Fe atom at the center of the tube has maximum stability in type 1, then type 2, followed by type 3 nanotubes. For type 1 (4, 0), C top, type 2 (4, 0) first hollow and type 3 (4, 0) Si-Si zigzag bridge sites are the most preferred sites for Fe atom adsorption. C top, first hollow and C top sites are the most stable sites for type 1 (6, 0), type 2 (6, 0) and type 3 (6, 0) nanotubes when outer wall Fe atom adsorption is concerned. The corresponding sites are hollow, first hollow and Si-Si zigzag bridge for type 1, type 2 and type 3 (10, 0) nanotubes respectively. Type 2 and type 3 nanotubes are predicted to be better candidates for coating with Fe than the most stable type 1 nanotubes, like armchair SiCNTs found in our previous work. However type 1 zigzag nanotubes were found to retain their original shape upon Fe atom adsorption, unlike other two types with smaller diameter. Fe coating on smaller diameter type 2 and 3 zigzag nanotubes are not very promising due to very strong interaction that can cause complete structural distortions with bond breakings. For all the adsorption sites Fe atom transferred charge to the nanotube with some exceptions. HOMO localization and redistribution associated with Fe atom interactions are intimately connected with adsorption energy and indicative to the position of the reactive regions. Type 1 zigzag nanotubes are not very sensitive to band gap modification upon encapsulation of Fe atom like type 1 armchair nanotubes. When Fe atom is adsorbed on external tube wall band gap tailoring is feasible for higher diameter nanotubes in all three configurations. All the armchair and zigzag nanotubes studied here have magnetic ground states with very high magnetic moments compared to nonmagnetic ground states of the corresponding bare nanotubes. When the interaction between the Fe atom and the nanotube is stronger, magnetic moment of the Fe atom gets quenched. These small magnetic structures could be useful in magnetic device and spintronic applications. We hope this analysis will be helpful for further exploration of the interactions of other transition metal atoms with silicon carbide nanotubes.

REFERENCES

[1] S. Iijima, Nature **354**, 56 (1991); S. Iijima and T. Ichihashi, Nature **363**, 603 (1993).

[2] *Carbon Nanotubes-Synthesis, Structure, Properties and Applications*, Topics in Applied Physics Vol. **80**, edited by M. S. Dresselhaus, G. Dresselhaus, and Ph. Avouris (Springer, Berlin, 2001).

[3] N. Hamada, S. I. Sawada, and A. Oshiyama, Phys. Rev. Lett. **68**, 1579 (1992).

[4] R. Saito, M. Fujiata, G. Dresselhaus, and M. S. Dresselhaus, App. Phys. Lett. **60**, 2204 (1992).

[5] T. W. Odom, J. L. Huang, P. Kim, and C. M. Lieber, Nature **391,** 62 (1998).

[6] R. A. Jishi, J. Bragin, and L. Lou, Phys. Rev. B **59**, 9852 (1999).

[7] O. Gulseren, T. Yildirim, and S. Ciraci, Phys. Rev. Lett. **65,** 3405 (2002).

[8] S. Wind, J. Appenzeller, R. Martel, V. Derycke, and Ph. Avouris, Appl. Phys. Lett. **80**, 3817 (2002).

[9] Javey, J. Guo, Q. Wang, M. Lundstrom, and H. Dai, Nature, **427**, 654 (2003).

[10] J. Appenzeller, Y. M. Lin, J. Knoch, Z. Chen, and P. Avouris, IEEE Trans. On Electron Devices, **52**, 2568 (2005).

[11] J. Guo, M. Lundstrom, S. Datta, Appl. Phys. Lett. **80**, 3192 (2002).

[12] W.A. de Heer, A. Chatelain and D. Ugarte. Science, **270,** 1179 (1995).

[13] W. Zhu, C. Bower, O. Zhou, G. Kochanski and S. Jin, Appl. Phys. Lett. **75,** 873 (1999).

[14] C. Bower, D. Shalóm, W. Zhu, D. López, G. P. Kochanski, P. L. Gammel and S. Jin, IEEE Trans. On Electron Devices, **49**, 1478 (2002).

[15] T. Durkop, S. A. Getty, E. Cobas, M. S. Fuhrer, Nano Lett., **4**, 35 (2004).

[16] J. Suehiro, G. Zhou, and M. Hara, Sensor and Actuators B: Chemical, **105**, 164 (2005).

[17] M. Penza, G. Cassano, P. Aversa, A. Cusano, A. Cutolo, M. Giordano, and L. Nicolais,

Nanotechnology, **16**, 2536 (2005).

[18] J. Kong, N. Franklin, C. Zhou, S. Peng, J.J. Cho, and H. Dai, Science **287**, 622 (2000).

[19] S. Wind, J. Appenzeller, P. Avouris, Phys. Rev. Lett. **91**, 58301 (2003).

[20] A. Javey, J. Guo, M. Paulsson, Q. Wang, D. Mann, M. Lundstrom, H. Dai, Phys. Rev. Lett. **92**, 106804 (2004).

[21] J. Cumings and A. Zettl, Chem. Phys. Lett. **316**, 211 (2000).

[22] Q. Wu, Z. Hu, X. Wang, Y. Lu, X. Chen, H. Xu, and Y. Chen, J. Am. Chem. Soc. **125**, 10176 (2003).

[23] J. Goldberger, R. He, Y. Zhang, S. Lee, H. Yan, H. Chol, and P. Yang, Nature (London) **422**, 599 2003).

[24] Y. R. Hacohen, E. Grunbaum, R. Tenne , J. Sloand, and J. L. Hutchinson, Nature **395,** 336 (1998); Y. R. Hacohen, R. Popovitz-Biro, E. Grunbaum, Y. Prior, and R. Tenne, Adv. Mater. **14,** 1075 (2002).

[25] Q. Chen , W. Zhou , G. Du, and L. M. Peng , Adv. Mater. **14**, 1208 (2002).

[26] G. R. Patzke, F. Krumeich, and R. Nesper, Angew. Chem. Int. Ed. **41**, 2446 (2002).

[27] J. Sha, J. Niu, X. Ma, J. Xu. X. Zhang, Q. Yang and D. Yang, Adv. Mater, **14**, 1219 (2002).

[28] A. Srinivasan, M. N. Huda and A. K. Ray, Phys. Rev. A **72**, 063201 (2005).

[29] M. N. Huda and A. K. Ray, Phys. Rev. A (R) **69**, 011201 (2004); A. K. Ray and M. N. Huda, *Review Article*, J. Comp. Th. Nanosci. **3**, 315 (2006) and references therein.

[30] M. N. Huda, L. Kleinman and A. K. Ray, J. Comp. Th. Nanosci. **4**, 739 (2007).

[31] R. J. Baierle, S. B. Fagan, R. Mota, A. J. R. da Silva and A. Fazzio, Phys. Rev. B **64** 085413 (2001).

[32] M. T. Yin and M. L. Cohen, Phys. Rev. B **29**, 6996 (1984).

[33] X. H. Sun, C. P. Li, W. K. Wong, N. B. Wong, C. S. Lee, S. T. Lee, and B.T. Teo, J. Am. Chem. Soc. **124**, 14464 (2002).

[34] N. Keller, C. Pham-Huu, G. Ehret, V. Keller, and M. J. Ledous, Carbon, **41**, 2131 (2003).

[35] E. Borowiak-Palen, M. H. Ruemmeli, T. Gemming, M. Knupfer, K. Biedermann, A. Leonhardt, T. Pihler, R. J. Kalenczuk, J. Appl. Phys. **97**, 056102 (2005).

[36] T. Taguchi, N. Igawa, H. Yamamoto, S. Shamoto, S. Jitsukawa, Phys. E **28**, 431 (2005).

[37] J. Q. Hu, Y. Bando, J. H. Zhan, D. Goberg, Appl. Phys. Lett. **85**, 2923 (2004).

[38] J.M. Nhut, R. Vieira, L. Pesant, J.-P. Tessonnier, N. Keller, G. Ehet, C. Pham-Huu, M.J. Ledoux: Catalysis Today **79**, 11 (2002).

[39] C. Pham-Huu, N. Keller, G. Ehet, M. J. Ledoux: J. Catal. **200**, 400 (2001).

[40] T. Taguchi, N. Igawa, H. Yamamoto, S. Jitsukawa, J. Am. Ceram. Soc. **88**(2) 459 (2005).

[41] A. Huczko, M. Bystrzejewski, H. Lange, A. Fabianowska, S. Cudzilo, A. Panas, and M. Szala, J. Phys. Chem. B **109**, 16244 (2005).

[42] M. W. Zhao, Y. Y. Xia, F. Li, R. Q. Zhang, and S.-T. Lee, Phys. Rev. B **71**, 085312 (2005).

[43] G. Mavrandonakis, E. Froudakis, M. Schnell, and M. Muhlhä, Nano Lett. **3**, 1481 (2003).

[44] M. Menon, E. Richter, and A. N. Andriotis, Phys. Rev. B, **69**, 115322 (2004).

[45] A.N. Andriotis, M. Menon, and G. Froudakis, Phys. Rev. Lett. **85**, 3193 (2000).

[46] Y.H. Lee, S.G. Kim, and D. Tomanek, Phys. Rev. Lett. **78**, 2393 (1997).

[47] K. Kong, S. Han, and J. Ihm, Phys. Rev. B **60**, 6074 (1999).

[48] S. B. Fagan, R. Mota, A. J. R. da Silva, and A. Fazzio, Phys. Rev. B **67**, 205414 (2003).

[49] E. Durgun, S. Dag, V. M. K. Bagci, O. Gülseren, T. Yildirim, and S. Ciraci, Phys. Rev. B **67**, 201401(R (2003). E. Durgun, S. Dag, S. Ciraci, and O. Gülseren, J. Phys. Chem. B **108**, 575 (2004); S. Dag, E. Durgun, and S. Ciraci, Phys. Rev. B **69**, 121407(R) (2004);

[50] Y. Zhang, N.W. Franklin, R.J. Chen, and H. Dai, Chem. Phys. Lett. **331**, 35 (2000);
Y. Zhang, H. Dai, Appl. Phys. Lett., ***77***, 3015 (2000).

[51] A. K. Singh, T. M. Briere, V. Kumar and Y. Kawazoe, Phys. Rev. Lett. **91**, 146802 (2003).

[52] H. Hiura, T. Miyazaki and T. Kanayama, Phys. Rev. Lett., **86**, 1733 (2001).

[53] T. Meng, C-Y. Wang, S.-Y. Wang, Chem. Phys. Lett. **437,** 224 (2007).

[54] J.-x. Zhao and Y.-h. Ding, J. Phys. Chem. C **112**, 2558 (2008).

[55] S. Mukherjee and A. K. Ray, J. Comp. Th. Nanosci., (in press).

[56] R. G. Parr and W. Yang, *Density Functional Theory of Atoms and Molecules* (Oxford University Press, New York, 1989).

[57] P. Hohenberg and W. Kohn, Phys. Rev. **136,** B864 (1964);

[58] W. Kohn and L. J. Sham, Phys Rev. **140,** A1133 (1965)

[59] D. M. Ceperley and B. J. Adler, Phys. Rev. Lett. **45**, 566 (1980).

[60] W. Kohn, A.D. Becke and R. G. Parr, J. Phys. Chem. **100**, 12974(1996).

[61] R. O. Jones and O. Gunnarsson, Rev. Mod. Phys. **61**, 689 (1989).

[62] G. Sentore and N. H. march, Rev. Mod. Phys. **66**, 445(1996).

[63] J. F. Dobson, G. Vignale, and M. P. Das (Eds.), *Electronic Density Functional Theory: Recent Progress and New Directions, (Plenum Press, New York and London, 1998).*

[64] D. R. Hartree, Proc. Cambridge PHilos. Soc. **24**, 89(1928)

[65] V. Fock, Z. Phys. **61**, 126(1930)

[66] J. C. Slater, Phys. Rev. **35**, 210 (1930)

[67] C. Coulson, Rev. Mod. Phys. **32**, 170(1960).

[68] L. H. Thomas, Proc. Cambridge Plilos. Soc. **23**, 542(1927).

[69] E. Fermi, Z. Phys. **48**, 73(1928).

[70] P. A. M. Dirac, Proc. Cambridge Plilos. Soc. **26**, 376(1930).

[71] U. von Barth and L. Hedin, J. Phys. C:Solid State Phys. **5**, 1629(1972).

[72] O. Gunnarsson and B. I. Lundqvist, Phys. Rev. **13**, 4274(1976).

[73] S. H. Vosko, L. Wilk, and M. Nusair, Can. J. Phys. **58**, 1200 (1980).

[74] M. Rasolt and D. J.W. Geldart, Phys. Rev. B **34, 1325(1986).**

[75] J. P. Perdew, Phys. Rev. B **33**, 8822(1986); **34**, 7406 (1984).

[76] A. D. Becke, J. Chem. Phys. **98**, 1372(1993); **98**, 5648(1993)

[77] C. Lee, W. Yang, and R. G. Parr, Phys. Rev. B **37**, 785 (1988)

[78] J. P. Perdew, J. A. Chevary, S. H. Vosko, K. A. Jackson, M. R. Pederson, D. J. Singh, and C. Fiolhais, Phys. Rev. B **48,** 4978 (1993); K. Burke, J. P. Perdew, and Y. Wang, in *Electronic Density Functional Theory: Recent Progress and New Directions,* Ed. J. F. Dobson, G. Vignale, and M. P. Das (Plenum, New York, 1998).

[79] J. P. Perdew, K. Burke, and M. Ernzerhof, Phys. Rev. Lett. **77**, 3865(1996); **78**, 1396(1997).

[80] J. P. Perdew, *Electronic Structure of Solids'91*, edited by P. Ziesche and H. Eschig (Akademie Verlag, Berlin, 1991); J. P. Perdew and Y. wang, Phys. Rev. B **46**, 12947(1992); Phys. Rev. B **46**, 6671(1992).

[81] W. J. Hehre, L. Radom, P. v. R. Schleyer, and J. A. Pople, *Ab Initio Molecular Orbital Theory* (Wiley, New York, 1986).

[82] J. P. Perdew, R. G. Parr, M. Levy, J. L. Balduz, Phys. Rev. Lett. **49**, 1691 (1982).

[83] J. P. Perdew, M. Levy, Phys. Rev. Lett. **51**, 1884 (1983).

[84] J. Muscat, A. Wander, and N. Harrison, Chem. Phys. Lett. **34**, 397 (2001).

[85] J. Heyd and G. Scuseria, J. Chem. Phys. **121**, 1187 (2004).

[86] V. Barone, J. E. Peralta, M. Wert, J. Heyd, and G. E. Scuseria, Nano Lett. **5**, 1621 (2005).

[87] V. Barone, J. E. Peralta, and G. E. Scuseria, Nano Lett. **5**, 1830 (2005).

[88] V. Barone, O. Hod, and G. E. Scuseria, Nano Lett. **6**, 2748 (2006).

[89] M. Y. Han, B. Ozyilmaz, Y. Zhang, and P. Kim, Phys. Rev. Lett. **98**, 206805 (2007).

[90] T. H. Dunning Jr. and P. J. Hay, in *Modern Theoretical Chemistry*, p. 1-28 (Plenum, New York, 1976).

[91] *Gaussian 03*, Revision A.1, M. J. Frisch, M. J. Frisch, G. W. Trucks, H. B. Schlegel, G. E. Scuseria, M. A. Robb, J. R. Cheeseman, J. A. Montgomery, Jr., T. Vreven, K. N. Kudin, J. C. Burant, J. M. Millam, S. S. Iyengar, J. Tomasi, V. Barone, B. Mennucci, M. Cossi, G. Scalmani, N. Rega, G. A. Petersson, H. Nakatsuji, M. Hada, M. Ehara, K. Toyota, R. Fukuda, J.

Hasegawa, M. Ishida, T. Nakajima, Y. Honda, O. Kitao, H. Nakai, M. Klene, X. Li, J. E. Knox, H. P. Hratchian, J. B. Cross, C. Adamo, J. Jaramillo, R. Gomperts, R. E. Stratmann, O. Yazyev, A. J. Austin, R. Cammi, C. Pomelli, J. W. Ochterski, P. Y. Ayala, K. Morokuma, G. A. Voth, P. Salvador, J. J. Dannenberg, V. G. Zakrzewski, S. Dapprich, A. D. Daniels, M. C. Strain, O. Farkas, D. K. Malick, A. D. Rabuck, K. Raghavachari, J. B. Foresman, J. V. Ortiz, Q. Cui, A. G. Baboul, S. Clifford, J. Cioslowski, B. B. Stefanov, G. Liu, A. Liashenko, P. Piskorz, I. Komaromi, R. L. Martin, D. J. Fox, T. Keith, M. A. Al-Laham, C. Y. Peng, A. Nanayakkara, M. Challacombe, P. M. W. Gill, B. Johnson, W. Chen, M. W. Wong, C. Gonzalez, and J. A. Pople, Gaussian Inc. Pittsburgh*, Pa*, (**2003).**

[92] P. J. Hay and W. R. Wadt, J. Chem. Phys. **82,** 270 (1995).

[93] E. Hernandez, C. Goze, P. Bernier, and A. Rubio, Phys. Rev. Lett. **80**, 4502 (1998).

[94] R. J. Baierle, P. Piquini, L. P. Neves, and R. H. Miwa, Phys. Rev. B **74**, 155425 (2006)

[95] Y. Miyamoto and B.D.Yu, Appl. Phy. Lett, **80**, 4, 586 (2002).

[96] M. W. Zhao, Y. Y. Xia, D. J. Zhang, and L. M. Mei, Phys. Rev. B **68**, 235415 (2003)

[97] S. M. Lee, Y. H. Lee, Y. G. Hwang, J. Elsner, D. Porezag, and Th.Frauenheim, Phys. Rev. B **60**, 7788 (1999).

[98] M. Menon and D. Srivastava, Chem. Phys. Lett. **307**, 407 (1999).

[99] S. P. Mehandru and A. B. Anderson, Phys. Rev. B **42**, 9040 (1990).

[100] D. H. Lee and J. D. Joannopoulos, J. Vac. Sci. Technol. **21**, 351 (1982).

[101] T. Takai, T. Halicioglu, and W. A. Tiller, Surf. Sci. **164**, 341 (1985).

[102] B. Wenzien, P. Ka¨ckell and F. Bechstedt, Surf. Sci. **308-309**, 989 (1994).

[103] M. W. Zhao, Y. Y. Xia, R. Q. Zhang, and S.-T. Lee, J. Chem. Phys. **122**, 214707 (2005).

[104] F. Li, Y. Y. Xia, M. W. Zhao, X. D. Liu, B. D. Huang, Z. H. Yang, Y. J. Ji, and C. Song, J. Appl. Phys. **97**, 104311 (2005).

[105] G. Mpourmpakis, G. E. Froudakis, G. P. Lithoxoos, and J. Samios, Nano Lett. **6**,1581 (2006).

[106] R. Saito, T. Takeya, T. Kimura, G. Dresselhaus, and M. S. Dresselhaus, Phys. Rev. B **59**, 2388 (1999).

[107] J. Wu, W. Duan, B.-L. Gu, J.-Z. Yu and Y. Kawazoe, Appl. Phys. Lett. **77**, 2554 (2000)

[108] R. B. Chen, C. P. Chang, F. L. Shyu, J. S. Hwang, and M. F. Lin, Carbon, **42**, 531 (2004)

[109] O. Hod, J. E. Peralta, and G. E. Scuseria, arXiv:physics/0609091 (2006).

[110] T. He, M. Zhao, Y. Xia, W. Li, C. Song, X. Lin, X. Liu, and L. Mei, J. Chem. Phy. **125**, 194710 (2006).

[111] F. Leonard, and J. Terso, Phys. Rev. Lett. **83**, 5174 (1999).

[112] S. M. Sze, *Physics of Semiconductor Devices*, 2nd edition (John Wiley & Sons, (1981)

[113] K. M. Alam, and A. K. Ray, Phys. Rev. B **77**, 035436 (2008); Nanotech. **18**, 495706 (2007).

[114] J. Appenzeller, M. Radosavljevic, J. Knoch, and Ph. Avouris, Phys. Rev. Lett. **92**, 048301 (2004).

[115] Y. L. Mao, X. H. Yan, and Y. Xiao, Nanotech. **16**, 3092 (2005).

[116] Y. Yagi, T. M. Briere, M. H. F. Sluiter, V. Kumar, A. A. Farajian, and Y. Kawazoe, Phys. Rev. B **69,** 075414 (2004).

[117] K. M. Alam, and A. K. Ray, submitted for publication.

BIOGRAPHICAL INFORMATION

The author completed his undergraduate degree in Mechanical Engineering from Bangladesh University of Engineering and Technology, Bangladesh. He has earned a Master of Science degree (non thesis) in Mechanical Engineering with a minor in Electrical Engineering from Texas A & M University, College Station. He started another Master of Science program in Electrical Engineering at The Ohio State University but did not complete it. During these programs he has completed numerous courses on semiconductor device physics, electronic and optoelectronic device engineering and fiber optic communication. In order to have a deeper understanding of device phenomena he decided to pursue a Master of Science degree in physics in the area of condensed matter physics before starting a PhD in nanotechnology.

His current research interests are theoretical and experimental nanotechnology, quantum devices and their potential applications in cutting edge, state of the art technological areas such as fiber optic communication, semiconductor lasers, spintronic devices, novel information processing and computation. He has authored few papers in scientific journals and presented papers at national conferences under the mentorship of Dr. A. K. Ray. Recently he has got the opportunity to work (both experimental and theoretical) as a PhD student at Canada's only national lab for nanotechnology, NINT (National institute for nanotechnology) housed in Edmonton and in collaboration with the University of Alberta. He intends to continue his research activities in academia or industry after completion of his PhD.